Universidad de Jaén

Escuela de Doctorado

**TESIS DOCTORAL**

# OPTIMAL DISTRIBUTED GENERATION ALLOCATION CONSIDERING UNCERTAINTY OF POWER GENERATION AND TIME-VARYING LOAD


**PRESENTADA POR:**

**ALI SELIM MOHAMED IBRAHIM**

**DIRIGIDA POR:**

**FRANCISCO JURADO MELGUIZO**

**SALAH MOHAMED KAMEL**



**JAÉN, Enero 2021**

**ISBN…….**

Universidad de Jaén

Escuela de Doctorado

**TESIS DOCTORAL**

# OPTIMAL DISTRIBUTED GENERATION ALLOCATION CONSIDERING UNCERTAINTY OF POWER GENERATION AND TIME-VARYING LOAD


## Ali Selim Mohamed Ibrahim


El acto de defensa y lectura de Tesis se celebra el día…25 de enero…de 2021 en la Universidad de Jaén, ante el siguiente Tribunal evaluador, quien decide otorgar la calificación de:

.....

**El Presidente** **El Secretario**

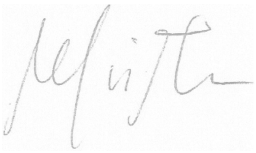

**El vocal**

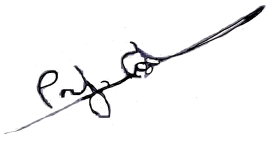

Universidad de Jaén

Escuela de Doctorado

**TESIS DOCTORAL**

# OPTIMAL DISTRIBUTED GENERATION ALLOCATION CONSIDERING UNCERTAINTY OF POWER GENERATION AND TIME-VARYING LOAD


**Director de Tesis:**

**Francisco Jurado Melguizo** *Catedrático de Universidad (Universidad de Jaén)*
**Salah Mohamed Kamel** *Titular de Universidad (Aswan University)*


**TRIBUNAL EVALUADOR**

**Presidente: Francisco Gonzalez-Longatt, University of South-Eastern, Noruega**
**Secretario: Marcos Tostado, Universidad de Jaén**
**Vocal: Ghada Mohammed Amer, Benha University, Egipto**
**Suplente: Mohamed Ebeed, Sohag University, Egipto**
**Suplente: María Reyes Sánchez Herrera, Universidad de Huelva**

**Jaén, Enero 2021**

# *Acknowledgment*

*At the end of this work, I remember many people who have participated somehow to make it possible. Let me express with brief words my deep acknowledgment. I would like to take this opportunity to extend my heartfelt appreciation to the following persons who contribute directly or indirectly towards the completion of the study.*

*I owe my deepest appreciation to my supervisors Prof. Francisco Jurado Melguizo and Prof. Salah Mohamed Kamel for the continuous support of my Ph.D. study and research, for their motivation, patience, and eagerness. Their support helped me in all the time of researching and finishing this thesis. My appreciation also goes to my colleagues from the Electrical Engineering Department of the University of Jaén.*

*Finally, my warmest thanks are dedicated to my family: my wife, and my friends for supporting me spiritually throughout my life.*

*Ali Selim Mohamed*

# ABSTRACT

The interest in incorporating distributed generators (DGs) into radial distribution systems (RDSs) has grown over the last few decades due to their advantages, such as improving the efficiency of the power grid, reducing power losses, and improving the voltage profile. However, if the integration of DGs is not properly planned, this can bring some technical issues such as over-voltage, fluctuation, and system unbalance. Besides, dealing with DG-based renewable energy resources, such as wind power and photovoltaic (PV), which are characterized by the intermittent nature of power generation besides the load variation led to increasing the change in the power losses and voltage level.

To avoid these issues and increase the benefits of DG integration, the optimal DG allocation (location and size) into RDS is essentially required. The allocation of the DG has been achieved in the literature based on analytical and metaheuristic optimization algorithms.

However, these algorithms face some issues, the analytical algorithms are a very time-consuming task. On the other hand, metaheuristic algorithms face low convergence rate issues, and they are trapping in local solutions during phases of exploration and exploitation. These issues can be solved by developing improved versions of the original optimization algorithms.

Based on the above discussion, the main contributions of this thesis can be summarized as follows.:

- Proposing efficient single- and multi-objective optimization algorithms using different improved methods to improve the performance of the original algorithm.
- Applying the proposed algorithms to find the optimal allocation of DG into RDS in order to minimize the overall power losses, voltage deviation, and maximize the VSI.
- Scheduling for BES charge/discharge during 24 hrs is proposed to avoid the uncertain nature of PV power generation besides the variation of the load.
- A comprehensive comparison with the other competitive optimization algorithms is performed to test the efficiency of the proposed algorithms through standard and practical RDSs with various operating scenarios.

# Contents

# List of Figures

# List of Tables

# Chapter 1

# Introduction

## 1.1.- Context and Motivation

In recent years, the growing interest in decreasing the effects of $CO_2$ emissions has led the power systems community to think about exploiting clean renewable energy resources [1]. Part of the renewable energy resources is usually known as distribution generators (DGs), which are small generation units that are directly connected with distribution systems at strategic locations to improve customer reliability [2]. Consequently, the integration of DGs changes the radial distribution systems (RDSs) from their passive structures with one direction power flow (see Fig. 1.1) into active distribution systems (ADS) with multi-directional power flows. However, based on different points of view, the potential large-scale penetration of DGs can result in both positive and negative consequences. Key negative effects include power flows, voltage levels, and power loss. [3]. In consequence, the assessment of these resources and their effects on electricity is essential.

Regarding the voltage level, distribution network operators (DNOs) concern to preserve the distribution system voltage level within limits. However, the existence of DGs in the RDS in the absence of load demand increases the generation and reverses power flow along the line in which voltage rise becomes critical. Hence, many control schemes have

been investigated for voltage control in active distribution systems [4-7]. In order to guarantee the optimal operation of RDSs, voltage control should be carried out with the integration of DGs [8].

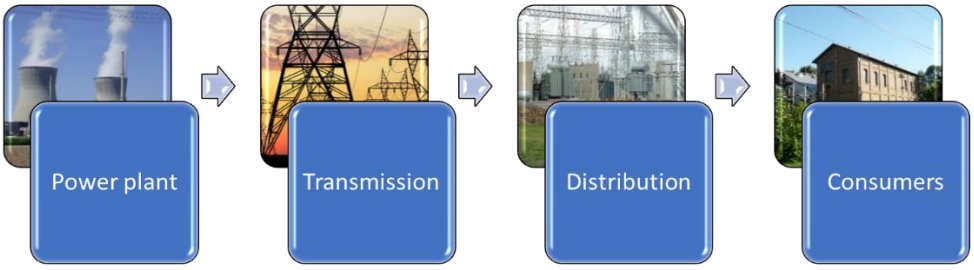


*Fig. 1.1 – Electrical power system structure*

# 1.2.- Introduction

The allocation of the DG in the RDS has been studied in many types of research works. This section provides a summary of the optimization techniques and their application to the DG allocation.

## 1.2.1- Optimization algorithms

It is possible to describe optimization as a procedure of accomplishing the most appropriate solutions for a combination of variables that achieve the objective of a problem in terms of maximization or minimization [9]. Recently, many algorithms for optimization have been proposed. to find the appropriate solutions to the optimization problems. These optimization algorithms can be classed based on the nature of the algorithm to different groups, such as numerical algorithms and stochastic algorithms [10, 11].

In the numerical based algorithm, a mathematical model should be adopted for the optimization problem. However, this algorithm requests some gradient information to assess better solutions nearly to initial points in the local search. Besides, it is more sensitive to the initial points [10].

On the other hand, the stochastic based algorithms have a random character in which a different result could be obtained every time [11]. The metaheuristic optimization algorithm is the most popular of the stochastic algorithms characterized by its simplicity and efficiency. Metaheuristic optimization algorithms are categorized into four groups

based on the nature of inspiration. These groups are; evolutionary, swarm, physics, and human behavior based algorithms[12] [13].

In the first category (evolutionary-based algorithm), the main inspiration comes from the nature of genetic evolution. Where a generation of better offspring that inherit the characteristic of the parents leads to achieving global optima. Thus, mutation, selection, and crossover have been applied in this type of algorithms. Good examples of these algorithms which proved their effectiveness in optimization problems are; genetic algorithm (GA) [14], differential evolution (DE) [15], human evolutionary model [16], Physarum inspired computational model (PCM) [17], and biogeography based optimization [18].

The second group is swarm-based algorithms that are motivated by the social behavior of groups of particles and animals. The intelligence behavior of the individual search agent in the swarm and the combination of these behaviors gives these types the superiority in accomplishing the global optima over the other algorithms. The most popular swarm algorithms are; Particle swarm optimization (PSO) [19], social spider optimization (SSO)[20], artificial bee colony (ABC) [21], moth-flame optimization algorithm (MFO) [22], grey wolf optimizer (GWO) [23], grasshoppers optimization algorithm (GOA) [24], whale optimization algorithm (WOA) [13], salp swarm algorithm (SSA) [25], Harris hawk optimization (HHO) [26], border collie optimization BCO [11], and bonobo optimizer (BO) [27].

Indeed, the physical-based algorithms use the occurrence of the physical phenomena to implement the optimization paradigm such as; simulated annealing (SA) [28], gravitational search optimization algorithm (GSA) [29], water cycle algorithm (WCA) [30], water evaporation optimization (WEO) [31], atom search optimization (ASO) [32], equilibrium optimizer (EO) [33], lightning search algorithm (LSA) [34], and artificial ecosystem-based optimization (AEO) [10].

The fourth category is the human behavior based algorithms which mimic the social activities and ideology of humans some of these algorithms known as; human-inspired algorithm (HIA) [35], social group optimization (SGO) [36], Teaching–learning-based optimization (TLBO) [37], most valuable player algorithm (MVPA) [38], and league championship algorithm (LCA) [39].

The powerful of meta-heuristic optimizations are coming from their simplicity of the implementation. Besides, they are more efficient in dealing with many optimization problems. However, based on the theorem of optimization called no-free-lunch [40], which rises that no optimization algorithm able to deal with all optimization problems and achieve the best results so far. Hence, many researchers tended to improve existing optimization algorithms or tried to develop new algorithms.

Different methods were used. to improve the metaheuristic optimization algorithms. Chaos theory [41] has been widely utilized in metaheuristic algorithms to change their random parameters. Ten chaotic maps have been employed to enhance many optimization algorithms, and better results have been achieved [42]. The application of chaos in GA has been introduced in [43] and improved chaotic PSO proposed in [44]. Besides, the chaos theory has been used in the new optimization algorithms such as chaotic antlion optimization (CALO) [45], CWOA [46], CGWO [47], chaotic biogeography-based optimization (CBBO) [48], and recently in chaotic sine cosine algorithm (CSCA) [49] and CHHO [50].

Also, opposition based learning (OBL) [51] has been handled to improve metaheuristic optimization algorithms where the improvement can be accomplished using both the candidate solutions and their opposites at the same time, and then the best one will be applied for the next process. Some of the applications of OBL are in quasi-oppositional TLBO (QOTLBO) [52, 53], Quasi-oppositional swine influenza model-based optimization with quarantine (QOSIMBO-Q)[54], and oppositional Jaya algorithm [55].

Moreover, a multi-population algorithm has been proposed and applied to metaheuristic algorithms. The economic dispatch problem has been solved using a multi-population Jaya algorithm in [56], in [57], a multi-population genetic algorithm has been presented to control the adjustable hydraulic torque converter.

### 1.2.2- Application of optimization algorithms in DG allocation

The problem of the DG allocation was tackled based on single and multi-objective optimization problems. One objective function has been applied in order to optimize the single-objective optimization-based problem and thus the main objective function in this form has been considered to minimize power losses. On the other hand, in multi-objective optimization problems, more than one objective function can be simultaneously optimized.

Numerous optimization algorithms have been used in the literature to identify the best location and size of the DGs unit of both transmission and distribution networks. [58, 59]. In the power system, three optimization algorithms were implemented; analytical algorithm, heuristic algorithm, and a hybrid between the analytical and heuristic algorithms [60].

A mathematical formulation for the power system is thoroughly articulated in analytical algorithms to investigate the influence of the injected DG power on the performance of the power system, as provided in the improved analytical (IA) and exhaustive load flow (ELF) optimization algorithms [61]. In addition, several indices were determined with differential equations [62]. However, some of the analytical algorithms are not suitable to find the optimal size and location of multiple DGs due to their dependency on the topology of the system[63].

As a result, several researchers switched to metaheuristic-based optimization algorithms. The key feature of using metaheuristic algorithms is their ability to solve optimization problems without getting too deep into the complexity of the problem. Metaheuristic optimization algorithms have also been commonly used in the DG allocation for both single-and multi-objective problems.

A genetic algorithm (GA), which optimizes the DG in the distribution system, has been used to minimize the total power consumption for the single objective problem. [64]. In order to minimize the active power loss, the optimization of the Particle Swarm (PSO) has been implemented for the DG allocation including various load models. [60, 65]. Optimization algorithms based on artificial intelligence have been used to evaluate the optimum location for multiple DGs in [61, 66]. An algorithm for fuzzy and clonal selection has been developed for DG allocation in [67]. Recently, a variety of nature-inspired optimization algorithms were used in the DG allocation problem such as backtracking optimization algorithm (BSOA) [68], bacterial foraging optimization algorithm (BFOA) [69], stud krill herd algorithm (SKHA) [70], whale optimization algorithm (WOA) [71], and chaotic sine cosine (CSCA) [72].

On the other hand, based on two methodologies, the multi-objective optimization problem has been used to deal with the allocation of DGs. A weighting total for individual target functions was used in the first one. Based on this approach, several research papers have been introduced to optimize three objective functions, namely power loss, voltage

deviation (VD), and voltage stability index (VSI), for example, GA [73], PSO [73], GA/PSO [73], teaching-learning based optimization (TLBO), its quasi-oppositional version (QOTLBO) [74], swine influenza model-based optimization with quarantine SIMBO-Q, its quasi-oppositional QOSIMBO-Q [54], and imperialist competitive algorithm and genetic algorithm (ICA/GA) [75]. However, this approach faces some of the difficulties raised in the selection of the weighting element. The second multi-objective approach utilizes a trade-off focused on the Pareto dominance principle among the objective functions. The obtained solutions are graded in Pareto dominance into dominated and non-dominated solutions. Then the decision-maker should choose the best solution from the non-dominated solutions. [59].

Different algorithms have been devised based on this approach, such as Pareto Archived Evolution Strategy (PAES), Non-Dominated Genetic Sorting Algorithm (NSGA-II), Strength Pareto Evolutionary Algorithm (SPEA), Enhanced Edition SPEAII, and Multi-Objective Particle Optimization (MOPSO) [76]. In the case of the DG allocation problem, MOPSO has been introduced with fuzzy decision-making in order to reduce power loss and VD [77]. Multi-objective whale optimization (MOWOA) was introduced to optimize the VSI and reduce VD and active power loss. [78]. In [79], a multi-objective bat shuffled algorithm has been suggested to analyze the effect of DGs with various load models. The Taguchi method (TM) and the multi-objective Taguchi technique (MOTA) were used to optimally incorporate the DG unit into the distribution networks. [80].

## 1.3.- Problem Statement

Many research works focused on sizing the DG units at the peak load demand however, many factors have been ignored in the previous research works, namely when dealing with DG units utilize green energies such as wind and photovoltaic energy (PV). In this regard, the availability of the primary energy resource conditions and the load time-varying have been ignored. Thus, power loss and voltage problems became an issue in case of low or high DG power penetration and light or heavy load demand. Only Some research works explored the time variance of the load demand and the volatility in DG power generation [81-84]. Besides, the issues of the optimization algorithms which are represented in the massive calculation (analytical algorithms) and the trapping in the local optima (metaheuristic algorithms).

# 1.4.- Thesis Objectives

The objective of this thesis is to allocate the DG into RDS using efficient optimization algorithms to gain the benefits of the DG and avoid the drawbacks. Besides, study the impact of the intermittent nature of the PV power and load variation in the RDS and find a suitable setting of the battery energy storage (BES) to mitigate the PV power generation. To achieve that, developed optimization algorithms are validated compared to other competitive algorithms then used in PV and BES settings.

In this context, the thesis objective can be summarized as follows:

- A power flow solver based on forward/backward sweep will be implemented to compute the objective functions (total power loss, VD, and VSI).
- To study the impact of the intermittent nature of the PV power and the load variation on the performance of the RDSs, an uncertainty model for PV power is formulated based on statistical data of the solar irradiance. In addition, to avoid the uncertainty of the PV power, BES is modeled to be optimally scheduled over 24 hrs.
- Three optimization algorithms are used to allocate the DG into RDS such as analytical, metaheuristic, hybrid optimization algorithms. In the analytical based algorithms, a formulation based on the power loss formula will be derived to calculate the optimal sizes of different types of DG. Besides, loss and voltage sensitivity factors will be used to determine the candidate DG location.
- Various metaheuristic optimization algorithms such as sine cosine algorithm (SCA), salp swarm algorithm (SSA), Harris hawk's optimizer (HHO), tree growth algorithm (TGA), and barnacle mating optimizer (BMO) are applied for DG allocation.
- Different multi-objective optimization algorithms are implemented based on the single-objective algorithms such as MOSCA, MSSA, and MOHHO. Where a Pareto dominance is constructed using two structures called archive and leader selection. Additionally, two decisions making named fuzzy and grey relation analysis are proposed to find the best compromise solution.

- To enhance the optimization algorithms, improved versions of the original single- and multi-objective optimization algorithms are proposed. Several improved methods are applied based on chaos theory, quasi oppositional theory, and hybridization method.
- Various RDSs are used to check the performance of the improved algorithms. These systems are divided into standard systems such as IEEE and practical (Portuguese) RDSs. The numerical results section and compared to the other competitive algorithms.
- Finally, integration of the PV+BES into RDSs using the improved optimization algorithms leads to significant enhancements in the energy reduction and voltage profile.

## 1.5.- Thesis Layout

The thesis is organized into several chapters. A brief explanation about the content and purpose of each chapter is provided below while the.

- Chapter 2 – Formulation of DG Allocation problem: this chapter presents the mathematical formulation of the DG problem besides the uncertainty model of the PV power generation.
- Chapter 3 - Analytical Optimization Algorithm for DG Allocation: this chapter presents some analytical algorithms used to find the proper location and sizes of DG.
- Chapter 4 - Metaheuristic Optimization Algorithms for DG Allocation: this chapter gives brief overviews of the metaheuristic optimization algorithms and includes the nature of inspiration for each algorithm with their pseudocode.
- Chapter 5 - Multi-objective Optimization Algorithms and Decision Making: in this chapter, several multi-objective optimization algorithms and decision-making theories are presented.
- Chapter 6 - Improved Optimization Algorithms for DG Allocation: in this chapter, various improved methods are introduced and employed for

enhancing the metaheuristic algorithms to optimally allocate the DG into RDS.

- Chapter 7 - Numerical results: various numerical results on standard and practical RDS in order to show the performance of the improved algorithms.
- Chapter 8 - Conclusions and Future works: the main conclusions and potential future lines are suitably drawn in this chapter.

# Chapter 2

# Formulation of DG Allocation Problem

## 2.1.- Introduction

This chapter presents a mathematical formulation of the DG allocation problem. The forward/ backward load flow method is used to find the main objective functions. The uncertainty model is introduced to represent the intermittent nature of the PV power generation. Additionally, to convert the non-dispatchable PV power to dispatchable, BES is modeled and integrated with the PV system.

## 2.2.- Forward/Backward Power Flow Method

The use of DGs in RDSs has an inappropriate effect on the performance of the system. Using power flow analysis, these impacts are fully observed. To solve the power flow problem in power systems, many approaches have been implemented. The most powerful power flow method used in the RDS is called forward/backward load flow. The

Forward/backward power flow approach is mainly based on the voltage and current laws of Kirchhoff. For the RDS, the basic equivalent circuit is shown in Fig. 2.1. For this system, the forward/backward power flow algorithm can be accomplished by adding the steps below. [6]:

**Step 1:** Based on the active and reactive powers and the initial bus voltage, determine the load currents in the phasor format for each bus *i* as:

$$\overline{I_i} = \left(\frac{\overline{S_i}}{\overline{V_i}}\right)^* \tag{2.1}$$

Where, $\overline{I_i}$, $\overline{V_i}$, and $\overline{S_i}$are current, voltage, and apparent power respectively at bus *i*.

**Step 2** (backward step): Determine the cumulative branch current, $I_z$ From sub-lines $p$, to bus # 1, as demonstrated in (2.2).

$$\overline{I_z} = \overline{I_k} + \sum_{p \in M} \overline{I_p} \tag{2.2}$$

**Step 3:** (forward Step): Upgrade the voltage of the buses from the main no. 1 bus feeder to the final bus. :

$$\overline{V_k} = \overline{V_i} - (R_{ik} + jX_{ik})\overline{I_z} \tag{2.3}$$

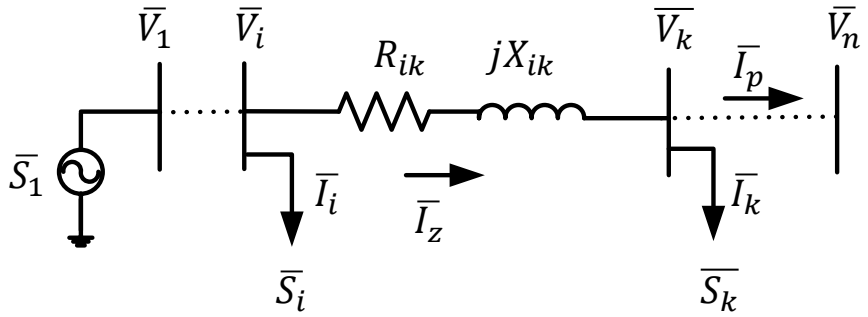


*Fig. 2.1.- Equivalent circuit for RDS*

## 2.3.- Objective Functions

Numerous objective functions are often used to optimally incorporate DG into the RDSs, and the following three major objective functions are considered in this work:

### 2.3.1- Total power loss:

The key goal of the optimum allocation of DGs to the RDSs is to minimize the overall loss of power $P_{loss}$:

$$f_1 = min\ (P_{loss}\ ) \tag{2.4}$$

where the power loss in each branch is calculated as:

$$P_{loss\_z} = R_{ik}|I_z|^2 \tag{2.5}$$

where, $|I_z|$ is the magnitude value of the branch current.

The cumulative power losses in the RDS can be determined by summing up the power losses of all the $n\_br$ branch of the system as follows.:

$$P_{loss} = \sum_{z=1}^{n\_br} P_{loss\_z} \tag{2.6}$$

### 2.3.2- Total voltage deviation (VD)

The overall voltage deviation $VD$ shows the RDS voltage level and how far from the defined value, $V_{sep}$. Based on a given voltage, $V_{sep}$, the total $VD$ for the distribution system can be determined using the voltage at bus $i$:

In literature, many formulas have been used for the VD. However, in this thesis two formulas are used as follows:

$$VD = \sum_{i=1}^{n\_bus} \left(V_{sep} - V_i\right)^2 \tag{2.7}$$

Or,

$$VD = \sum_{i=1}^{n\_bus} \left(\frac{V_i - V_{sep}}{V_{max} - V_{min}}\right)^2 \tag{2.8}$$

where, $V_{sep}$ is taken 1.00 p.u, $V_{max}$ and $V_{min}$ are the maximum and the minimum limits of the RDS, respectively. Therefore, the second objective function is:

$$f_2 = \min\ (VD) \tag{2.9}$$

### 2.3.3- Voltage stability index (VSI)

Voltage stability is known to be one of the most important indices used to signify the intensity of the system to withstand irregular conditions. Hence, optimizing the minimum VSI is necessary. For each $ik$ branch, the voltage stability index (VSI) can be defined as follows:

$$VSI_{ik} = V_i^4 - 4\left(P_k R_{ik} + Q_j X_{ik}\right)V_i^2 - 4(P_k X_{ik} - Q_k R_{ik}) \tag{2.10}$$

$$f_3 = max\ (min(VSI_{ik})) \tag{2.11}$$

## 2.4.- Modeling of PV Power Generation

The stochastic behavior of PV can be modeled using probability distribution functions (PDF) [81]. The historical data obtained on time for solar irradiance was used to produce a standard day's frequency distribution of irradiance. Beta PDF is used to implement PV power generation as follows:

### 2.4.1- Solar irradiance model

Beta PDF reflects the probability nature of solar radiance, $s^t(\mathrm{kW/m^2})$, at any hour of the average day as follows:

$$f_b(s^t) = \begin{cases} \dfrac{\boldsymbol{\Gamma}(\alpha^t + \beta^t)}{\boldsymbol{\Gamma}\alpha^t + \boldsymbol{\Gamma}\beta^t}\ (s^t)^{\alpha^t - 1}(1 - s^t)^{\beta^t - 1} & \\ \qquad\qquad\qquad\qquad 0 \le s^t \le 1, & \\ \qquad\qquad\qquad\qquad \alpha^t, \beta^t > 0 & \\ 0, \qquad\qquad\qquad otherwise & \end{cases} \tag{2.12}$$

where, $\alpha^t$ and $\beta^t$ are the Beta PDF parameters which can be calculated using the mean $\mu_s^t$ and the standard deviation $\sigma_s^t$ of the solar irradiance $s$ at time $t$ as:

$$\beta^t = (1 - \mu_s^t)\left(\frac{(1 + \mu_s^t)\mu_s^t}{(\sigma_s^t)^2}\right) \tag{2.13}$$

$$\alpha^t = \frac{\mu_s^t * \beta^t}{(1 - \mu_s^t)} \tag{2.14}$$

### 2.4.2- PV Power Generation

To determine the PV output power, the continuous PDF for a specific time hour $t$ is separated into several states. Power generation of PV array is produced by the probability

of all possible states for that hour. The hourly average output power $P_{PV}^{t}$ array corresponds to a specific time segment $t$ can be calculated as follows:

$$P_{PV}^{t} = \sum_{i=1}^{n_s} P_o(s_i^t) f_b(s_i^t) \tag{2.15}$$

where, $P_o(s^t)$ is the output power of the PV module and it is expressed as [81]:

$$P_o(s^t) = N_m * V_c * I_c \left(\frac{V_{MPP} * I_{MPP}}{V_o * I_s}\right) \tag{2.16}$$

where, $N_m$ is the number of PV modules, $V_{MPP}$ and $I_{MPP}$ the voltage and current at maximum power point respectively, $V_o$ is the open-circuit voltage and $I_s$ is the short circuit current, and $V_c$, $I_c$ are the cell voltage and current respectively and they can be calculated using the following equations:

$$V_c = V_o - K_v * T_c \tag{2.17}$$

$$I_c = s^t(I_s + K_i(T_c - 25)) \tag{2.18}$$

where, $K_v$ , $K_i$ are the voltage and current temperature coefficient (V/ºC), (A/ºC) respectively,$T_c$ is the cell temperature ºC and it can be determined using the ambient temperature $T_A$ and the nominal operating temperature $T_0$ as:

$$T_c = T_A + s^t \left(\frac{T_0 - 20}{0.8}\right) \tag{2.19}$$

In this work, the solar irradiance data given in [83] for $\mu_s^t$ and $\sigma_s^t$ during three years and the PV module parameters are adopted to represent the Beta PDF of the solar irradiance as shown in Fig. 2.2. a. It is clear that the mean and standard deviation (SD) of the solar irradiance is weather and time-dependent which starts from 06:00 to 19:00. For this period, 20 states of solar irradiance with step 0.05 (kW/m2) are considered for each hour, and the expected PV powers are calculated as shown in Fig. 2.2.b. Finally, the typical day for the three years is generated in p.u as shown in Fig. 2.2.c.

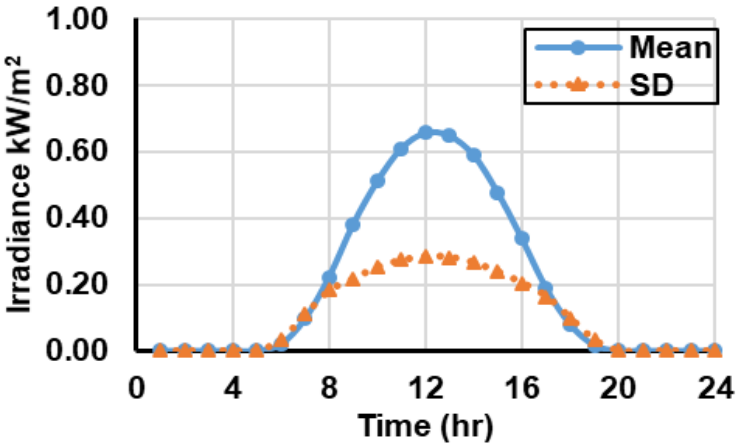


*a. Mean and standard deviation of solar irradiance*

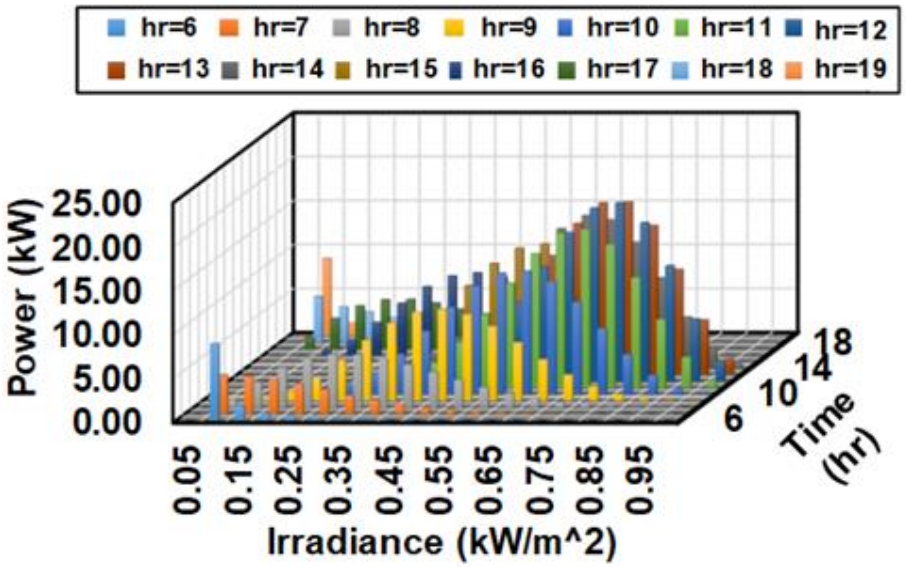


*b. Expected PV power*

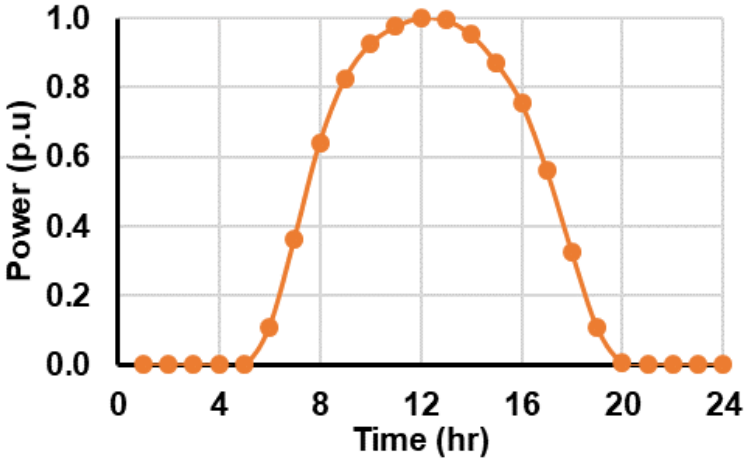


*c. Normalized expected PV output power*

*Fig. 2.2.- PV power generation stochastic modeling*

## 2.5.- Modeling of Battery Energy Storage (BES)

As mentioned, BES plays an important role in the integration of the PV system to convert it to a dispatchable energy source. In this regard, the BES unit can work as a charging load or a discharging generator. Hence, The BES charging/discharging energy $E^t_{BES_i}$ at bus $i$ in period $t$ can be expressed as [85]:

$$E^t_{BES_i} = \begin{cases} E^{t-1}_{BES_i} - \dfrac{(P^t_{BES_i})_d}{\eta_d}\,\Delta t, & P^t_{BES_i} > 0 \\ E^{t-1}_{BES_i} - \eta_c * (P^t_{BES_i})_c * \Delta t, & P^t_{BES_i} \le 0 \end{cases} \tag{2.20}$$

where,$(P^t_{BES_k})_c$ and $(P^t_{BES_k})_d$ are the charge and discharge power of the BES, respectively; $\eta_c$ and $\eta_d$ are efficiencies of the charge and discharge, $\Delta t$ is the sampling time. However, the$E^t_{BES_i}$ must satisfy the minimum $E^{min}_{BES_i}$and maximum $E^{max}_{BES_i}$ energy limits of the BES unit as follows:

$$E^{min}_{BES_i} \le E^t_{BES_i} \le E^{max}_{BES_i} \tag{2.21}$$

In this work, the $E^{min}_{BES_i}$and $E^{max}_{BES_i}$ limits are taken to be 20% and 90% of the connected size of the BES unit, respectively.

## 2.6.- Modeling of PV and BES power

Distinct to the non-dispatchable PV integration, the hourly PV+BES power can be dispatched over the day using the charging/discharging BES power as shown in Fig. 2.3, hence the daily charging $(E_{BES_i})_c$ and discharging $(E_{BES_i})_d$ energies at bus $i$ are obtained as:

$$(E_{BES_i})_c = \sum_{t=1}^{24} (P^t_{BES_i})_c * \Delta t \tag{2.22}$$

Therefore, the total output energies $E_{(PV+BES)_i}$ of the PV+BES and $E_{PV_i}$ of the PV generation unit at bus $i$ in case of BES discharging and charging is calculated respectively as:

$$E_{(PV+BES)_i} = (E_{BES_i})_d + (E_{PV_i})_G \tag{2.23}$$

$$E_{PV_i} = (E_{BES_i})_c + (E_{PV_i})_G \tag{2.24}$$

where $(E_{PV_i})_G$ is the quantity of PV energy transporting to the grid at bus $i$. The charging and discharging energies of the BES unit at bus $k$ with a roundtrip efficiency ($\eta_B = \eta_d * \eta_c$ ) is expressed as:

$$(E_{BES_i})_d = \eta_B (E_{BES_i})_c \tag{2.25}$$

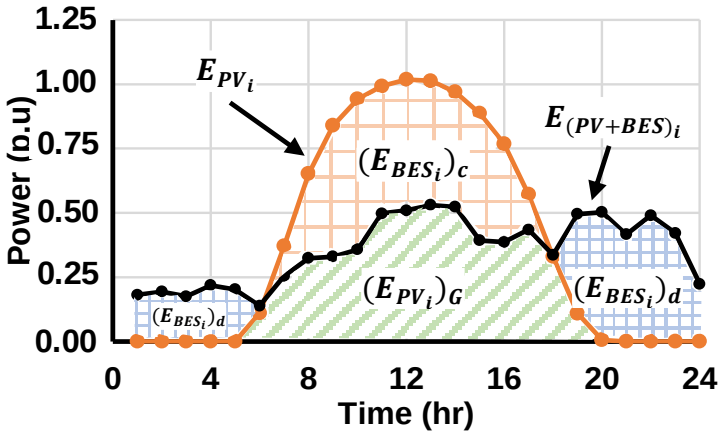


*Fig. 2.3.- PV+BES output power generation per unit.*

Using (20) to (22), the $E_{PV_i}$ of the PV generation unit can be calculated as:

$$E_{PV_i} = \frac{E_{(PV+BES)_i} - (1-\eta_B)(E_{PV_i})_G}{\eta_B} \tag{2.26}$$

To find the maximum PV unit output power at bus $i$, a capacity factor for the module unit $C_{PV}^U$ can be used as follows:

$$P_{PV_i} = C_{PV}^U E_{PV_i} \tag{2.27}$$

where,

$$C_{PV}^U = \frac{P_{PV}^U}{E_{PV}^U} \tag{2.28}$$

$P_{PV}^U$ is the maximum output of a PV module unit, and $E_{PV}^U$ is the amount of PV generated energy over a 24-hr day. Based on the normalized values shown in Fig. 2.2. The capacity factor is $C_{PV}^U$ =0.1063.

Consequently, the $P_{PV_i}$ can be calculated using the following equation:

$$P_{PV_i} = C_{PV}^U \left( \frac{E_{(PV+BES)_i} - (1-\eta_B)(E_{PV_i})_G}{\eta_B} \right) \tag{2.29}$$

# Chapter 3

# Analytical Optimization Algorithm for DG Allocation

## 3.1.- Introduction

This chapter presents the analytical algorithm that has been developed to allocate the DG into RDS. The main advantage of the analytical algorithm is represented in its accuracy in finding the optimal sizes. However, it is very time-consuming and exhausted in the calculation.

## 3.2.- Analytical Algorithm

A mathematical formulation for the power system is thoroughly expressed in an analytical algorithm to analyze the effect of the injected DG power on the overall performance of the power system. The analytical algorithm can be derived based on the exact power loss formula as $P_{loss}$ [63] :

$$P_{loss} = \sum_{i=1}^{N_{bus}} \sum_{k=1}^{N_{bus}} [\alpha_{ik}(P_i P_k + Q_i Q_k) + \beta_{ik}(Q_i P_k - P_i Q_k)] \quad (3.1)$$

where, $P_i$ , $Q_i$ are the active and reactive power at bus $i$, $N_{bus}$ is the total bus number, and $\alpha_{ik}$ , $\beta_{ik}$ can be calculated using the voltage magnitude $V$ and phase angle $\theta$ at bus $i, k$ as follows:

$$\alpha_{ik} = \frac{r_{ik}}{V_i V_k} cos\ (\theta_i - \theta_k)$$
$$\beta_{ik} = \frac{r_{ik}}{V_i V_k} \sin\ (\theta_i - \theta_k) \quad (3.2)$$

$r_{ik}$ is the real part element in $Z_{bus_{ik}}$ matrix where, $Z_{bus_{ik}}$ can be formulated using:

$$Z_{bus_{ik}} = [BIBC]^T [Z_{ik}][BIBC] \quad (3.3)$$

where, $Z_{ik} = R_{ik} + jX_{ik}$ the primitive impedance in a diagonal matrix.

Groups of DGs are categorized based on their injected power, where Type I DGs can only inject active power, Type II can only inject reactive power, Type III injects active and reactive powers, and Type IV injects active but absorbs reactive power. The first three forms are included in this work.

The consequences of the active and reactive power injected by the DGs are formulated as:

$$P_i = PG_i - PD_i$$
$$Q_i = QG_i - QD_i \quad (3.4)$$

$PD_i$ , $QD_i$ are the demand active and reactive power at bus $i$, and $PG_i$ , $QG_i$ are the generated active and reactive power.

Assume there are $n$ numbers for DG type I and their location are $a_1, a_2, \dots a_n$ hence the generated active power at these buses are $PG_{a_1}, PG_{a_2}, PG_{a_n}$. and the injected active powers are:

$$P_{a_1} = PG_{a_1} - PD_{a_1}\ , P_{a_2} = PG_{a_2} - PD_{a_2}, \dots P_{a_{nDG_{\mathrm{I}}}} = PG_{a_n} - PD_{a_n}$$

Also, $m$ numbers for DG type II and their location are $b_1, b_2, \dots b_m$ hence the generated reactive power at these buses are $QG_{b_1}, QG_{b_2}, QG_m$. And the injected reactive powers are:

$$Q_{b_1} = QG_{b_1} - QD_{b_1}, Q_{b_2} = QG_{b_2} - QD_{b_2}, \ldots Q_{b_{nDG_{\mathrm{II}}}} = QG_{b_m} - QD_{b_m}$$

The first derivative of the exact power loss formula for the injected active or reactive powers should be equal to zero to detect the minimal power loss with the integration DGs. For the DG type I, then:

$$\frac{\partial P_{loss}}{\partial P_{a_1}} = 0 \tag{3.5}$$

$$\frac{\partial P_{loss}}{\partial P_{a_1}} = 2\sum_{k=1}^{N_{bus}} \left[\alpha_{a_1 k} P_k - \beta_{a_1 k} Q_k\right] = 0$$

.

.

$$\frac{\partial P_{loss}}{\partial P_{a_n}} = 2\sum_{k=1}^{N_{bus}} \left[\alpha_{a_n k} P_k - \beta_{a_n k} Q_k\right] = 0 \tag{3.6}$$

Similarly, for DG type II $\frac{\partial P_{loss}}{\partial Q_{b_m}} = 0$

$$\frac{\partial P_{loss}}{\partial Q_{b_1}} = 2\sum_{k=1}^{N_{bus}} \left[\alpha_{b_1 k} Q_k + \beta_{b_1 k} P_k\right] = 0$$

.

.

$$\frac{\partial P_{loss}}{\partial Q_{b_m}} = 2\sum_{k=1}^{N_{bus}} \left[\alpha_{b_m k} Q_k + \beta_{b_m k} P_k\right] = 0 \tag{3.7}$$

However, if the distribution system includes a mixture of $n$ DG type I and $m$ DG type II, the latter equation can be rewritten by different DG bus positions $a_1, a_2, \ldots a_n$ and $b_1, b_2, \ldots b_m$ from the summation as follow:

$$\alpha_{a_1 a_1} P_{a_1} + \alpha_{a_1 a_2} P_{a_2} \ldots + \alpha_{a_1 a_n} P_{a_n} - \beta_{a_1 b_1} Q_{b_1} - \beta_{a_1 b_2} Q_{b_2} \ldots - \beta_{a_1 b_m} Q_{b_m} = -\sum_{\substack{k \neq a_1, a_2 \ldots a_n \\ k \neq b_1, b_2 \ldots b_m}}^{N_{bus}} \left[\alpha_{a_1 k} P_k - \beta_{a_1 k} Q_k\right] \tag{3.8}$$

$$\alpha_{a_n a_1} P_{a_1} + \alpha_{a_n a_2} P_{a_2} \ldots + \alpha_{a_n a_n} P_{a_n} - \beta_{a_n b_1} Q_{b_1} - \beta_{a_n b_2} Q_{b_2} \ldots - \beta_{a_n b_m} Q_{b_m} = - \sum_{\substack{k \neq a_1, a_2 \ldots . a_n \\ k \neq b_1, b_2 \ldots . b_m}}^{N_{bus}} \left[ \alpha_{a_n k} P_k - \beta_{a_n k} Q_k \right] \tag{3.9}$$

$$\beta_{b_1 a_1} P_{a_1} + \beta_{b_1 a_2} P_{a_2} \ldots \ldots + \beta_{b_1 a_n} P_{a_n} + \alpha_{b_1 b_1} Q_{b_1} + \alpha_{b_1 b_2} Q_{b_2} \ldots \ldots + \alpha_{b_1 b_m} Q_{b_m} = - \sum_{\substack{k \neq a_1, a_2 \ldots . a_n \\ k \neq b_1, b_2 \ldots . b_m}}^{N_{bus}} \left[ \alpha_{b_1 k} Q_k + \beta_{b_1 k} P_k \right] \tag{3.10}$$

$$\beta_{b_m a_1} P_{a_1} + \beta_{b_m a_2} P_{a_2} \ldots \ldots + \beta_{b_m a_n} P_{a_n} + \alpha_{b_m b_1} Q_{b_1} + \alpha_{b_m b_2} Q_{b_2} \ldots \ldots + \alpha_{b_m b_m} Q_{b_m} = - \sum_{\substack{k \neq a_1, a_2 \ldots . a_n \\ k \neq b_1, b_2 \ldots . b_m}}^{N_{bus}} \left[ \alpha_{b_m k} Q_k + \beta_{b_m k} P_k \right] \tag{3.11}$$

The general formula for the above equations can be expressed as follows when the two types of DG are presented:

$$\begin{bmatrix} \alpha_{a_1 a_1} & \alpha_{a_1 a_2} & \cdots & \alpha_{a_1 a_n} & -\beta_{a_1 b_1} & -\beta_{a_1 b_2} & \cdots & -\beta_{a_1 b_m} \\ \alpha_{a_2 a_1} & \alpha_{a_2 a_1} & & \alpha_{a_2 a_n} & -\beta_{a_2 b_1} & -\beta_{a_2 b_2} & & \beta_{a_1 b_m} \\ \vdots & & \ddots & \vdots & \vdots & & \ddots & \vdots \\ \alpha_{a_n a_1} & \alpha_{a_n a_2} & \cdots & \alpha_{a_n a_n} & -\beta_{a_n b_1} & -\beta_{a_n b_2} & \cdots & -\beta_{a_n b_m} \\ \beta_{b_1 a_1} & \beta_{b_1 a_2} & \cdots & \beta_{b_1 a_n} & \alpha_{b_1 b_1} & \alpha_{b_1 b_2} & \cdots & \alpha_{b_1 b_m} \\ \beta_{b_2 a_1} & \beta_{b_2 a_2} & & \beta_{b_2 a_n} & \alpha_{b_2 b_1} & \alpha_{b_2 b_2} & & \alpha_{b_2 b_m} \\ \vdots & & \ddots & \vdots & \vdots & & \ddots & \vdots \\ \beta_{b_m a_1} & \beta_{b_m a_2} & \cdots & \beta_{b_m a_n} & \alpha_{b_m b_1} & \alpha_{b_m b_2} & \cdots & \alpha_{b_m b_m} \end{bmatrix} \begin{bmatrix} P_{a_1} \\ P_{a_2} \\ \vdots \\ P_{a_n} \\ \ldots \\ Q_{b_1} \\ Q_{b_2} \\ \vdots \\ Q_{b_m} \end{bmatrix} = - \begin{bmatrix} C_{a_1} \\ C_{a_2} \\ \vdots \\ C_{a_n} \\ \ldots \\ E_{b_1} \\ E_{b_2} \\ \vdots \\ E_{b_m} \end{bmatrix} \tag{3.12}$$

where, $C_{a_i}$ and $E_{b_i}$ are calculated using:

$$C_{a_i} = \sum_{\substack{k \neq a_1, a_2 \ldots a_n \\ k \neq b_1, b_2 \ldots b_m}}^{N_{bus}} \left[\alpha_{a_i k} P_k - \beta_{a_i k} Q_k\right] \qquad i = 1,2, \ldots n \tag{3.13}$$

$$E_{b_i} = \sum_{\substack{k \neq a_1, a_2 \ldots a_n \\ k \neq b_1, b_2 \ldots b_m}}^{N_{bus}} \left[\alpha_{b_i k} Q_k + \beta_{b_i k} P_k\right] \qquad i = 1,2, \ldots m \tag{3.14}$$

For simplicity Eq (3.12) can be expressed as:

$$\begin{bmatrix} [H_{11}]_{n\times n} & [H_{12}]_{n\times m} \\ [H_{21}]_{m\times n} & [H_{22}]_{m\times m} \end{bmatrix} \begin{bmatrix} [P_{a_i}]_{n\times 1} \\ [Q_{b_i}]_{m\times 1} \end{bmatrix} = \begin{bmatrix} [C_{a_i}]_{n\times 1} \\ [E_{b_i}]_{m\times 1} \end{bmatrix} \tag{3.15}$$

Consequently, $[P_{a_i}]_{n\times 1}$ and $[Q_{b_i}]_{m\times 1}$ are calculated using the inverse matrix:

$$\begin{bmatrix} [P_{a_i}]_{n\times 1} \\ [Q_{b_i}]_{m\times 1} \end{bmatrix} = \begin{bmatrix} [H_{11}]_{n\times n} & [H_{12}]_{n\times m} \\ [H_{21}]_{m\times n} & [H_{22}]_{m\times m} \end{bmatrix}^{-1} \begin{bmatrix} [C_{a_i}]_{n\times 1} \\ [E_{b_i}]_{m\times 1} \end{bmatrix} \tag{3.16}$$

Let $H^{inv} = H^{-1}$

$$\begin{bmatrix} [{H_{11}}^{inv}]_{n\times n} & [{H_{12}}^{inv}]_{n\times m} \\ [{H_{21}}^{inv}]_{m\times n} & [{H_{22}}^{inv}]_{m\times m} \end{bmatrix} = \begin{bmatrix} [H_{11}]_{n\times n} & [H_{12}]_{n\times m} \\ [H_{21}]_{m\times n} & [H_{22}]_{m\times m} \end{bmatrix}^{-1} \tag{3.17}$$

Then,

$$[P_{a_i}]_{n\times 1} = [{H_{11}}^{inv}]_{n\times n} [C_{a_i}]_{n\times 1} + [{H_{12}}^{inv}]_{n\times m} [E_{b_i}]_{m\times 1} \tag{3.18}$$

$$[Q_{b_i}]_{m\times 1} = [{H_{21}}^{inv}]_{m\times n} [C_{a_i}]_{n\times 1} + [{H_{22}}^{inv}]_{m\times m} [E_{b_i}]_{m\times 1} \tag{3.19}$$

The final DGs active and reactive power at bus $i$ can be calculated as:

$$[PG_{a_i}]_{n\times 1} = [P_{a_i}]_{n\times 1} + [PD_{a_i}]_{n\times 1} \tag{3.20}$$

$$[QG_{b_i}]_{m\times 1} = [Q_{b_i}]_{m\times 1} + [QD_{b_i}]_{m\times 1} \tag{3.21}$$

For DG type III, the injected active and reactive power can be calculated using (3.20) and (3.21) where $a = b$ and $n = m$.

# Chapter 4

# Metaheuristic Optimization Algorithms for DG Allocation

## 4.1.- Introduction

The powerful of meta-heuristic optimizations are coming from their simplicity of the implementation. Besides, they are more efficient in dealing with many optimization problems. However, based on the theorem of optimization called no-free-lunch [40], which rises that no optimization algorithm able to deal with all optimization problems and achieve the best results so far. This chapter exhibits various single metaheuristic optimization algorithms based on the different nature of inspiration.

## 4.2.- Single Objective Algorithms

This section presents different optimization algorithms that are used to the optimal allocation of DG in RDS for minimization of the power loss as a single objective problem.

### 4.2.1- Sine Cosine Algorithm (SCA)

SCA is set in a modern metaheuristic algorithm that has been introduced [86]. The main idea behind this algorithm is to use the sine and cosine functions to find the optimal global solution.

Several individual solutions are randomly distributed in the SCA and then the fitness function is determined for each solution. The update equation for the incoming solutions can then be determined as follows:

$$X_i^{k+1} = X_i^k + r_1 \sin(r_2)\left|r_3 D_i^k - X_i^k\right| \tag{4.1}$$

$$X_i^{k+1} = X_i^k + r_1 \cos(r_2)\left|r_3 D_i^k - X_i^k\right| \tag{4.2}$$

where, $X_i^k$ is the current position of $i$ dimension at $k^{th}$ iteration and $r_1, r_2,$ and $r_3$ are random values, $D_i^k$ is the goal position.

As seen in Fig. 4.1.a, the circular attribute of the sine and cosine functions allows the individual solutions the ability to update their locations in the circumference of another solution. The exploitation process can be easily achieved in this manner. On the other hand, the region of the search space can be chosen in the exploration process to formulate the boundary of the functions of the sinus and cosine to travel in the direction of the local optima or step out as seen in Fig. 4.1.b.

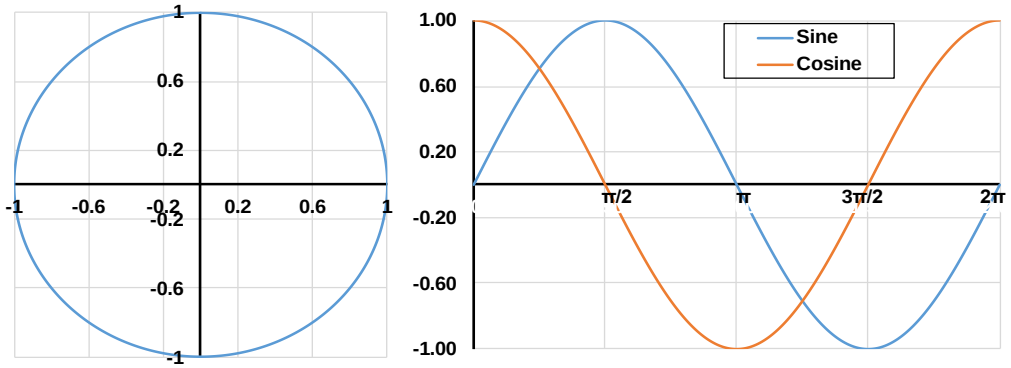


*a. Sine cosine functions*

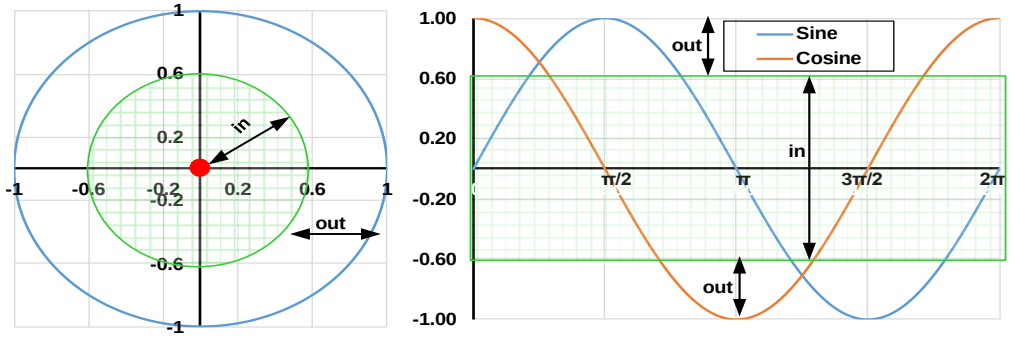


*b. Sine cosine with a search space area*

*Fig. 4.1.- Sine cosine circular characteristics*

It is possible to merge equations (4.1) and (4.2) to determine the modified location in one equation where the transition between the function of sine and cosine is done by a new parameter, $r_4$ It has a random value of [0,1]. As has been proposed in [86]:

$$X_i^{k+1} = \begin{cases} X_i^k + r_1 \sin(r_2) \left| r_3 D_i^k - X_i^k \right|, & r_4 < 0.5 \\ X_i^k + r_1 \cos(r_2) \left| r_3 D_i^k - X_i^k \right|, & r_4 \geq 0.5 \end{cases} \tag{4.3}$$

The purpose of the parameters $r_1, r_2,$ $r_3$ and $r_4$ is to preserve search inside the search area, $r_1$ guides to the next place area. In order to maintain a balance between exploration and exploitation, $r_1$ can be estimated using the following equation as described in [86]:

$$r_1 = c - k \frac{c}{K_{max}} \tag{4.4}$$

where, $K_{max}$ is the maximum iteration number, and $c$ is constant. To demonstrate the function of r-1 SCA, Fig. 4.2 indicates an example of the variance of the updated value at c=1, $K_{max}$=10. The figure indicates that the location comes near the destination point, while the full maximum value is reached by the number of iterations.

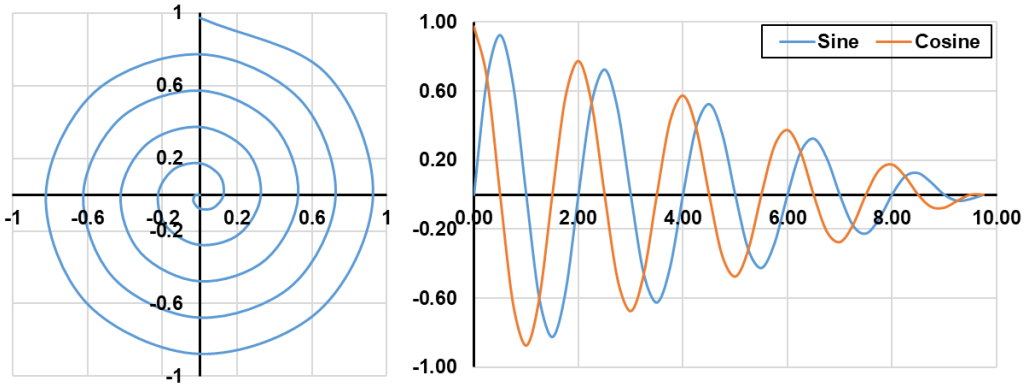


*Fig. 4.2.- Effect of $r_1$ on the sine cosine functions at c=1, $K_{max}$=10*

Moreover, the parameter $r_2$ is modified to change the individual positions toward or outward to or from the destination as previously explained in Fig. 4.1. The value of $r_2$ varies between $[0, 2\pi]$. Finally, $r_3$ is an arbitrary weighting parameter that gives a more significant designation value if $r_3 \leq 1$ or unconcern $r_3 > 1$ .

In principle, the SCA's terminology is presented as provided in Algorithm 4.1:

**Algorithm 4.1:** SCA formulation

1: **Initialize** a set of random search agents $X_i = (X_1, X_2, \dots, X_n,)$
within the limits $X^L \leq X_i \leq X^U$.
2: **Calculate** the objective function for each search agent.
3: **Store** the best solution as a destination point $D = X^*$
4: **while** ($k < K_{max}$)
5: **for** each search agents $X_i$
6: **Update** the parameters $r_1$ using (4.4)
7: $r_2 = 2\pi * \underline{rand1}$
8: $r_3 = 2 * \underline{rand2}$
9: $r_4 = \underline{rand3}$
10: **if** $r_4 < 0.5$
11: Update the agents position using sine function (4.1)
12: **else** $r_4 \geq 0.5$
13: Update the agents position using cosine function (4.2)
14: **end if**
15: **Calculate** the objective function.
16: **Update** the destination $D$ if there is a better solution.
17: $K = K + 1$
18: **end while**
19: **return** the final best solution stored $D$

## 4.2.2- Salp Swarm Algorithm (SSA)

The SSA is an algorithm based on a swarm that simulates the activity of the Salp chain in the search for food [25]. SSA's mathematical structure is broken into two populations. The first population is the leader who is positioned on the front of the chain where the rest are the followers. For the leader position solutions, the updating equation is expressed as follows:

$$X_i^1 = \begin{cases} F_i + r_1\left[r_2\left(U^i - L^i\right) + L^i\right], & r_3 < 0.5 \\ F_i - r_1\left[r_2\left(U^i - L^i\right) + L^i\right], & r_3 \geq 0.5 \end{cases} \quad (4.5)$$

where, $X_i^1$ is the current leader position of the $i$ dimension and $F_i$ is the target (food) position of the $i$ dimension $r_1, r_2,$ and $r_3$ are random values used to keep the populations

within the search space, $U^i, L^i$ are the upper and lower limits., $r_1$ is used to ensure the balance between exploration and exploitation phases as:

$$r_1 = 2e^{-\left(\frac{4k}{K_{max}}\right)^2} \tag{4.6}$$

where, $K_{max}$ is the maximum iteration number and $k$ is the current iteration, $r_2$ is adopted movement parameter and $r_3$ is a random switching parameter. The position of followers can be adopted with the iteration as follows:

$$X_i^j = \frac{1}{2}\left(X_i^j + X_i^{j-1}\right) \tag{4.7}$$

where $j \geq 2$ and $X_i^j$ gives $j$ Salp position in $i$ dimension. The formulation of the SSA is exhibited in Algorithm 4.2

**Algorithm 4.2:** SSA formulation

1: **Initialize** a set of searches Salps within the limits $X_i = (X_1, X_2, \dots, X_n,)$
within the limits $L^i \leq X_i \leq U^i$.
2: **while** ($k < K_{max}$)
3: Calculate the objective function for each search salp.
4: Store the best solution as a destination point $F = X^*$
5: Update the parameters $r_1$ using (4.6)
6: $r_2 = rand1$_and_ $r_3 = rand2$
7: for each search salp $X_i$
8: if $j == 1$
9: Update the leader position using (4.5)
10: else
11: Update the position of followers (4.7)
12: end if
13: $K = K + 1$
14: end while
19: **return** the final best solution stored $F$

## 4.2.3- Harris Hawks Optimizer (HHO)

HHO was suggested in [26] based on the Harris hawks' hunting algorithm. HHO is a population-based algorithm applied through the exploration and exploitation process. As provided in the following paragraphs, the mathematical formula can be derived:

### 4.2.3.1 Exploration phase

The main aim of the Harris hawks is to chase the rabbit prey. Therefore, firstly, the hawks explore for rabbits, there are two methods for the exploration process. The first assumes that the hawks' sites are near the members of their families and their prey. The second technique, though, hawks pinpoint on random trees. These methods are mathematically applied as follows:

$$X(t+1) = \begin{cases} X_{rand}(t) - r_1|X_{rand}(t) - 2r_2X(t)|, & q \geq 0.5 \\ (X_{rab}(t) - X_m(t)) - r_3\big(LB + r_4(UB - LB)\big), & q < 0.5 \end{cases} \quad (4.8)$$

where $X(t)$ and $X(t+1)$ are the hawk's positions at the current iteration $t$ the next iteration $t+1$ respectively, $X_{rand}(t)$ is randomly selected hawks' position, and $X_{rab}(t)$ reveals the position of the rabbit (prey). $r_1, r_2, r_3, \ and \ r_4$ are utilized as random numbers within [0,1], $LB \ and \ UB$ are the lower and upper boundaries of the search space. The two exploration schemes can be changed using a random variable $q$ that can be altered between [0,1].

$X_m(t)$ is the mean hawk's position and can be achieved as:

$$X_m(t) = \frac{1}{n}\sum_{i=1}^{n} X_i(t) \quad (4.9)$$

where, $X_i(t)$ is the $i$ hawk position, and $n$ reveals the total number of hawks.

### 4.2.3.2 Switch between exploration and exploitation

During the chase, the escape energy of rabbit $E$ was used to switch between exploration and exploitation in the HHO and can be articulated as follows. :

$$E = 2E_0\left(1 - \frac{t}{T}\right) \quad (4.10)$$

Where $T$ is the overall number of iterations, $E_0$ specifies the random initial energy of the rabbit and it is between [-1,1]. On the one side, in the case of $E \geq 1$, this suggests the ability of the rabbit to run, and that the exploration process can be pursued by the hawks.

On the other side, $E < 1$, which indicates the vulnerability of the rabbit, so that the hawks can begin to exploit near the rabbit position.

#### 4.2.3.3 Exploitation phase

Subject to the opportunity of the rabbit to escape $r$ and escape energy $E$, the exploitation process was applied in the HHO. In which place, the rabbit will escape successfully at $r < 0.5$, and unsuccessful one when $r \geq 0.5$. However, based on the escaping energy, the hawks make soft besiege when $|E| \geq 0.5$, and a hard besiege when $|E| < 0.5$.

Therefore, the exploitation of the HHO can be modelled mathematically on four chasings besieges.

*a) Soft besiege*

When $r \geq 0.5$ and $|E| \geq 0.5$, the soft besiege is carried out, which illustrates the rabbit's efforts to escape with the help of random jumps despite the softly surrounding hawks. This besiege is represented:

$$X(t+1) = \Delta X(t) - E|JX_{rab}(t) - X(t)| \tag{4.11}$$

where,

$$J = 2(1 - r_5) \tag{4.12}$$

and,

$$\Delta X(t) = X_{rab}(t) - X(t) \tag{4.13}$$

Where $\Delta X(t)$ is the distance between the rabbit location and the hawks' position, $J$ indicates the random jump of the rabbit for escaping, and $r_5$ is a random number between [0,1].

*b) Hard besiege*

The hard besiege could occur if $r \geq 0.5$ and $|E| < 0.5$.Here, the rabbit is worn out and the hawks are not circling the prey. this activity may present as:

$$X(t+1) = X_{rab}(t) - E|\Delta X(t)| \tag{4.14}$$

*c) Soft besiege with progressive rapid dives*

This besiege is seen as a tactic of intelligence that differentiates the HHO from other swarm algorithms. In the case of $r < 0.5$ and $|E| \geq 0.5$, The rabbit is allowed to escape and the haws gently surround it. A Levy flight (LF) theory has been utilized to draw up this besiege as follows:

$$Y = X_{rab}(t) - E|JX_{rab}(t) - X(t)| \tag{4.15}$$

where $Y$ signifies the soft besiege position. the LF is used to describe the hawks dive as:

$$Z = Y + S \times LF(D) \tag{4.16}$$

where $D$ is the problem dimension, $S$ is a vector of random values with size $1 \times D$. The LF is expressed as:

$$LF(x) = 0.01 \times \frac{\mu \times \sigma}{|v|^{\frac{1}{\beta}}} \tag{4.17}$$

$$\sigma = \left( \frac{\Gamma(1+\beta) \times \sin\left(\frac{\pi\beta}{2}\right)}{\Gamma\left(\frac{1+\beta}{2}\right) \times \beta \times 2^{\left(\frac{\beta-1}{2}\right)}} \right)^{\frac{1}{\beta}} \tag{4.18}$$

where $\beta$ is a constant value set to 1.5, $\mu$, and $v$ are random values between [0,1].

Hence, the hawk's position at the next iteration is obtained as:

$$X(t+1) = \begin{cases} Y, & F(Y) < F(X(t)) \\ Z, & F(Z) < F(X(t)) \end{cases} \tag{4.19}$$

*d) Hard besiege with progressive rapid dives*

In this case, $r < 0.5$ and $|E| < 0.5$, the rabbit is very tired, and It has barely been encircled by the hawks. Likewise, the Levy flight (LF) theory is used to present this besiege as in Eq (4.15) to (4.18), but $Y$ are assessed by follows:

$$Y = X_{rab}(t) - E|JX_{rab}(t) - X_m(t)| \tag{4.20}$$

The whole HHO process is presented in Algorithm 4.3

**Algorithm 4.3:** HHO formulation

1: **Initialize** a set of random search hawks $X_i = (X_1, X_2, \dots, X_n,)$
within the limits $LB \leq X_i \leq UB$.
2: **while** $(t < t_{max})$
3: **Calculate** the objective function for hawks.
4: **Store** the best solution as a rabbit location of $X_{rab}$
5: **for** each search hawks $X_i$
6: **Update** the initial energy $E_0 = 2rand() - 1$ and jump strength using (4.12)
7: **Update** the energy using (4.10)
8: **if1** $|E| \geq 1$
9: **Update** hawks' position using (4.8)
10: **elseif1** $|E| < 1$
11: **if2 (** $r \geq 0.5$ and $|E| \geq 0.5$**)**
12: **Update** hawks' position using (4.11)
13: **elseif2 (** $r \geq 0.5\ and\ |E| < 0.5$**)**
14: **Update** hawks' position using (4.14)
15: **elseif2 (** $r < 0.5\ and\ |E| \geq 0.5$**)**
16: **Update** hawks' position using (4.19)
17: **elseif2 (** $r < 0.5\ and\ |E| < 0.5$**)**
18: **Update** hawks' position using (4.20)
19: **endif2**
20: **endif1**
21: $t = t + 1$
22: **end while**
23: **return** the final best solution stored $X_{rab}$

## 4.2.4- Tree Growth Algorithm (TGA)

TGA was implemented on the basis of the actions of trees in the processing of light and food [87]. In this algorithm, mathematical formulas were modelled based on competition between trees to rise. Four classes of trees were used to model this completion and organized as best trees, competition for light, remove /replace, and reproduction. TGA has been used in problems with electrical power systems and has shown its efficacy and

viability as presented in [88]. The TGA has developed accordingly:

- **Group 1 ($G_1$):** The best trees that have received ample light and begin to fight for food only in the roots comprised this category. Since they have excellent opportunities to grow old and taller trees quicker.
- **Group 2 ($G_2$):** This category explains the light contests, where certain trees attempt to hit the light from different angles pass close to the best trees.
- **Group 3 ($G_3$):** This group called for the elimination and replacement of a group where, because of their poor condition, certain trees could be cut and substituted with new trees.
- **Group 4 ($G_4$):** The reproduction community, where the best trees have a high rate of growth and new plants are simply produced and created. Since the mother tree inherits some of the variables from that location.

The complete TGA algorithm is illustrated in the steps below:

1. Initialize the TGA parameters includes a maximum number of iterations $k_{max}$, the number of variables, the population of trees, lower and upper variable's limits.
2. Randomly create the initial tree population and calculate the fitness function.
3. Find the global best tree among all trees at iteration $k$ and store it in $T_{GB}^{k}$.
4. For $\boldsymbol{G_1}$ (Best trees) update the better solution with a local search using the following equation:

$$T_i^{k+1} = \frac{T_i^k}{\theta} + rT_i^k \tag{4.21}$$

where $\theta$ is the reduction rate due to the trees aging and reduced food, and $r$ is the uniform distributed between [0,1] to indicate the satisfaction of light. However, use Eq. (4.21) if the fitness function of the local search is better than the initial position.

5. Move $\boldsymbol{G_2}$ to compete over light close to the best solutions with different angle $\alpha$ using the following formula:

$$d_i = \sqrt{\sum_{i=1}^{G_1+G_2} \left(T_{G_2}^k - T_i^k\right)^2} \quad \left| \quad \& \; d_i = \begin{cases} d_i, & T_{G_2}^k \neq T_i^k \\ \infty, & T_{G_2}^k = T_i^k \end{cases} \right. \tag{4.22}$$

After that choose two minimal distance solutions $x_1$ and $x_2$ and find the combination between the trees as:

$$y = \mu x_1 + (1-\mu)x_2 \tag{4.23}$$

Where $\mu$ is uniformly distributed factor [0,1]. Then they move the tree between the adjacent best tree by the angle $\alpha_i = [0,1]$ as follows:

$$T_{G_2}^k = T_{G_2}^k + \alpha_i y \tag{4.24}$$

6. Eliminate the worst solution $\boldsymbol{G_3}$ **(**poor trees**)** and generate new random solutions instead of them.

$$T_{G_3}^k = rand\,(LB,\ UB,\ variables) \tag{4.25}$$

7. Create a new population $G = G_1 G_2 + G_3$.
8. Generate $\boldsymbol{G_4}$ (reproducing trees) and randomly use a mask operator to adjust the new solutions with respect to the best solution from $G_1$ and combine it to the new population (new population= new population+ $\boldsymbol{G_4}$).
9. Sort the new population and consider it as an initial population for the next iteration.
10. Check the stopping criteria and $k_{max}$ if not satisfied go to 3.

The formulation of the TGA is shown in Algorithm 4.4.

## 4.2.5- Barnacles mating optimizer (BMO)

The structure of the BMO algorithm involves three main steps that starting with the initialization of the barnacles, then the mating process, and finally, the reproduction of the offspring [9]. These steps are mathematically implemented in the next subsections.

### 4.2.5.1 Initialization of the barnacles

In the BMO, barnacles are randomly initialized based on control variables number *N* and the number of barnacles $n$ as follows:

$$X = \begin{bmatrix} x_1^1 & \cdots & x_1^N \\ \vdots & \ddots & \vdots \\ x_n^1 & \cdots & x_n^N \end{bmatrix} \tag{4.26}$$

where the barnacles $X$ should be within the boundary limits as:

$$X_{lb} \leq X \leq X_{ub} \tag{4.27}$$

where, $X_{lb}$ and $X_{ub}$ are the lower and upper vector bounds, respectively, and can be expressed as:

**Algorithm 4.4:** TGA formulation

**Initialize** a set of random search trees $T_i = (T_1, T_2, \dots, T_n,)$
within the limits $LB \leq T_i \leq UB$.
**Split** the population $N$ into four groups ($N_1$, $N_2$, $N_3$, $N_4$)
**while** ($k < k_{max}$)
    **Calculate** the objective function for trees.
    **Store** the global best $T_{GB}^k$
    **for** $G_1(i = 1: N_1)$
        **Update** the better solution with a local search (4.21)
        **if** $\left(f\left(T_i^k\right) \leq f\left(T_i^{k-1}\right)\right)$
            $T_i^k = T_i^k$
        **else**
            $T_i^k = T_i^{k-1}$
        **endif**
    **end**
    **for** $G_2(i = N_1 + 1: N_1 + N_2)$
        **Update** the tree position using (4.24)
    **end**
    **for** $G_3(i = N_1 + N_2 + 1: N)$
        **Update** the tree position using (4.25)
    **end**
    **for** $G_4(i = 1: N_4)$
        **Product** new tree from bests tree
    **end**
    **Sort** the new trees population.
    $k = k + 1$
**end while**
**return** the final best solution stored $T_{GB}^k$

$$X_{lb} = [x_{lb}^1 \quad ... \quad x_{lb}^N] \tag{4.28}$$

$$X_{ub} = [x_{ub}^1 \quad ... \quad x_{ub}^N] \tag{4.29}$$

#### 4.2.5.2 Mating process

In real life, each barnacle able to inject its sperm as well as absorb it from other barnacles. Hence, three mating scenarios can occur. These scenarios are named normal mating, self-mating, and sperm cast mating. However, as assumed in the BMO algorithm [9], the mating process occurs only between two barnacles. Hence, the self-mating is not considered in BMO.

On the one hand, the normal mating (exploitation) occurs when the absolute distance between two barnacles is less than the penis length $pl$ that has been set. On the other hand, the sperm cast (exploration) happens when the absolute distance is more than $pl$.

The mathematical formulation of this behavior can be achieved by forming two vectors of parents' IDs from the overall barnacles' population as follows:

$$ID_D = randperm(N) \tag{4.30}$$

$$ID_M = randperm(N) \tag{4.31}$$

where, $ID_D$ and $ID_M$ are vectors of identification numbers of Dads and Mums respectively. $randperm$ is a function that returns a vector including a random variation of the integers 1to N.

#### 4.2.5.3 Reproduction process

The reproduction of the new offspring in the BMO has been achieved based on the mating scenario in a simple formulation. For normal mating, the latest offspring can be expressed as:

$$x_i^{N\_new} = \alpha x_{ID_D}^N + \beta x_{ID_M}^N \tag{4.32}$$

where, $\alpha$ is a random number between [0,1], $\beta = (1 - \alpha)$, $x_{ID_D}^N$, and $x_{ID_M}^N$ are the Dad and Mum variables of the selected barnacles.

On the other hand, if the barnacles exceed the range of $pl$ then the sperm cast should occur as follows:

$$x_i^{N\_new} = \gamma x_{ID_M}^N \tag{4.33}$$

Where $\gamma$ is a random variable between [0,1]. It can be noticed that the new offspring is generated by the Mum, and thus due to the Mum receives the sperm from the water that has been injected by other barnacles elsewhere.

Algorithm 4.5 illustrates the procedure of the BMO

**Algorithm 4.5:** BMO formulation

1: **Initialize** a set of random barnacles $X_i = (X_1, X_2, \dots, X_n,)$
within the limits $X_{lb} \leq X_i \leq X_{ub}$.
2: **Calculate** the objective function for each search barnacles.
3: **Sort** the fitness in ascending order and store the best solution in$X_{Best}$
4: **Set** the value of $pl$
4: **while** ($iter < iter_{max}$)
5: **Form** two vectors of parents' IDs using (4.30)and (4.31)
6: **for** each search agents $X_i$
7: **if** $|ID_D - ID_M| \leq pl$
11: Generate a new offspring using (4.32)
12: **else**
13: Generate a new offspring using (4.33)
14: **end if**
15: **Calculate** the objective function.
16: **Sort** the fitness in ascending order and update the best solution $X_{Best}$
17: $iter = iter + 1$
18: **end while**
19: **return** the final best solution stored $X_{Best}$

# Chapter 5

# Multi-objective Optimization Algorithms and Decision-Making Methods

## 5.1.- Introduction

This chapter describes the implementation of the multi-objective optimization algorithms based on the single-objective algorithms and two structures. Archive and leader selection structures are applied to obtain the Pareto optimal set. Also, two decision-making methods are introduced to achieve the best compromise solution among the non-dominated Pareto solutions. Additionally, to check the performance of the multi-objective algorithms, the SP metric is formulated.

## 5.2.- Multi-objective Algorithms

The multi-objective algorithm employs a compromise among the objective functions that are based upon the Pareto dominance model. In Pareto domination, the solutions obtained are categorized as dominated and non-dominated solutions. The optimal solution will then be selected from the non-dominated alternatives by the

decision-maker. [59]. In this regard, the single objective algorithms are considered the main core of the multi-objective algorithms. Therefore, two functions are used to formulate the Pareto optimal solutions from the single-objective algorithms, namely archive and leader selection. [89]. The archive is responsible for organizing the non-dominant solutions accomplished so far and the selection of leaders used to direct the other agents to obtain the right solution.

### 5.2.1- Multi-objective SCA

The full description of the MOSCA is shown in Algorithm 5.1. The SCA is adopted to create dominated and non-dominated solutions as written in Algorithm 5.1.

**Algorithm 5.1:** MOSCA formulation

1: **Initialize** a set of random search agents $X_i = (X_1, X_2, \dots, X_n,)$
within the limits $X^L \leq X_i \leq X^U$.
2: **Calculate** the objective functions for each search agent.
3: **Find** the non-dominate solutions and store them in the archive.
4: **Select** the leader using leader selection.
5: **while** ($k < K_{max}$)
6: **for** each search agents $X_i$
7: **Update** SCA parameters $r_1$, $r_2$, $r_3$, and $r_4$
8: **Update** the agents' position using SCA (4.3)
9: **Calculate** the objective functions.
10: **Find** the non-dominate solutions and update the archive.
11: **if** the archive is full.
12: **Run** the grid mechanism to omit one of the current archive's members.
13: **Add** the new solution to the archive.
14: **endif**
15: **if** any of the new added solutions to the archive is located outside the hypercubes.
16: **Update** the grids to cover the new solution(s)
17: **endif**
18**:** **Perform** the leader selection.
19: $K = K + 1$
20: **end while**
21: **return** final non-dominated solutions stored in the archive.

## 5.2.2- Multi-objective SSA

To implement the MSSA, the two structures repository (archive), and food selection (leader) are used. The food selection is used to guide the SSA agents to update their position directly to the food location. Algorithm 5.2 shows the formulation of the MSSA.

**Algorithm 5.2:** MSSA formulation

1: **Initialize** a set of searches Salps within the limits $X_i = (X_1, X_2, \dots, X_n,)$

within the limits $L^i \leq X_i \leq U^i$.

2: **while** ($k < K_{max}$)

3: **Calculate** the objective functions for each search salp.

4: **Find** the non-dominate solutions and store them in the repository.

5: **if** the repository is full.

6: **Run** the grid mechanism to omit one of the current repository's members.

7: **Add** the new solution to the repository.

8: **endif**

9: **if** any of the newly added solutions to the repository is located outside the hypercubes.

10: **Update** the grids to cover the new solution(s)

11: **endif**

12: **Select** the food location using food selection.

13: **Update** the parameters $r_1$ (4.6), $r_2$, and $r_3$

14: **for** each search salp $X_i$

15: Update the leader position using (4.5)

16: Update the position of followers (4.7)

17: $K = K + 1$

18: **end while**

19: **return** final non-dominated solutions stored in the repository.

## 5.2.3- Multi-objective HHO

Similarly, the two structures (archive, and leader selection) are adopted to implement the MOHHO. The full implementation is exhibited in Algorithm 5.3.

**Algorithm 5.3:** MOHHO formulation

1: **Initialize** a set of random search hawks $X_i = (X_1, X_2, \dots, X_n,)$

within the limits $LB \leq X_i \leq UB$.

2: **while** ($t < t_{max}$)

3: **Calculate** the objective functions for hawks.

4: **Find** the non-dominate solutions and store them in the archive.

5: **if** the archive is full.

6: **Run** the grid mechanism to omit one of the current archive members.

7: **Add** the new solution to the archive.

8: **endif**

9: **if** any of the newly added solutions to the archive is located outside the hypercubes.

10: **Update** the grids to cover the new solution(s)

11: **endif**

12: **Select** the leader using leader selection.

14: **for** each search hawks $X_i$

15: **Update** the initial HHO parameters and the energy using (4.10)

16: **Update** hawks' position of using HHO.

17: $t = t + 1$

18: **end while**

19: **return** final non-dominated solutions stored in the archive.

# 5.3.- Decision Making Methods

Several optimal Pareto solutions are found among the multi-objective optimization problems and the best compromise solutions are necessary to select from the non-dominated Pareto solutions. [90]. So it is important to make appropriate decisions through decision making [91]. In this work, two decisions making are developed and used to find the best compromise solutions. The first one is based on the fuzzy control theory while the other one is based on the grey relation analysis.

### 5.3.1- Fuzzy decision making

Developed fuzzy decision-making is used to achieve the best compromise solution. The advantage of using the developed fuzzy decision-making is to permit the planner to give a priority to an objective function over the other through the fuzzy rules.

The fuzzy output can be obtained through three stages, fuzzification, IF-then rules, and defuzzification. The input and output are replaced by a different membership function (MF) based on its value. Hence, the value of the objective function *F* of individual *n* can be normalized as follows:

$$u_i^n = \frac{F_i^{max} - F_i}{F_i^{max} - F_i^{min}} \tag{5.1}$$

where, $F_i^{min}$and $F_i^{max}$ are the minimum and maximum values of the $i^{th}$ objective function.

For DG allocation, fuzzy decision making can be implemented as follows:

Fig. 5.1 displays the three normalized target functions of fuzzy memberships. The performance is a weighting value computed by 27 rules in Table 5.1 which reflects the weighting by five memberships as in Fig. 5.1.d. The fuzzy logic controller chooses the best compromise solution which has the highest weighting value subject to all non-dominated solutions.

However, the rules described in the Table 5.1must be validated with the decision-maker, since they are intended to describe the DM's preferences. Table 5.1 shows the symmetry between the two objective functions.

To interpret the rules in Table 5.1, a simple example can be performed as follows: If the normalized value of $P_{loss}$ , $VD$ , and $VSI$ have arbitrary values; 0.9, 0.5, and 0.2 respectively then based on the memberships illustrated in Fig. 5.1, the fuzzy input is H, M, and L respectively which represents rule 22. The output weighting of the fuzzy is 0.5049 which represents M as in Fig. 5.1.d

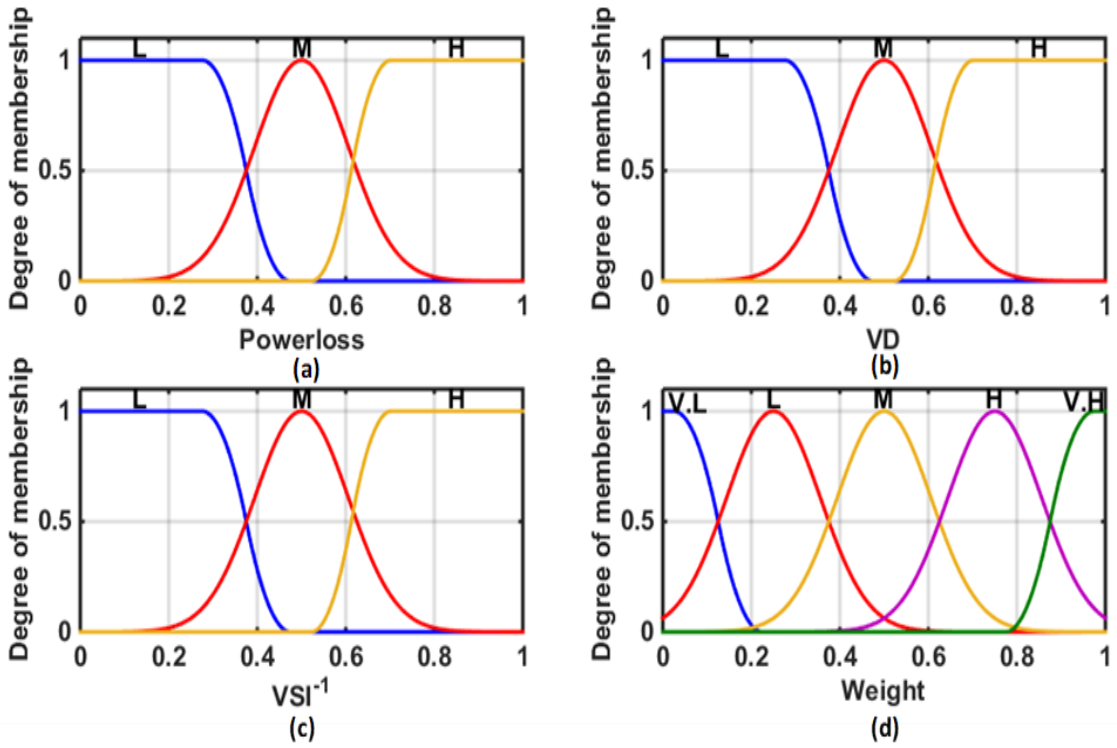


*Fig. 5.1.- Fuzzy memberships (a) Power loss, (b) VD, (c) VSI, (c) Output weight*

**VL =Very Low, L= Low, M =Medium, H =, and VH =Very High.*

*Table 5.1.- Input/output fuzzy rules*

| R | Input Linguistic | | | Out | R | Input Linguistic | | | Out |
|---|---|---|---|---|---|---|---|---|---|
| | $P_{loss}$ | $VD$ | $VSI$ | W | | $P_{loss}$ | $VD$ | $VSI$ | W |
| 1 | L | L | L | V.L | 15 | M | M | H | H |
| 2 | L | L | M | L | 16 | M | H | L | M |
| 3 | L | L | H | L | 17 | M | H | M | H |
| 4 | L | M | L | L | 18 | M | H | H | H |
| 5 | L | M | M | L | 19 | H | L | L | L |
| 6 | L | M | H | M | 20 | H | L | M | M |
| 7 | L | H | L | L | 21 | H | L | H | M |
| 8 | L | H | M | M | 22 | H | M | L | M |
| 9 | L | H | H | M | 23 | H | M | M | H |
| 10 | M | L | L | L | 24 | H | M | H | V.H |
| 11 | M | L | M | M | 25 | H | H | L | V.H |
| 12 | M | L | H | M | 26 | H | H | M | V.H |
| 13 | M | M | L | M | 27 | H | H | H | V.H |
| 14 | M | M | M | M | | | | | |

* R = Rule, and W= weighting

## 5.3.2- Grey Relational Analysis

Appropriate decision-making is needed to achieve the best compromise solution between the optimum Pareto set [91]. A grey relational analysis is carried out in this work to find the best solution using the following steps. [92].

### 5.3.2.1 Grey relational generation

In order to obtain the grey relation, for all objective functions $m$, all non-dominated solution $n$ is normalized within the maximum and minimum values as follows. :

$$u_i^j = \frac{F_i^{max} - F_i^j}{F_i^{max} - F_i^{min}} \quad for\ i = 1,2,.m\ and\ j = 1,2.n \tag{5.2}$$

where, $u_i^j$ is the normalized value of the nondominated solution $j$ of the objective function $i$, $F_i^{max}$ , $F_i^{min}$ are the maximum and minimum of the objective function values, respectively.

### 5.3.2.2 Reference sequence definition

Now all objective functions are normalized between [0,1], hence the reference sequence $u_i^{max}$ value for all objective functions is 1.

### 5.3.2.3 Grey relational coefficient

To present how close the solution $u_i^j$ to the reference $u_i^{max}$, a grey relation coefficient $\zeta_i^j$ is used as:

$$\zeta_i^j = \frac{\Delta^{min} + \zeta\Delta^{max}}{\Delta_i^j + \zeta\Delta^{max}} \tag{5.3}$$

where,

$$\Delta_i^j = \left|u_i^{max} - u_i^j\right| \tag{5.4}$$

$\Delta^{min}$ and $\Delta^{max}$ are the minimum and maximum values of the $\Delta_i^j$ , respectively, and $\zeta$ is the distinguishing coefficient $\in$ [0,1].

### 5.3.2.4 Grey relational grade

Finally, the grey relation grad $\gamma^j$ for all non-dominated solutions is calculated as:

$$\gamma^j = \frac{1}{n}\sum_{i=1}^{n} \zeta_i^j \tag{5.5}$$

where $n$ is the number of objective functions.

According to the above steps, the best compromise solution is the one has the highest-grade value subject to all non-dominated solutions.

## 5.4.- Spacing metric (SP-metric)

A spacing metric is used to measure the efficiency of the multi-objective optimization algorithms, measuring the divergence size of nearby trajectories in the Pareto front as a spacing metric [93]:

$$SP = \sqrt{\frac{1}{n-1}\sum_{i=1}^{n}\left(\bar{d} - d_i\right)^2} \tag{5.6}$$

$$d_i = \min\left(\sum_{k=1}^{m}\left|f_k^i - f_k^j\right|\right) \tag{5.7}$$

where, $i, j = 1,2, \ldots \ldots n,\ m$ is the number of objective functions and $\bar{d}$ is the mean of all $d_i$. The SP-metric value shows how similar the Pareto alternatives are to each other.

# Chapter 6

# Improved Optimization Algorithms for DG Allocation

## 6.1.- Introduction

This chapter introduces the improved optimization algorithms that are used to allocate the DG into the RDS. The main objective of the improved method is to enhance the performance of the optimization algorithm to achieve the optimal solution. The improved methods are implemented based on the chaotic theory, quasi oppositional theory, and hybridization method between the analytical and metaheuristic algorithms.

## 6.2.- Chaotic Maps

As a solution for forecasting erratic behaviors such as atmosphere, brain conditions, or turbulent movement of air or water, chaos maps are applied, these beliefs can be converted to a system of chaotic equations known as chaotic maps. In recent time, in optimization algorithms, several chaotic maps have been used. The key benefit of using chaotic maps in optimization is to increase the algorithm's convergence rate by using various chaotic maps as an alternative for using random variables [48, 94]. The chaotic

maps (see Table 6.1) that are widely used to enhance optimization algorithm efficiency are presented. In this work, the developed algorithm involves these chaotic maps to improve its convergence rate.

It can be observed from Table 6.1 that every chaotic map's behavior depends on the initial value $y_1$, so it is necessary to set an acceptable initial value. For all chaotic maps, though, the initial value is selected at $y_1 = 0.7$ as used in [48, 94].

*Table 6.1.- Chaotic maps*

| No | Name | Chaotic map formula |
|---|---|---|
| 1 | Chebyshev | $y_{k+1} = cos(k\cos^{-1}(y_k))$ |
| 2 | Circle | $y_{k+1} = mod\left(y_k + b_1 - \left(\frac{b_2}{2\pi}\right) sin(2\pi y_k), 1\right)$ $b_1 = 0.5, b_2 = 0.2$ |
| 3 | Gauss/mouse | $y_{k+1} = \begin{cases} 1, & y_k = 0 \\ \frac{1}{mod(y_k)}, & otherwise \end{cases}$ |
| 4 | Iterative | $y_{k+1} = sin\left(\frac{b\pi}{y_k}\right),\ b = 0.7$ |
| 5 | Logistic | $y_{k+1} = by_k(1 - y_k), b = 4$ |
| 6 | Piecewise | $y_{k+1} = \begin{cases} \frac{y_k}{H}, & 0 \le y_k \le H \\ \frac{y_k - H}{0.5 - H}, & H \le y_k \le 0.5 \\ \frac{1 - H - y_k}{0.5 - H}, & 0.5 \le y_k \le 1 - H \\ \frac{1 - y_k}{H}, & 1 - H \le y_k \le 1 \end{cases}, H = 0.4$ |
| 7 | Sine | $y_{k+1} = \frac{b}{4} sin(\pi y_k)\ ,\ b = 4$ |
| 8 | Singer | $y_{k+1} = u(7.86y_k^1 - 23.31y_k^{12} - 28.75y_k^3 - 13.302875y_k^4), u = 1.07$ |
| 9 | Sinusoidal | $y_{k+1} = by_k^1 sin(\pi y_k)\ , b = 2.3$ |
| 10 | Tent | $y_{k+1} = \begin{cases} \frac{y_k}{0.7}\ , & y_k < 0.7 \\ \frac{10}{3}(1 - y_k)\ , & y_k \ge 0.7 \end{cases}$ |

## 6.2.1- Chaotic SCA

The proposed CSCA and MOCSCA and how the chaotic maps in the original SCA optimization algorithm are covered in this section. There are four parameters used in the SCA, ( $r_1, r_2,\ r_3$ and $r_4$)., as stated in the previous section. $r_1$ is updated using (4.4) after each iteration, but the other three parameters are arbitrarily updated, as seen in Algorithm 4.1. Therefore, a specific chaotic map can be used to change certain three parameters instead of using a random variable. Thus, in each parameter, the ten chaotic maps are evaluated separately, and then a mixture is applied between them.

As a result, the chaotic maps are numbered from 1 to 10 as seen in Table 6.1, and the numbering for the use of the chaotic map with the parameters is examined in Table 6.2.

*Table 6.2.- Arrangement of the proposed CSCA algorithms*

| No | Name | Parameter |
|---|---|---|
| 1 | SCA | NA |
| 2 | CSCA_1 | $r_2$ |
| 3 | CSCA_2 | $r_3$ |
| 4 | CSCA_3 | $r_4$ |
| 5 | CSCA_4 | $r_2$, $r_3$ |
| 6 | CSCA_5 | $r_2$, $r_4$ |
| 7 | CSCA_6 | $r_3$ , $r_4$ |
| 8 | CSCA_7 | $r_2$, $r_3$ , and $r_4$ |

To study the effect of chaotic maps on SCA parameters, ten maps are used for each arrangement of the proposed CSCA algorithms, for example when Chaotic Map 1 (Chebyshev) includes CSCA_2, a case study called CSCA_21, and so on. The same method applies to MOSCA.

#### 6.2.1.1 Application of CSCA in Optimal DGs allocation

The optimal size and location of DG into RDS can be achieved using the proposed CSCA as presented in Fig. 6.1 and described in the following steps:

**Step 1:** Read the system data (line data and load data) and define the objective function.

**Step 2:** Randomly initialize a set of search agents, SCA parameters, and Max. number of iterations $K_{max}$ .

**Step 3:** Initialize the chaotic map parameter $y_1 = 0.7$.

**Step 4:** Run power flow and calculate the objective function for each of the search agents and store the best solution.

**Step 5:** Update the selected chaotic map parameter $y_k$ .

**Step 6:** For each search agent, update the parameters $r_1$.

**Step 7:** Using the chaotic $y_k$, update the parameters, $r_2, r_3$ $and$ $r_4$.

**Step 8:** Check the value of $r_4$ and update the position of the current search agents using equation (4.4).

**Step 9:** Calculate the objective function for each search agent.

**Step 10:** Update the best solution.

**Step 11:** Check if $k < K_{max}$, repeat Step 5.

**Step 12:** Return the stored best solution obtained so far.

**Step 13:** Use the search agents' position obtained at the best solution as the optimal size and location for the DGs.

**Step 14:** Run the power flow and obtain the voltage profile.

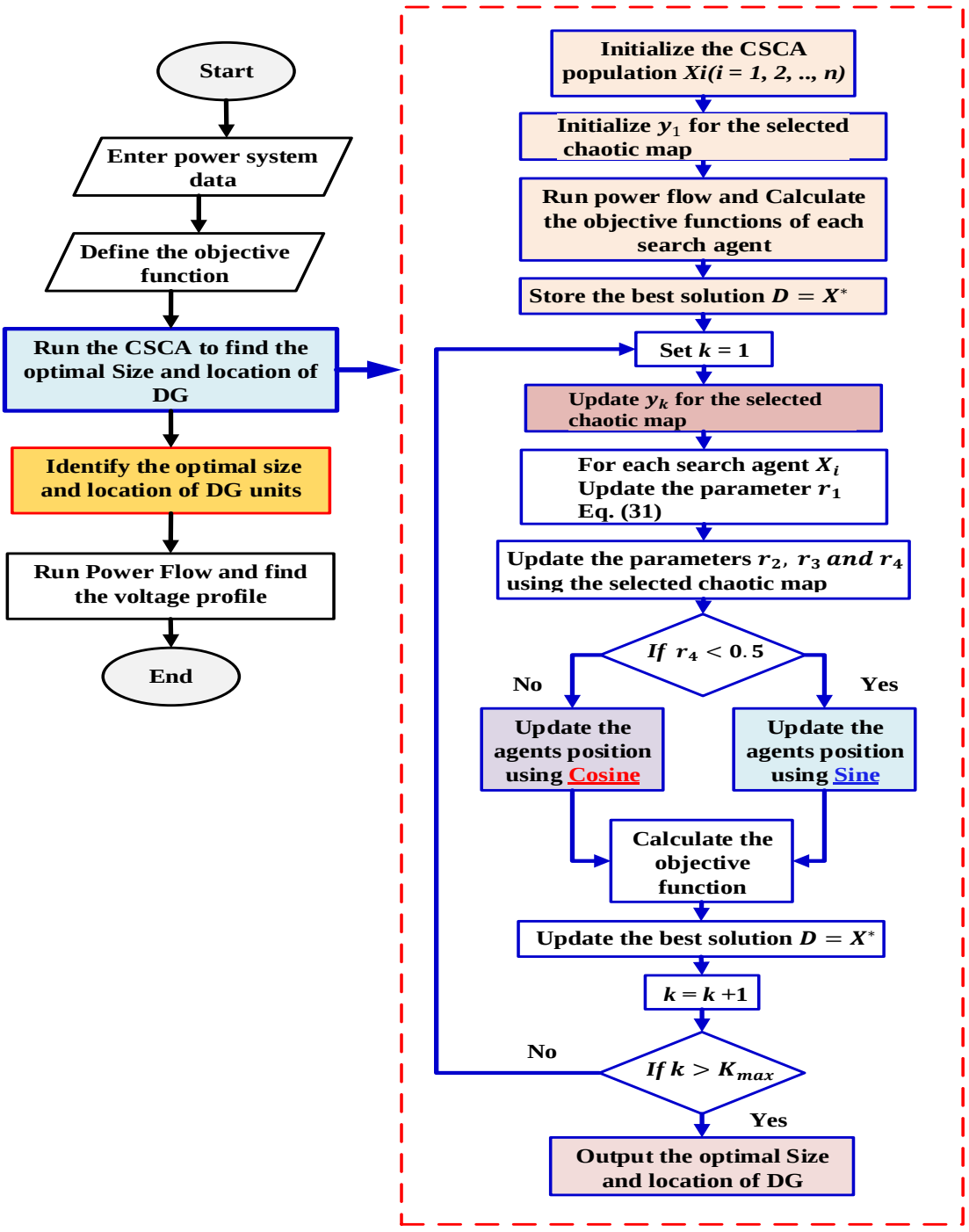


*Fig. 6.1.- DGs allocation using proposed CSCA algorithm*

### 6.2.1.2 Application of MOCSCA in Optimal DGs allocation

Fig. 6.2 shows the flowchart for allocating the DG unit into the RDS using the MOCSCA with grey relation analysis.

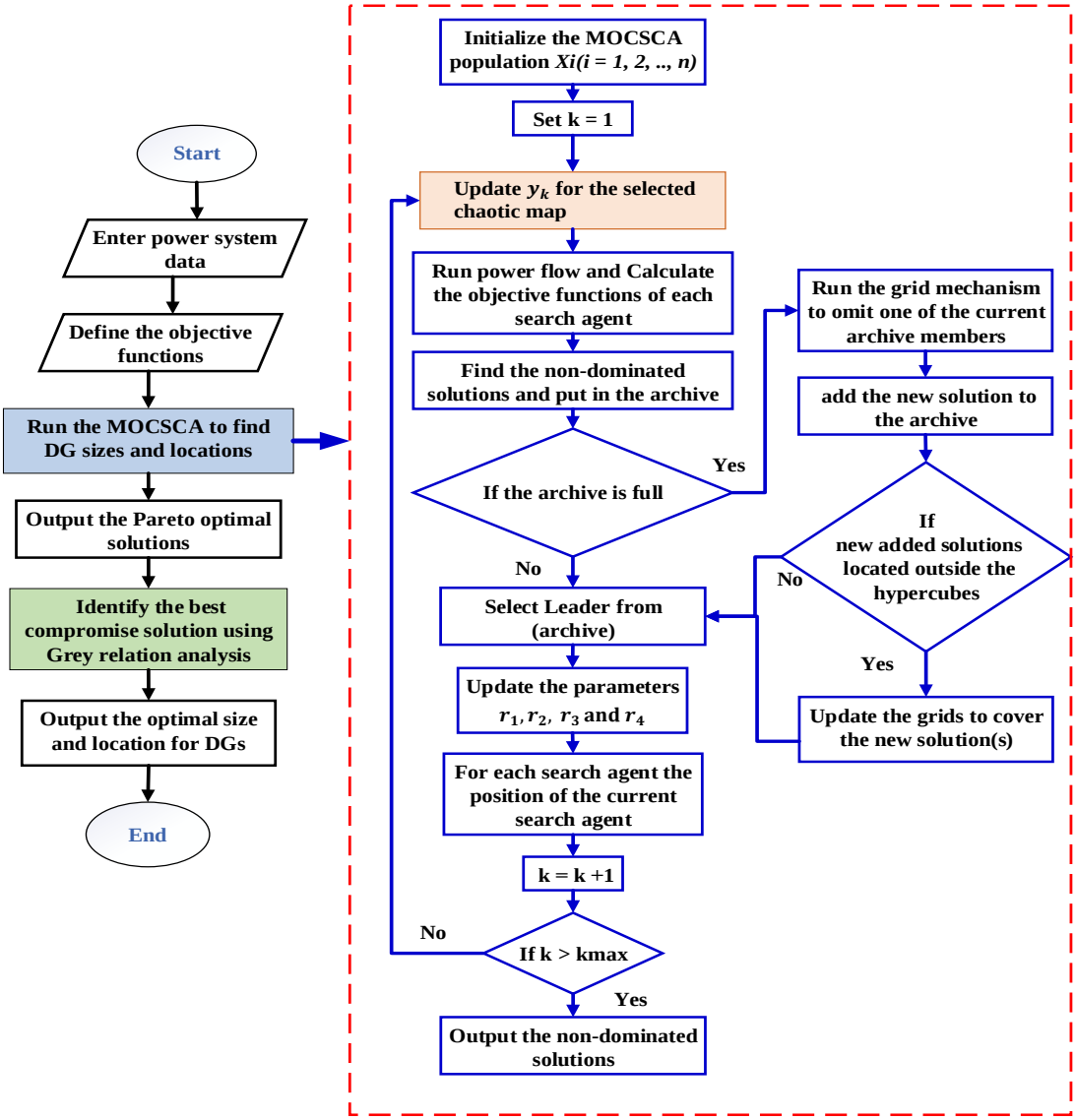


*Fig. 6.2.- DG unit allocation using MOCSCA with Grey relation decision making*

## 6.2.2- Chaotic SSA

Ten chaotic maps exhibited in Table 6.1 are incorporated into the MSSA to update its parameter $r_2$ instead of using random probability as follows:

$$r_2 = y_{k+1} \tag{6.1}$$

#### 6.2.2.1 Application of MCSSA in Optimal DGs allocation

The allocation DGs in the RDS using the MCSSA is exhibited in Fig. 6.3. The following steps show the full procedure of application of the MCSSA in the DG allocation problem:

**Step 1:** Read the system data (line data and load data) and define the objective functions.

**Step 2:** Randomly initialize a set of search agents, MSSA parameters, and Max. number of iterations $K_{max}$ .

**Step 3:** Initialize the chaotic map parameter $y_1 = 0.7$.

**Step 4:** Run power flow and compute the objective functions for each of the search agents.

**Step 5:** Find the non-dominate solutions and store them in the repository.

**Step 6:** Check the archive if full use grid mechanism to delete the current archive agent and insert the new solution.

**Step 7:** Perform food selection.

**Step 8:** Update the selected chaotic map parameter $y_k$ .

**Step 9:** Update the parameters $r_1$ (4.6), $r_2$, and $r_3$ then update the leader and followers' positions using (4.5) and (4.7) respectively.

**Step 10:** Check the archive if full use grid mechanism to delete the current archive agent and insert the new solution.

**Step 11:** Check if $k < K_{max}$repeat **Step 4**

**Step 12:** Return the stored final non-dominated solutions in the archive.

**Step 13:** Use the fuzzy decision making to obtain the best compromise solution and identify it as the optimal size and location for the DGs.

**Step 14:** Run the power flow and obtain the voltage profile.

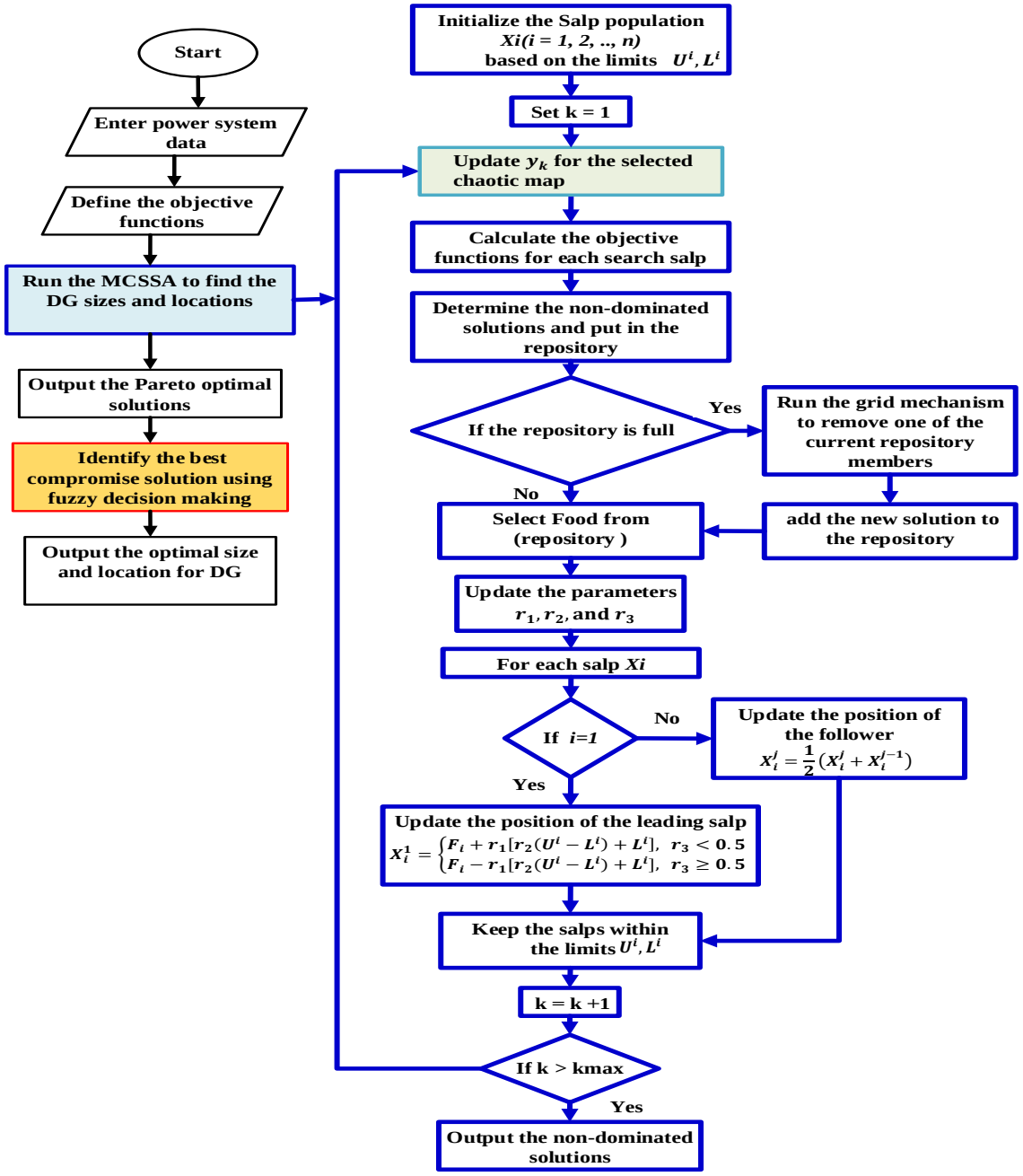


*Fig. 6.3.- DGs allocation using MCSSA with Fuzzy decision making*

# 6.3.- Other Improved Optimization Algorithms

## 6.3.1- Improved HHO

In the original HHO algorithm, the next equation is used to take back the hawk if the hawks go beyond the position limits:

$$X(t+1) = \begin{cases} X(t+1), & X_{min} \leq X(t+1) \leq X_{max} \\ X_{min}, & X(t+1) < X_{min} \\ X_{max}, & X(t+1) > X_{max} \end{cases} \quad (6.2)$$

Where, $X_{min}$ and $X_{max}$ are the minimum and maximum of the optimization problem variables. To enhance the HHO, the hawks can return to the place of a rabbit $X_{rab}$ if they reach the limits. Which is deemed to be the best solution as follows:

$$X(t+1) = \begin{cases} X(t+1), & X_{min} \le X(t+1) \le X_{max} \\ X_{rab}(t), & X(t+1) < X_{min} \\ X_{rab}(t), & X(t+1) > X_{max} \end{cases} \quad (6.3)$$

Fig. 6.4 shows the flowchart of the IHHO.

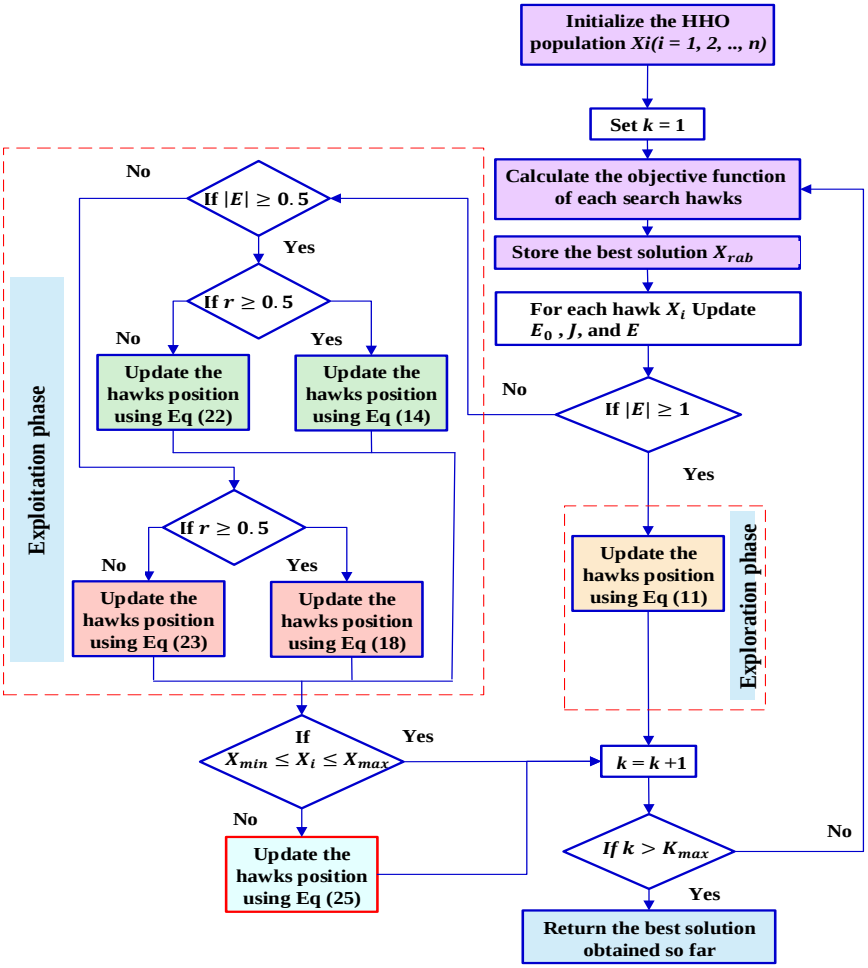


*Fig. 6.4.- Flowchart of IHHO*

### 6.3.1.1 Application of IHHO in DG allocation

The application of the IHHO into DG allocation can be summarized in the following steps:

**Step 1:** Read the system data (line data and load data) and define the objective function.

**Step 2:** Randomly initialize a set of hawks' searches within the upper and lower limits of the DG sizes and locations, HHO parameters, and Max. number of

iterations $K_{max}$ .

**Step 3:** Run the power flow and calculate the objective function (power loss) for each search hawk.

**Step 4:** Store the best solution $X_{rab}$ .

**Step 5:** Update the parameters of HHO ($E$, $E_0$, and $J$).

**Step 6:** Update the sizes and locations of the best solutions based on the exploration and exploitation phases' strategies.

**Step 7:** Check the sizes and locations' limits and update the position using (6.3)

**Step 8:** Check if ($k < K_{max}$) **Step 3.**

**Step 9:** Return the final best solution stored (DG locations and sizes).

**Step 10:** Run the power flow and obtain the voltage profile.

#### 6.3.1.2 Application of MOIHHO in DG allocation

Implementation of the MOIHHO for optimal DG allocation into RDSs is presented in the following steps:

**Step 1:** Read the system data (line data and load data) and define the objective functions ($P_{loss}$, $VD$, and $VSI$).

**Step 2:** Randomly initialize a set of search hawks, HHO parameters, and Max. number of iterations $K_{max}$ .

**Step 3:** Run power flow and calculate the objective functions for each search hawk,

**Step 4:** Arrange the non-dominate solutions in the archive and select the leader.

**Step 5:** Update the parameters of HHO ($E$, $E_0$, and $J$).

**Step 6:** Check the archive, if it is full, apply the grid mechanism.

**Step 7:** Run the leader selection.

**Step 8:** If $k < K_{max}$, repeat Step 2.

**Step 9:** Return the stored final non-dominated solutions in the archive.

**Step 10:** Run the grey relation decision making to find the best compromise solution.

**Step 11:** Run the power flow and obtain the voltage profile.

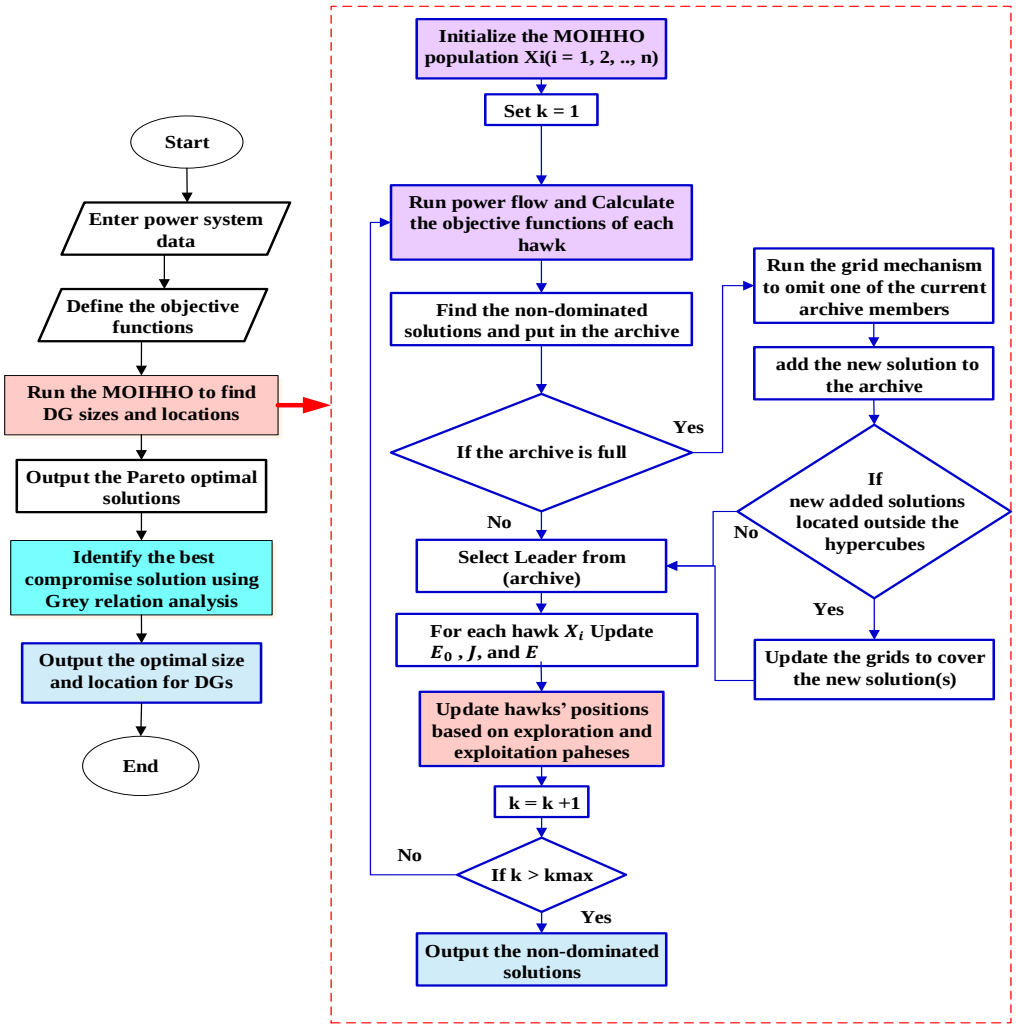


*Fig. 6.5.- DG allocation using MOIHHO.*

## 6.3.2- Hybrid Analytical and TGA optimization algorithm.

The key objective of the proposed ATGA is to optimally distribute multi-type DG units in the RDSs in order to reduce the total active powers and increase the stability of voltage based on the hybrid computation of analytical algorithms and the random metaheuristic initialization towards the satisfactory goal. The ATGA procedures are shown in Fig. 6.6 and summarized in the following steps:

**Step 1:** Randomly initialize a set of tree searches within the number of system limits.

**Step 2:** Calculate the initial injected active or/and reactive power for each agent using (3.20) or/and (3.21)

**Step 3:** Calculate the objective function for each of the search tree and store the best or worst trees.

**Step 4:** Update the parameters of TGA.

**Step 5:** Update the Sizes and locations of the best solutions.

**Step 6:** Check if ($k < K_{max}$) **Step 2**

**Step 7:** Return the final best solution stored.

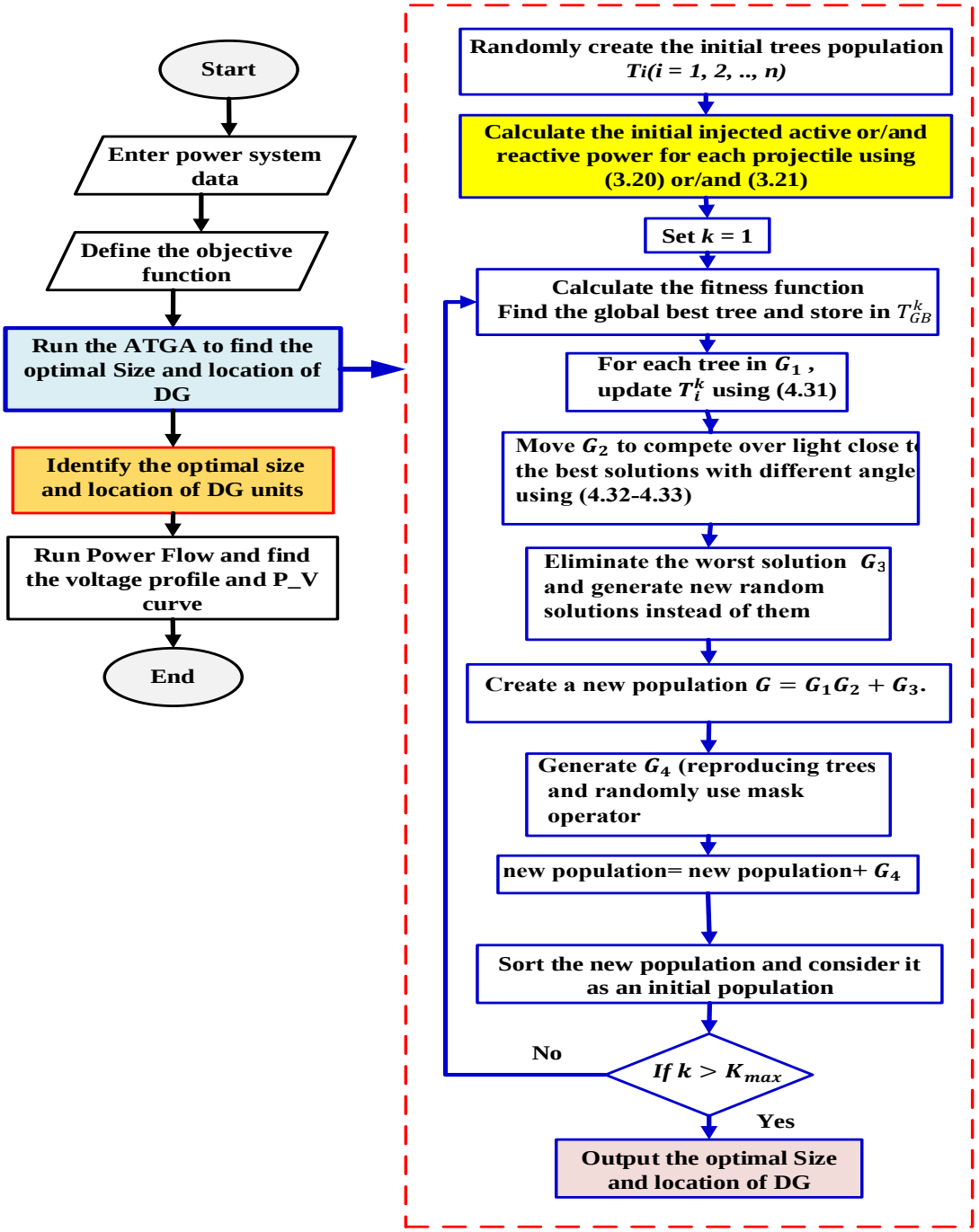


*Fig. 6.6.- Flowchart for the hybrid optimization algorithm ATGA*

## 6.3.3- Improved BMO

As discussed in Section I, different methods have been applied to improve the metaheuristic optimization algorithms. Therefore, quasi oppositional and chaos maps are handled to improve the performance of conventional BMO.

#### 6.3.3.1 Quasi oppositional

In this work, the opposite solutions of the BMO barnacles $X_i^{N\_new}$ can be expressed as:

$$X_i^{QN\_new} = \begin{cases} C + r_1(C - X_i^{N\_new}), & X_i^{N\_new} < C \\ C - r_1(X_i^{N\_new} - C), & X_i^{N\_new} \geq C \end{cases} \quad (6.4)$$

Where $X_i^{QN\_new}$ is quasi oppositional of the $X_i^{N\_new}$ barnacle and $C$ are calculated as:

$$C = \frac{x_{lb}^i + x_{ub}^i}{2} \quad (6.5)$$

Hence, $X_i^{N\_new}$ and $X_i^{QN\_new}$ are used to calculate the objective function, then the one who achieves the best objective is used in the next iterative process. The overall steps of the QOBMO are based on the quasi-oppositional algorithm is presented in Fig. 6.7.

#### 6.3.3.2 Chaos maps

The second improvement in the BMO is using chaos theory based on several chaotic maps to enhance the exploration. Where chaotic maps are used to improve the convergence by applying the chaotic equation instead of utilizing random parameters Thus, ten chaotic maps are adopted (see Table 6.1) and applied to the QOBMO algorithms to update the exploration parameter $\alpha$ instead of using random probability as follows:

$$\alpha = y_{iter+1} \quad (6.6)$$

where, $y_{iter+1}$ is the selected chaos map, as presented in Table 6.1. The overall steps of the CQOBMO are exhibited in the flowchart and shown in Fig. 6.8.

#### 6.3.3.3 Application of CQOBMO in Optimal DGs allocation

The optimal size and location of DG into RDS can be achieved using the proposed CQOBMO is described in the following steps:

**Step 1:** Read the system data (line data and load data) and define the objective function.

**Step 2:** Randomly initialize a set of search agents, BMO parameters, and Max. number of iterations $K_{max}$ .

**Step 3:** Initialize the chaotic map parameter $y_1 = 0.7$.

**Step 4:** Run power flow and calculate the objective function for each of the search barnacles.

**Step 5:** Sort the objective function in ascending order and store the best solution in $X_{Best}$

**Step 6:** Set the value of $pl$

**Step 7:** Update the selected chaotic map parameter $y_k$ .

**Step 8:** Form two vectors of parents' IDs using (4.30)and (4.31)

**Step 9:** Using the chaotic $y_k$, update the parameters, $\alpha$.

**Step 10:** Check the value $|ID_D - ID_M| \leq p$ and generate offspring.

**Step 11:** Calculate the objective function for each search barnacles.

**Step 12:** Update the best solution. $X_{Best}$

**Step 13:** Check if $k < K_{max}$, repeat Step 6.

**Step 14:** Return the stored best solution obtained so far.

**Step 15:** Use the search agents' position obtained at the best solution as the optimal size and location for the DGs.

**Step 16:** Run the power flow and obtain the voltage profile.

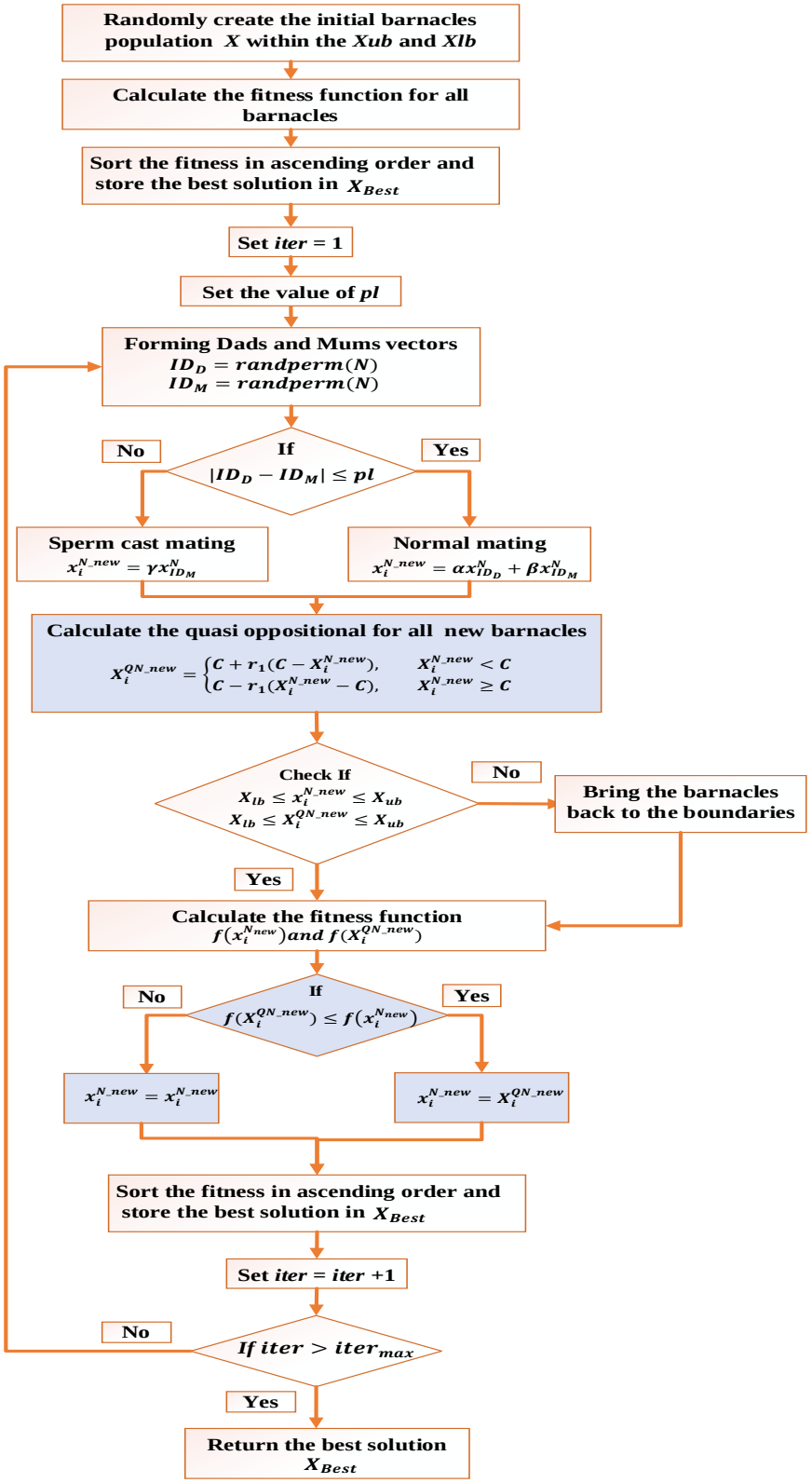


*Fig. 6.7.- QOBMO algorithm*

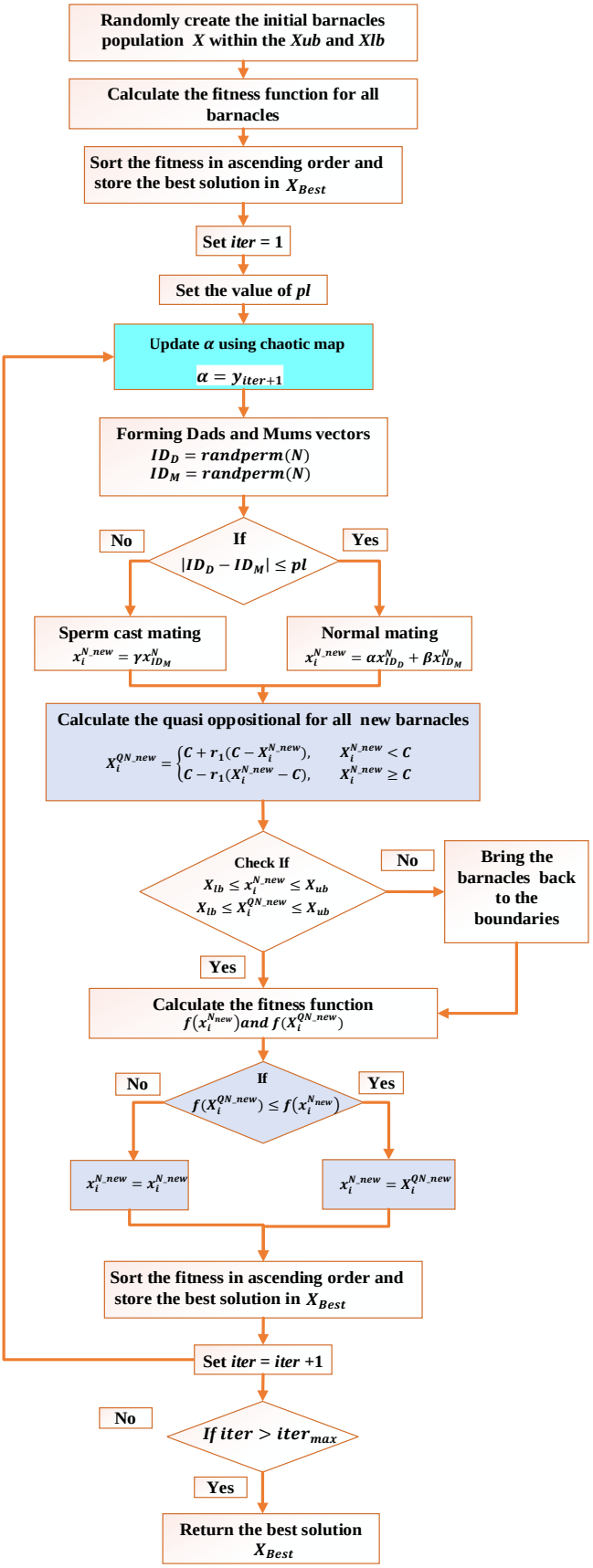


*Fig. 6.8.- Flowchart of the CQOBMO algorithm*

# Chapter 7

# Numerical Results

## 7.1.- Introduction

In this Chapter, the developed optimization algorithms are applied to optimally allocate the DG into RDSs and numerically compared in various scenarios. The improved algorithms are validated based on standard and realistic RDSs. The results are compared to other competitive optimization algorithms. Then, the improved algorithms are used to reduce the impact of the intermittent nature of the power generation represented in the PV system and load variation in the RDSs using optimal scheduling of the BES over 24 hrs besides, four typical days for the four seasons in the year.

## 7.2.- Simulation conditions

The developed algorithms have been programmed using MATLAB 2015 and run on Intel core i5, processor 2.9 GHz PC with capacity 8.0 GB RAM with operating system Win.10, and a developed GUI is proposed for all improved algorithms. To check the performance of the developed algorithms, 30 runs are carried out and the best, worst,

and average costs for the single objective algorithms are calculated while the SP-metric is computed for the multi-objective algorithms.

## 7.3.- Studied RDSs

In order to validate the tested methodologies, the following standard and realistic RDSs have been considered:

- IEEE 33-bus test system. [95].
- IEEE 69-bus test system [96].
- 94-bus Portuguese test system [97].

The full description of these test systems including the line data, load data, and single line diagram are given in the mentioned reference.

## 7.4.- Results of DG Allocation Using Improved Single-Objective Optimization Algorithms

This section presents the application of the improved single-objective algorithms in different scenarios of DG allocation.

### 7.4.1- CSCA

The proposed algorithm CSCA is applied on two standard IEEE 33-bus and 69-bus RDSs. As a single-objective optimization problem, the optimal size and sitting of several DGs units are calculated to minimize the overall power loss. A detailed analysis is made with other well-known optimization algorithms in order to show the viability and efficacy of the proposed algorithm. The parameters of CSCA are defined as; the number of agents = 100, the maximum number of iterations = 100.

For the single-objective problem in the two RDSs, the following four cases are considered:

**Case #1:** Base case (without DG);

**Case #2:** Integrating 1 DG.

**Case #3:** Integrating 2 DGs.

**Case #4:** Integrating 3 DGs.

### 7.4.1.1 Performance of CSCA

In [86], the efficiency of the SCA was shown and the results were checked with well-known optimization algorithms such as GA, PSO, and FA. But, with the chaotic maps, to evaluate the efficiency of the SCA, seven CSCAs (see Table 6.2) based on different chaotic maps are simulated with the IEEE 33-bus system to find the optimal size of the DG unit.

Fig. 7.1.a displays the convergence features of the various combination algorithms with iterative chaos maps. It can be observed from this figure that CSCA_6 provides the highest convergence rate relative to the other proposed algorithms. The iterative chaotic map proves its utility among the ten chaos maps, as seen in Fig. 7.1.b. It can be presumed that the effective chaotic algorithm for SCA is the CSCA_64 and can be used to assign DG units in the RDS. Consequently, the CSCA_64 is used in the IEEE 33- and 69-bus systems to find the best capacity and location of the DG.

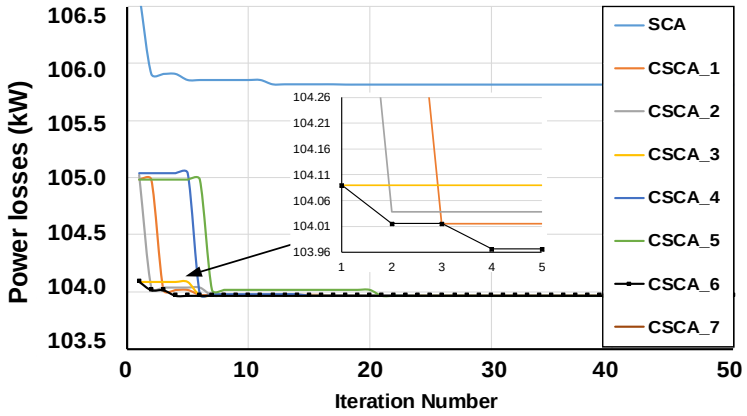


*a. SCA parameter combination*

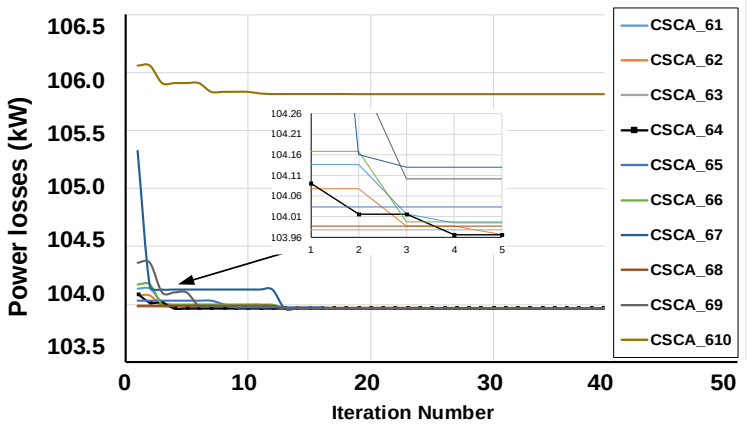


*b. Chaotic map convergence*

*Fig. 7.1.- CSCA Convergence characteristics using chaotic maps*

#### 7.4.1.2 IEEE 33-bus test system

The proposed CSCA_64 is tested using the IEEE 33-bus test system. In the literature, it has been noticed that there are two different power losses obtained at the base case for this system, the first one indicates that the active and reactive power losses are 202.68 kW and 134.14 kVAR, respectively, and the second one obtained the total active and reactive power loss for the base case as 210.98 kW and 143.13 kVAR. This has happened because some researchers have taken the resistance and reactance values of the 7th line as 0.7114 Ω and 0.2351Ω, whereas others have taken as 1.7114 Ω and 1.2351 Ω. Hence, in this case, study, the active and reactive power losses are 202.68 kW and 134.14 kVAR.

CSCA-64 is used to distinguish suitable positions and sizes of DGs depending on the above cases (1 DG, 2 DGs, and 3 DGs) to minimize overall power losses and improve voltage profiles. Table 7.1. summarizes the results obtained for each case, including the location of DGs, size, active, and reactive losses.

The active power losses decrease to 103.966 kW when a DG unit is integrated at bus 6 with a total capacity of 2575.26 kW. A significant decrease in the active power loss reach to 71.94 kW is obtained when 3 DG units. Fig. 7.2 shows the voltage profiles of the IEEE 33-bus system for the tested case studies. As seen, a significant improvement is achieved when 2 DGs and 3 DGs are incorporated. Besides, the voltage is kept within the limits.

*Table 7.1.- Optimal sizes and location using proposed CSCA-64 in IEEE 33-bus system*

| | Location | Size (kW) | Total power loss (kW) | Total reactive power loss (kVAR) |
|---|---|---|---|---|
| Base case | NA | NA | 202.68 | 135.14 |
| Case #2: 1 DG | 6 | 2575.26 | 103.966 | 74.79 |
| Case #3: 2 DGs | 12 | 973.82 | 85.96 | 58.49 |
| | 30 | 1106.22 | | |
| Case #4: 3 DGs | 13 | 871.00 | 71.94 | 49.54 |
| | 24 | 1091.47 | | |
| | 30 | 954.08 | | |

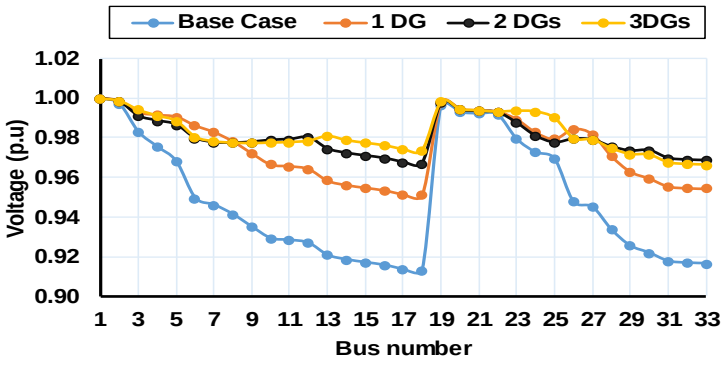


*Fig. 7.2.-Voltage profiles of IEEE-33 bus test system for CSCA_64*

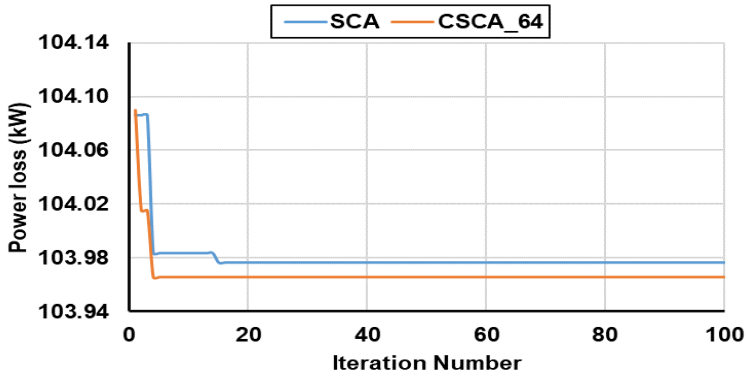


*a) Case 2: Integrating 1 DG*

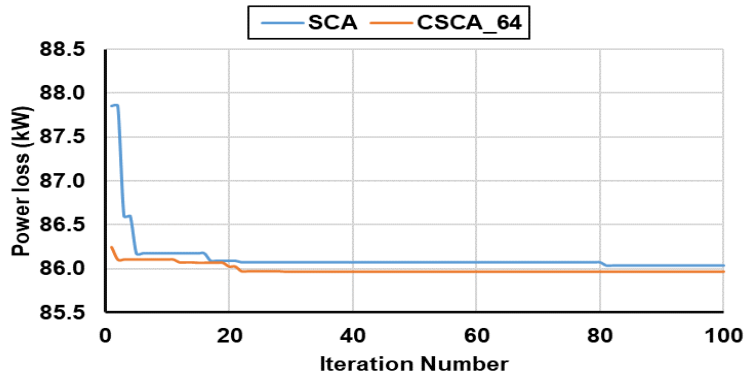


*b) Case 3: Integrating 2 DGs*

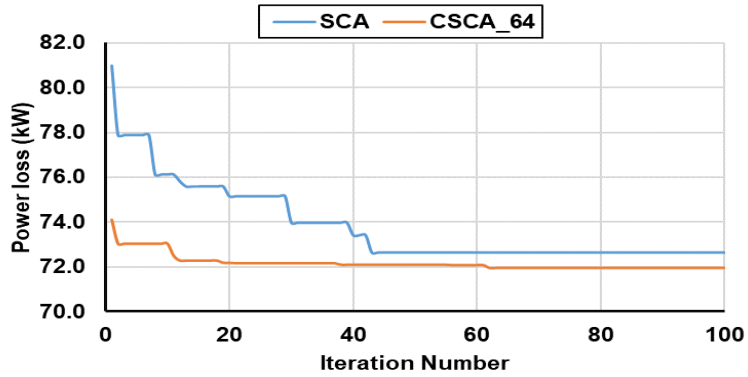


*c) Case 4: Integrating 3 DGs*

*Fig. 7.3.- SCA and CSCA-64 Convergence for DG integration in IEEE 33-bus test system*

It is necessary to examine the improvement in the convergence rate achieved by the proposed CSCA_64 compared to the original SCA. The convergence characteristics of the three DGs integration cases are seen in Fig. 7.3 and it is obvious that the CSCA_64 achieves the best solution quicker than the original SCA.

The statistical assessment, including the best, average, and worst value of the costing function is evaluated and presented in Table 7.2. to ensure the viability of results obtained for each analyzed scenario. From this table, the dominance of the proposed CSCA_64 over the original SCA can be found in all the tested cases.

*Table 7.2.- SCA and CSCA_64 statistical comparison (IEEE 33-bus test system)*

| Algorithm | | Best Cost | Average Cost | Worst Cost |
|---|---|---|---|---|
| Case #2: 1 DG | SCA | 103.98 | 104.40 | 105.81 |
| | CSCA-64 | 103.97 | 103.97 | 103.97 |
| Case #3: 2 DGs | SCA | 86.03 | 88.82 | 94.36 |
| | CSCA-64 | 85.96 | 87.39 | 91.52 |
| Case #4: 3 DGs | SCA | 72.51 | 80.36 | 89.67 |
| | CSCA-64 | 71.94 | 76.07 | 84.67 |

Compared with numerous well-known optimization algorithms, the proposed CSCA_64 results are presented in Table 7.3. It can be observed that the proposed CSCA_64 can significantly boost loss reduction (LR).

#### 7.4.1.3 IEEE 69-bus test system

Table 7.4 gives the optimal places, sizes, and active power losses, the total power losses reduced to 63.03%, 68.14%, and 68.86% by incorporating (1 DG, 2 DGs, and 3 DGs) respectively. Fig. 7.4 shows the voltage profiles for all cases, the voltage is raised compared to the base case and still within the allowable limits.

*Table 7.3.-Comparison of LR obtained by different optimization algorithms* and *CSCA_64 (IEEE 33-bus test system)*

| Algorithm | Case #2: 1 DG (Bus/Size (kW)) | LR % | Case #3: 2 DG (Bus/Size (kW)) | LR % | Case #4: 3 DG (Bus/Size (kW)) | LR % |
|---|---|---|---|---|---|---|
| LSF [61] | #18/ 743 | 30.48 | #18/ 720; #33/0.900 | 52.32 | #18/720; #33/0.810; #25/ 900 | 59.72 |
| Fuzzy - IAS[67] | #32/1931 | 37.71 | #32/383.6; #30/1150.6 | 42.43 | #32/2071; #30/1113.8; #31/150.3 | 42.45 |
| BSOA[68] | #8/ 1858 | 43.98 | #13/ 880; #31/ 924 | 57.62 | #13/632; #28/486; #31/550 | 57.76 |
| BFOA[98] | NA | NA | NA | NA | #14/652; #18/198.4; #32/1067.2 | 57.62 |
| SKHA[70] | #6/2590 | 47.38 | #13/851.6; #30/1157.6 | 58.7 | #30/1054; #24/1091; #13/802 | 65.40 |
| CSCA-64 | #6/ 2575 | 48.70 | #12/973.82; #30/1106.2 | 57.60 | #30/954.1; #24/1091.5; #13/871 | 64.5 |

** NA= Not Reported*

*Table 7.4.- Optimal sizes and location using proposed CSCA-64 in IEEE 69-bus system*

| | Location | Size (kW) | Total power loss kW | Total reactive power loss (kVAR) |
|---|---|---|---|---|
| Base case. | NA | NA | 224.95 | 102.15 |
| Case #2: 1 DG | 61 | 1872.60 | 83.19 | 40.52 |
| Case #3: 2 DGs | 18 | 511.28 | 71.67 | 35.95 |
| | 61 | 1794.11 | | |
| Case #4: 3 DGs | 17 | 365.97 | 70.07 | 35.14 |
| | 61 | 1675.85 | | |
| | 67 | 652.52 | | |

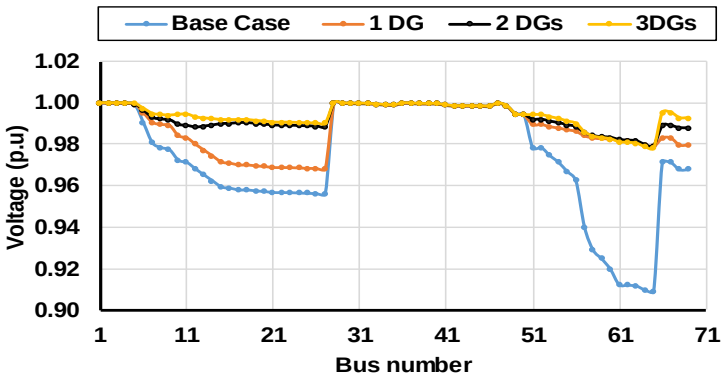


*Fig. 7.4.- Voltage profiles of IEEE-69 bus system for CSCA_64*

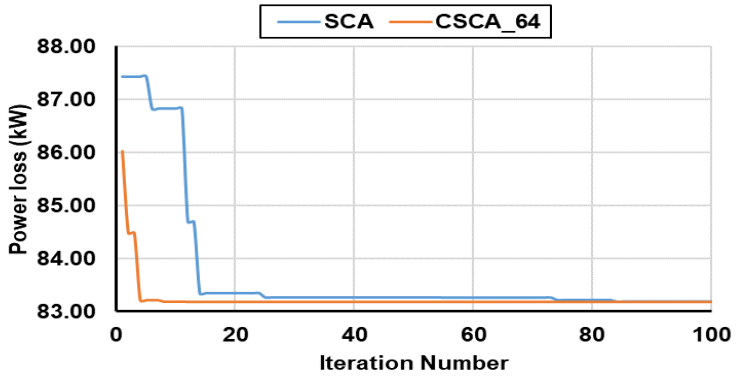


*a) Case 2: Integrating 1 DG*

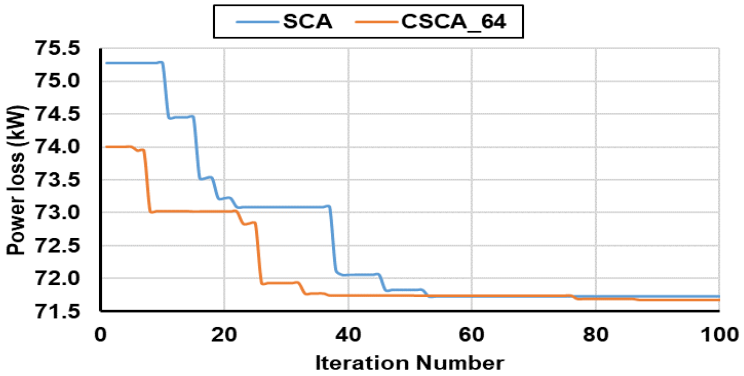


*a) Case 3: Integrating 2 DG*

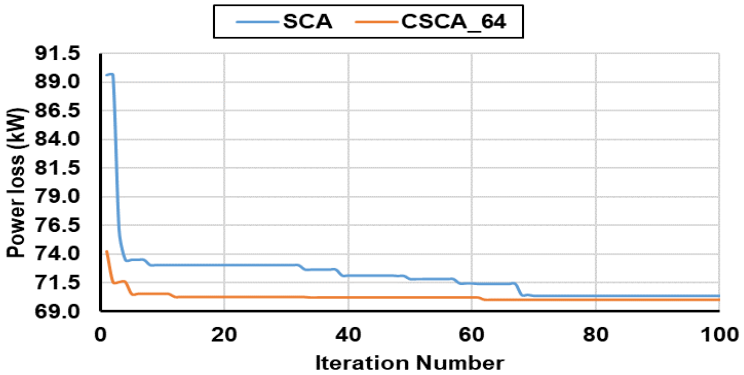


*a) Case 4: Integrating 3 DG*

*Fig. 7.5.- SCA and CSCA-64 Convergence for DG integration in IEEE 69-bus test system*

Similarly, it is worthy to track the performance of the proposed CSCA-64 by increasing the system size to prove the feasibility of the algorithm. The convergence characteristics of the proposed CSCA-64 and original SCA are shown in Fig. 7.5. From this figure, it can be observed that the chaotic map enhances the convergence of the original SCA algorithm. The statistical analysis is summarized in Table 7.5.

*Table 7.5.- SCA and CSCA_64 performance comparison (IEEE 69-bus test system)*

| Algorithm | | Best Cost | Average Cost | Worst Cost |
|---|---|---|---|---|
| Case #2: 1 | SCA | 83.19 | 83.23 | 83.73 |
| DG | CSCA-64 | 83.19 | 83.19 | 83.21 |
| Case #3: 2 | SCA | 71.73 | 78.67 | 86.20 |
| DGs | CSCA-64 | 71.67 | 76.06 | 83.23 |
| Case #4: 3 | SCA | 70.40 | 76.55 | 87.09 |
| DGs | CSCA-64 | 70.07 | 74.67 | 83.00 |

The effectiveness of the proposed algorithm is compared with the other optimization algorithms (Analytical, GAPSO, BFOA, MBFOA, and SKHA) used for allocating the DGs in the IEEE 69-bus system and the results are presented in Table 7.6. It can be noted that the proposed CSCA-64 can improve the LR compared to other optimization algorithms where the LRs are 63.03%, 68.14%, and 68.86% in case of integrating 1 DG, 2 DGs, and 3 DGs, respectively.

*Table 7.6.- Comparison of LR obtained by different optimization algorithms and CSCA_64 (IEEE 69-bus test system)*

| Algorithm | Case #2: 1 DG (Bus/Size (kW)) | LR % | Case #3: 2 DG (Bus/Size (kW)) | LR % | Case #4: 3 DG (Bus/Size (kW)) | LR % |
|---|---|---|---|---|---|---|
| Analytical [70] | #61/1800 | 62.95 | NA | NA | NA | NA |
| GAPSO [70] | NA | NA | NA | NA | #63/884.9; #61/1196; #21/910.5 | 63.96 |
| BFOA [70] | NA | NA | NA | NA | #27/295.4; #65/446; #61/1345.1 | 66.56 |
| MBFOA[70] | #61/1879 | 63.00 | NA | NA | NA | NA |
| SKHA[70] | #61/1865 | 63.00 | #17/5229.; #61/1778.9 | 68.07 | #61/1719.1; #17/371; #11/527.1 | 69.10 |
| CSCA-64 | #61/1873 | <u>63.03</u> | #18/511.3; #61/1794.1 | <u>68.14</u> | #67/652.5; #61/1675.9; #17/366 | <u>68.86</u> |

## 7.4.2- IHHO

The two standard IEEE 33-bus and 69-bus RDSs are utilized to study the performance of the IHHO algorithm. In the two systems investigated, the following four cases are examined:

**Case #1:** Base case (without DG);

**Case #2:** Integrating 3 DGs with unity power factor (p.f).

**Case #3:** Integrating 3 DGs with 0.95 p.f.

**Case #4:** Integrating 3 DGs with optimal p.f.

### 7.4.2.1 IEEE 33-bus test system

For the base case, the power flow outcomes reveal that the active and reactive power losses are 210.98 kW and 143.14 kVAR, respectively. Three DG units of different p.f. are optimally assigned using the IHHO to minimize the cumulative power losses.

Table 7.7 displays the optimum sizes and positions of the DG at unity p.f. From this table, it can be observed that the optimum positions of three DGs are 14, 24, and 30 with active power capacity equal 775.54 kW, 1080.83 kW, and 1066.69 kW respectively using the IHHO and that contributes to reducing power losses from 210.98 kW to 72.79 kW where the LR exceeds 65.50 percent. Besides, the developed IHHO provides the lowest power loss relative to the other optimization algorithms and the traditional HHO.

Table 7.8 also introduces the results with p.f of 0.95 for the multi- DG allocation. The results show that the developed IHHO seeks ideal positions and sizes with a minimal power loss (28.5 kW). The power loss from IHHO is smaller than the power loss from SIMBO-Q, and the traditional HHO, and nearly equal to the power of QOSIMBO-Q. Table 7.9 summarizes the results of the optimal p.f obtained by the IHHO in comparison with BSOA[68], BFOA [69], and HHO. A substantial LR in the power loss reaches 94.39 % is given by the IHHO.

The effect of the DG installation on the RDS voltage profile with different p.f. is seen in Fig. 7.6. This figure demonstrates a substantial improvement in the integration of many DGs with optimum p.f.

*Table 7.7.- Comparison of LR obtained by different optimization algorithms and IHHO at unity p.f (IEEE 33-bus system)*

| Algorithm | Optimal DG | | Power loss (kW) | LR % |
|---|---|---|---|---|
| | Bus | Size (kW) | | |
| LSF [61] | 18 | 720 | 85.07 | 59.72 |
| | 33 | 810 | | |
| | 25 | 900 | | |
| Fuzzy -IAS[67] | 32 | 2071 | 117.36 | 42.45 |
| | 30 | 1113.8 | | |
| | 31 | 150.3 | | |
| BSOA[68] | 13 | 632 | 89.05 | 57.76 |
| | 28 | 486 | | |
| | 31 | 550 | | |
| BFOA [69] | 14 | 779 | 73.53 | 65.14 |
| | 25 | 880 | | |
| | 30 | 1083 | | |
| TLBO [74] | 10 | 824.6 | 75.54 | 64.20 |
| | 24 | 1031.1 | | |
| | 31 | 886.2 | | |
| QOTLBO [74] | 12 | 880.8 | 74.10 | 64.88 |
| | 24 | 1059.2 | | |
| | 29 | 1071.4 | | |
| SIMBO-Q [54] | 14 | 763.8 | 73.4 | 65.21 |
| | 24 | 1041.5 | | |
| | 29 | 1135.2 | | |
| QOSIMBO-Q [54] | 14 | 770.8 | 72.8 | 65.49 |
| | 24 | 1096.5 | | |
| | 30 | 1065.5 | | |
| HHO | 14 | 745.69 | 72.98 | 65.40 |
| | 24 | 1022.69 | | |
| | 30 | 1135.78 | | |
| IHHO | 14 | 775.54 | 72.79 | 65.50 |
| | 24 | 1080.83 | | |
| | 30 | 1066.69 | | |

*Table 7.8.- Comparison of LR obtained by different optimization algorithms and IHHO at 0.95 p.f (IEEE 33-bus system)*

| Algorithm | Optimal DG | | | | Power loss (kW) | LR % |
|---|---|---|---|---|---|---|
| | Bus | Size | | | | |
| | | (kW) | kVAR | p. f | | |
| SIMBO-Q **[54]** | 13 | 887.5 | 291.7 | 0.95 | 29 | 86.26 |
| | 24 | 1085.3 | 356.7 | 0.95 | | |
| | 30 | 1309.2 | 430.3 | 0.95 | | |
| QOSIMBO-Q **[54]** | 13 | 830.3 | 272.9 | 0.95 | 28.5 | 86.49 |
| | 24 | 1123.9 | 369.4 | 0.95 | | |
| | 30 | 1239.8 | 407.5 | 0.95 | | |
| HHO | 13 | 871.34 | 286.40 | 0.95 | 29.71 | 85.92 |
| | 24 | 1326.76 | 436.08 | 0.95 | | |
| | 30 | 1076.05 | 353.68 | 0.95 | | |
| IHHO | 14 | 793.81 | 260.91 | 0.95 | 28.5 | 86.49 |
| | 24 | 1132.44 | 372.21 | 0.95 | | |
| | 30 | 1257.76 | 413.41 | 0.95 | | |

*Table 7.9.- Comparison of LR obtained by different optimization algorithms and IHHO at optimal p.f (IEEE 33-bus system)*

| Algorithm | Optimal DG | | | | Power loss (kW) | LR % |
|---|---|---|---|---|---|---|
| | Bus | Size | | | | |
| | | (kW) | kVAR | p.f | | |
| BSOA**[68]** | 13 | 698 | 414 | 0.86 | 29.65 | 85.97 |
| | 29 | 402 | 399 | 0.71 | | |
| | 31 | 658 | 671 | 0.7 | | |
| BFOA **[69]** | 14 | 600 | 307 | 0.89 | 27.5 | 86.97 |
| | 25 | 598 | 402 | 0.83 | | |
| | 30 | 934 | 504 | 0.88 | | |
| HHO | 12 | 913.05 | 557.01 | 0.85 | 14.94 | 92.92 |
| | 24 | 882.86 | 616.60 | 0.82 | | |
| | 30 | 1079.05 | 734.19 | 0.83 | | |
| IHHO | 14 | 761.82 | 373.50 | 0.90 | 11.83 | 94.39 |
| | 24 | 1141.92 | 536.07 | 0.91 | | |
| | 30 | 1013.83 | 1003.21 | 0.71 | | |

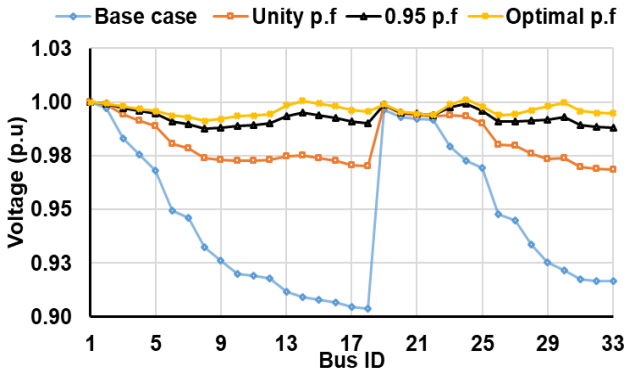


*Fig. 7.6.- Voltage profile of the IEEE 33-bus test system for IHHO*

For the traditional HHO and IHHO, a statistical analysis based on the best, average, and worst costs is carried out across ten runs to show the efficiency of the evolved algorithm. A description of this review is given in Table 7.10 and it is clear that the IHHO has the lowest values in all study cases. Additionally, the convergence characteristics for the HHO and IHHO are shown in Fig. 7.7.a, Fig. 7.7.b, and Fig. 7.7..c for unity p.f, 0.95 p.f, and optimal p.f respectively. These figures prove the efficiency of the IHHO over the conventional HHO.

*Table 7.10.- HHO and IHHO statistical analysis (IEEE 33-bus test system)*

| Algorithm | | Best Cost | Average Cost | Worst Cost |
|---|---|---|---|---|
| Unity p.f | HHO | 72.98 | 79.73 | 85.16 |
| | IHHO | 72.79 | 76.63 | 79.83 |
| 0.95 p.f | HHO | 29.71 | 37.38 | 45.89 |
| | IHHO | 28.55 | 36.81 | 46.00 |
| Optimal p.f | HHO | 14.94 | 21.70 | 27.32 |
| | IHHO | 11.83 | 15.83 | 24.98 |

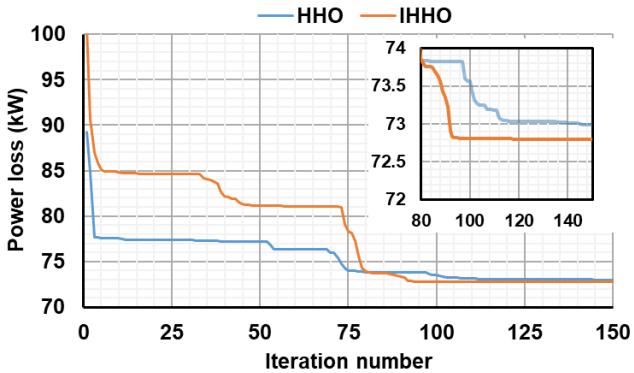


*(a) unity p.f,*

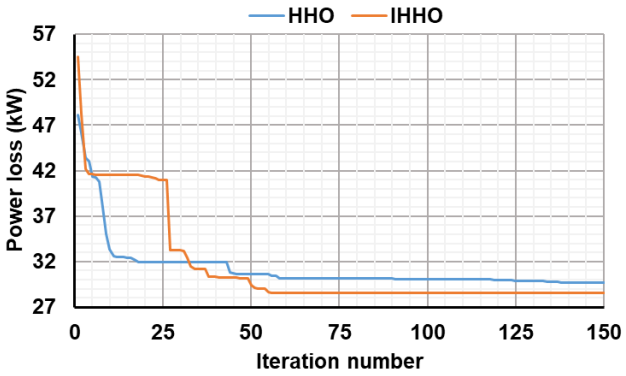


*(b) 0.95 p.f*

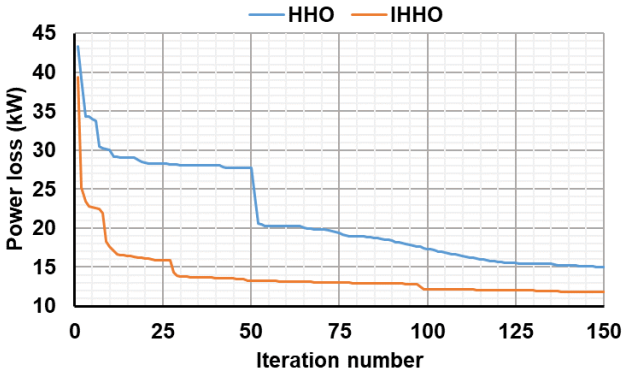


*(c) optimal p.f.*

*Fig. 7.7.- HHO and IHHO Convergence for DG integration in IEEE 33-bus test system at different operating p.f.*

### 7.4.2.2 IEEE 69-bus test system

Table 7.11, Table 7.12, and Table 7.13 summarize the result of the IHHO compared to the other optimization algorithms at unity, 0.95, and optimal p.f respectively. The highest LR is obtained by the HHO which equals 98.0 % at optimal p.f. the tables prove the feasibility of the IHHO in DG allocation.

The voltage profile of the IEEE 69-bus system has been improved due to the reduction of active power loss, as seen in Fig. 7.8.

The HHO and IHHO perform ten runs and the best, average, and worst costs are reported in Table 7.14. The robustness of the IHHO algorithm has been established. The results obtained suggest that the IHHO is more capable of achieving the optimum solution than the HHO, and this can be shown from the convergence features seen in Fig. 7.9.

*Table 7.11.- Comparison of LR obtained by different optimization algorithms and IHHO at unity p.f (IEEE 69-bus system)*

| Algorithm | Optimal DG | | Power loss (kW) | LR % |
|---|---|---|---|---|
| | Bus | Size (kW) | | |
| GAPSO [70] | 63 | 884.9 | 81.1 | 63.96 |
| | 61 | 1196 | | |
| | 21 | 910.5 | | |
| BFOA [69] | 27 | 295.4 | 75.23 | 66.56 |
| | 65 | 446 | | |
| | 61 | 1345.1 | | |
| SKHA[70] | 61 | 1719.1 | 68.15 | 69.10 |
| | 17 | 371 | | |
| | 11 | 527.1 | | |
| TLBO [74] | 15 | 591.9 | 72.41 | 67.82 |
| | 61 | 818.8 | | |
| | 63 | 900.3 | | |
| QOTLBO [74] | 18 | 533.4 | 71.63 | 68.17 |
| | 61 | 1198.6 | | |
| | 63 | 567.2 | | |
| SIMBO-Q [54] | 9 | 618.9 | 71.3 | 68.31 |
| | 17 | 529.7 | | |
| | 61 | 1500 | | |
| QOSIMBO-Q [54] | 9 | 833.6 | 71.0 | 68.44 |
| | 18 | 451.1 | | |
| | 61 | 1500 | | |
| HHO | 11 | 378.3 | 69.73 | 69.00 |
| | 17 | 480 | | |
| | 61 | 1706.1 | | |
| IHHO | 11 | 527.2 | 69.41 | 69.15 |
| | 17 | 382.5 | | |
| | 61 | 1719.4 | | |

*Table 7.12.- Comparison of LR obtained by different optimization algorithms and IHHO at 0.95 p.f (IEEE 69-bus system)*

| Algorithm | Optimal DG | | | | Power loss (kW) | LR % |
|---|---|---|---|---|---|---|
| | Bus | Size | | | | |
| | | (kW) | kVAR | p.f | | |
| SIMBO-Q [54] | 19 | 565.6 | 185.9 | 0.95 | 23.1 | 89.73 |
| | 61 | 1500.0 | 493.0 | 0.95 | | |
| | 64 | 422.0 | 138.7 | 0.95 | | |
| QOSIMBO-Q [54] | 17 | 582.8 | 191.6 | 0.95 | 22.8 | 89.87 |
| | 61 | 1500.0 | 493.0 | 0.95 | | |
| | 64 | 427.2 | 140.4 | 0.95 | | |
| HHO | 16 | 702.8 | 231.0 | 0.95 | 22.85 | 89.8 |
| | 50 | 286.6 | 94.2 | 0.95 | | |
| | 61 | 1890.9 | 621.5 | 0.95 | | |
| IHHO | 11 | 552.9 | 181.7 | 0.95 | 20.71 | 90.8 |
| | 18 | 419.5 | 137.9 | 0.95 | | |
| | 61 | 1879.2 | 617.7 | 0.95 | | |

*Table 7.13.- Comparison of LR obtained by different optimization algorithms and IHHO at optimal p.f (IEEE 69-bus system)*

| Algorithm | Optimal DG | | | | Power loss (kW) | LR % |
|---|---|---|---|---|---|---|
| | Bus | Size | | | | |
| | | (kW) | kVAR | p.f | | |
| PSO [60] | 11 | 498.0 | 334.7 | 0.83 | 4.61 | 97.7 |
| | 18 | 372.6 | 269.8 | 0.81 | | |
| | 61 | 1668.6 | 1208.1 | 0.81 | | |
| HHO | 17 | 270.8 | 385.5 | 0.57 | 6.58 | 97.1 |
| | 61 | 1541.4 | 1300.8 | 0.76 | | |
| | 66 | 696.8 | 177.7 | 0.97 | | |
| IHHO | 11 | 456.2 | 284.4 | 0.85 | 4.44 | 98.0 |
| | 18 | 389.2 | 275.6 | 0.82 | | |
| | 61 | 1714.8 | 1154.3 | 0.83 | | |

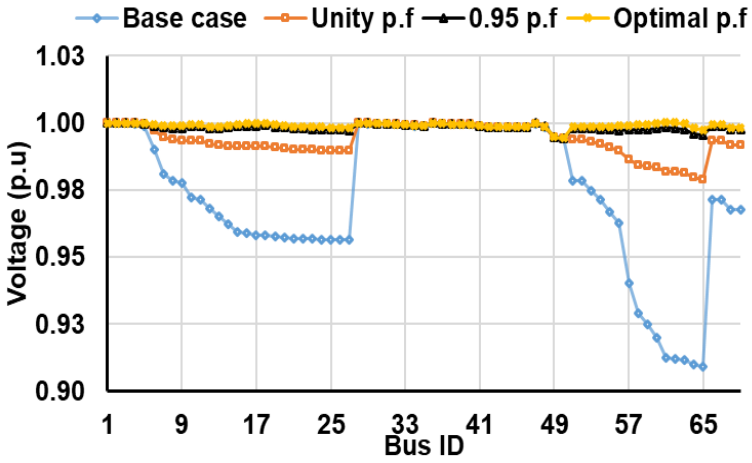


*Fig. 7.8.- Voltage profile of the IEEE 69-bus test system for IHHO.*

*Table 7.14.- HHO and IHHO statistical analysis (IEEE 69-bus test system)*

| Algorithm | | Best Cost | Average Cost | Worst Cost |
|---|---|---|---|---|
| Unity p.f | HHO | 69.73 | 73.03 | 80.11 |
| | IHHO | 69.41 | 69.94 | 71.14 |
| 0.95 p.f | HHO | 22.85 | 25.89 | 31.63 |
| | IHHO | 20.71 | 21.02 | 21.87 |
| Optimal p.f | HHO | 6.58 | 13.83 | 24.72 |
| | IHHO | 4.44 | 5.69 | 7.23 |

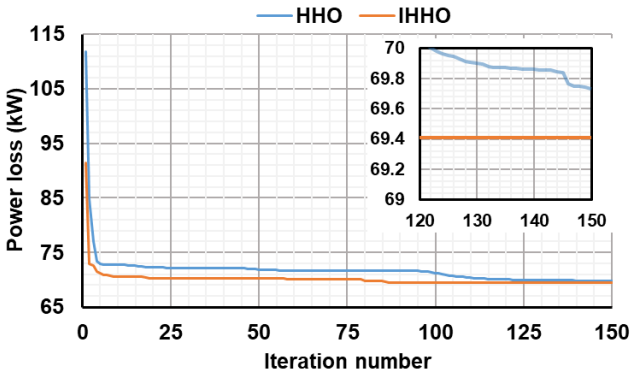


*(a) unity p.f,*

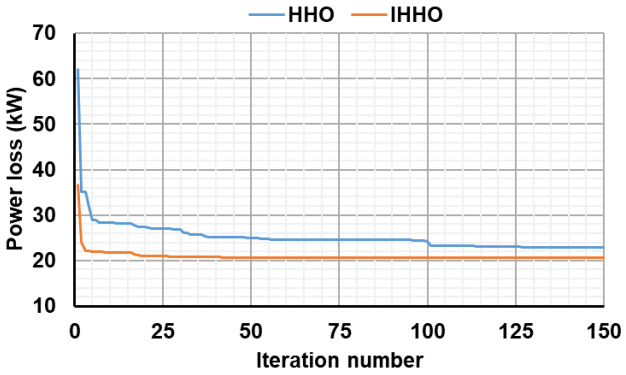


*(b) 0.95 p.f,*

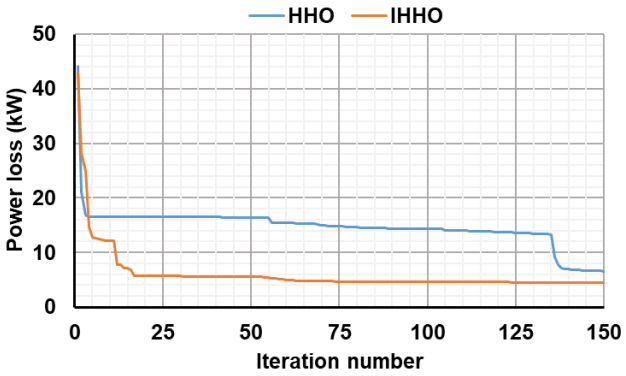


*(c) optimal p.f.*

*Fig. 7.9.- HHO and IHHO Convergence for DG integration in IEEE 69-bus test system at different operating p.f.*

## 7.4.3- CQOBMO

The problem of the DG allocation is studied using two IEEE test systems (IEEE 33-bus and IEEE 69-bus). The improved BMO based on the quasi oppositional and chaos map theories is applied to find the optimal size and location of the DG.

### 7.4.3.1 IEEE 33-bus test system

BMO, QOBMO, and CQOBMO are applied to find the best solutions (sizes and locations) of the three DG units for reducing the power loss (objective function), and

the results are given in Table 7.15.

It can be detected from Table 7.15 that using the CQOBMO_7, LR in the power loss quals 65.26% is achieved, which is higher than those obtained by LSF [61] (59.72 %), Fuzzy -IAS[67] which is 42.45%, 57.76% given in BSOA[68], 65.14% in BFOA [69], TLBO [74] which reaches 64.20 %, 64.88% in QOTLBO [74].

*Table 7.15.- Different optimization algorithms result for DG allocation in IEEE 33-bus system*

| Algorithm | DG allocation | | Power loss (kW) | LR % |
|---|---|---|---|---|
| | Location | Size (kW) | | |
| CQOBMO_7 | 13 | 788.58 | 73.29 | 65.26 |
| | 24 | 889.58 | | |
| | 30 | 1077.13 | | |
| QOBMO | 14 | 874.6 | 73.5 | 65.16 |
| | 24 | 960.36 | | |
| | 30 | 1012.29 | | |
| BMO | 14 | 749.59 | 75.81 | 64.04 |
| | 24 | 1234.59 | | |
| | 30 | 771.50 | | |
| QOTLBO [74] | 12 | 880.8 | 74.10 | 64.88 |
| | 24 | 1059.2 | | |
| | 29 | 1071.4 | | |
| TLBO [74] | 10 | 824.6 | 75.54 | 64.20 |
| | 24 | 1031.1 | | |
| | 31 | 886.2 | | |
| BSOA[68] | 13 | 632 | 89.05 | 57.76 |
| | 28 | 486 | | |
| | 31 | 550 | | |
| LSF [61] | 18 | 720 | 85.07 | 59.72 |
| | 33 | 810 | | |
| | 25 | 900 | | |
| BFOA [69] | 14 | 779 | 73.53 | 65.14 |
| | 25 | 880 | | |
| | 30 | 1083 | | |
| Fuzzy -IAS [67] | 32 | 2071 | 117.36 | 42.45 |
| | 30 | 1113.8 | | |
| | 31 | 150.3 | | |

Also, A comparison in the convergence characteristics between the improved algorithms and the conventional BMO is depicted in Fig. 7.10. The figure efficiency of the CQOBMO_7 over the QOBMO and BMO.

The impact of the DG placement on the voltage profile is displayed in Fig. 7.11. The optimal installation of the DGs in the distribution system leads to a significant enhancement in the voltage profile besides the minimization of power losses.

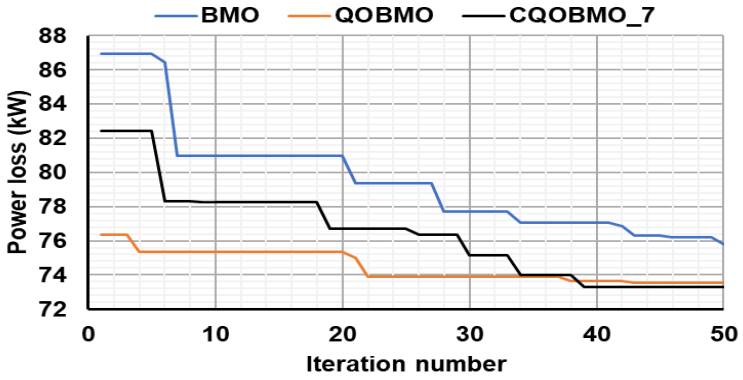


*Fig. 7.10.- Convergence characteristics of the BMO, QOBMO, And CQOBMO for the IEEE 33-bus test system*

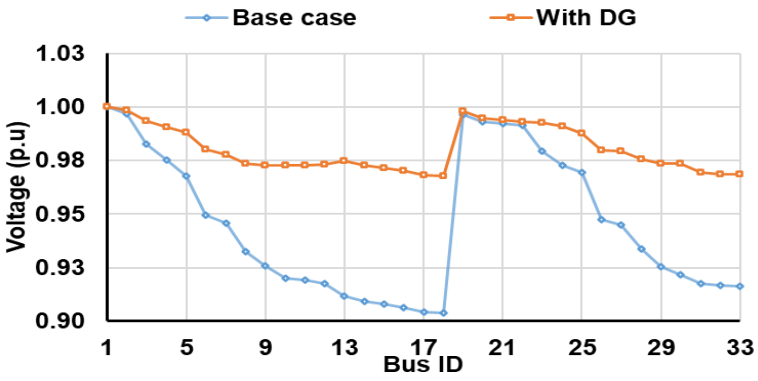


*Fig. 7.11.- Enhancement of the IEEE 33-bus voltage profile using optimal DG allocation.*

### 7.4.3.2 IEEE 69-bus test system

IEEE 69-bus is larger than the previous IEEE 33-bus, which is better to prove the performance of the improved algorithms. Three DG are suitably placed to minimize the power loss using the improved algorithms.

Table 7.16 yields the optimal allocations of the DGs in the IEEE 69 bus using different optimization algorithms compared to the CQOBMO_7, the QOBMO, and BMO. It is evident that the highest LR is 68.86 %, which obtained by CQOBMO_7 when integrated three DG at 11, 18, and 61 with active powers equal 573.02, 355.20, and 1583.50 kW, respectively. The convergence performance of CQOBMO_7, QOBMO, and BMO is displayed in Fig. 7.12. The figure shows the power of the CQOBMO_7 in reaching the optimal solution.

A considerable improvement in the voltage profile is accomplished when installing DGs in the IEEE 69 bus system, as presented in Fig. 7.13. And that approving the importance of the optimal settlement of the DG in the distribution systems.

*Table 7.16.- Different optimization algorithms result for DG allocation in IEEE 69-bus system*

| Algorithm | DG allocation | | Power loss (kW) | LR % |
|---|---|---|---|---|
| | Location | Size (kW) | | |
| CQOBMO_7 | 11 | 573.02 | 70.05 | 68.86 |
| | 18 | 355.20 | | |
| | 61 | 1583.50 | | |
| QOBMO | 21 | 246.45 | 70.43 | 68.69 |
| | 61 | 1704.45 | | |
| | 66 | 489.5 | | |
| BMO | 17 | 451.49 | 70.86 | 68.5 |
| | 55 | 569.4 | | |
| | 61 | 1683.92 | | |
| QOTLBO [74] | 18 | 533.4 | 71.63 | 68.17 |
| | 61 | 1198.6 | | |
| | 63 | 567.2 | | |
| TLBO [74] | 15 | 591.9 | 72.41 | 67.82 |
| | 61 | 818.8 | | |
| | 63 | 900.3 | | |
| BFOA [69] | 27 | 295.4 | 75.23 | 66.56 |
| | 65 | 446 | | |
| | 61 | 1345.1 | | |
| GAPSO [70] | 63 | 884.9 | 81.1 | 63.96 |
| | 61 | 1196 | | |
| | 21 | 910.5 | | |

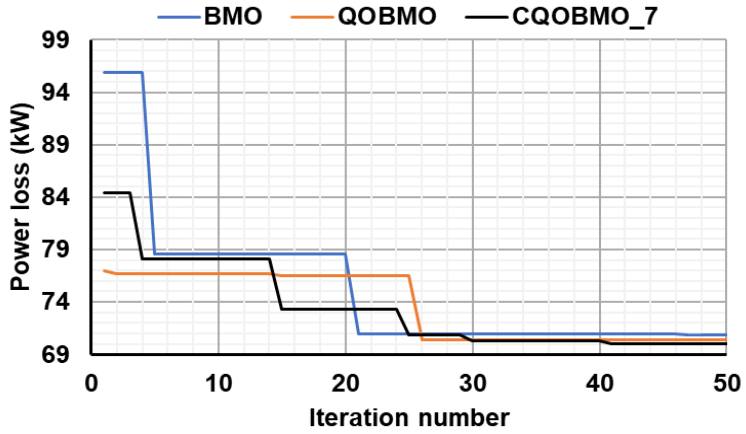


*Fig. 7.12.- Convergence characteristics of the BMO, QOBMO, And CQOBMO for the IEEE 69-bus test system.*

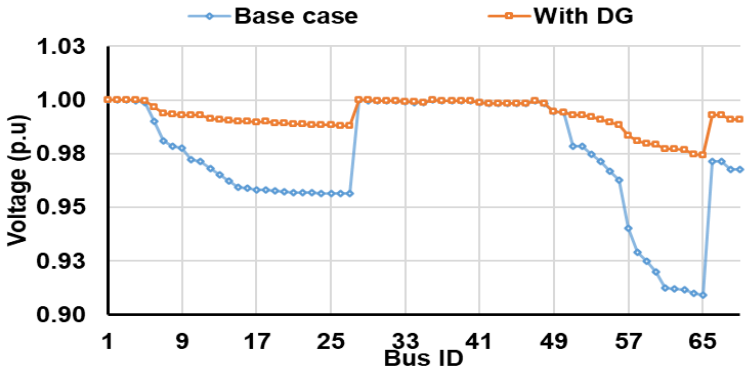


*Fig. 7.13.- Enhancement of the IEEE 69-bus voltage profile using optimal DG allocation.*

## 7.4.4- ATGA

The proposed ATGA is used to optimally allocate multiple types of DGs units in IEEE 33-bus, 69-bus RDSs. four case studies are performed on each test system. Hence, the results of Three different DG types are used to be presented: DG Type I, II, and III:

**Case 1:** Base case (without DGs).

**Case 2:** Integrating 3 DGs Type I.

**Case 3:** Integrating 3 DGs Type II.

**Case 4:** Integrating 3 DGs Type III.

ATGA's results are carried out with 30 runs to monitor their performance and extensively in contrast with original TGA and other optimization algorithms. The P_V curve is drawn using the PSAT package for the calculation of the voltage stability and maximum loadability.

### 7.4.4.1 IEEE 33-bus test system

Case 2 (see Table 7.17), the suggested ATGA provides LR attains 65.5 % which is better than 65.47 % in the original TGA, 64.82 % in PSO [99], 65.45 % from Hybrid [60], 65.14 % in BFOA, 57.76% in BSOA, and 61.62 % in the IA [61] and about the same as the metaheuristic (MVGWO, PSO [60], and SKHA). However, the proposed ATGA has the very best rate of convergence as demonstrated in Fig. 7.14.a. In comparison, the 30-run Boxplot is drawn and demonstrates the efficiency of the proposed ATGA to the original TGA.

In Case 3 (see Table 7.18), The LR of ATGA is greater than those of MVGWO, PSO, and Hybrid. Fig. 7.14.b Shows the viability of the proposed ATGA relative to the original TGA convergence rate and the Boxplot.

As three DG type III are combined (see Table 7.19), the significant LR is achieved. In this case, the LR for the ATGA amounts to 94.45%, in TGA, 94.41% of the PSO and 92.56% of BFOA, which is greater than 91.70%. In comparison, the ATGA still performs much better than the initial TGA as seen in Fig. 7.14.c.

*Table 7.17.- Comparison of LR obtained by different optimization algorithms and ATGA at Case 2 (IEEE 33-bus system)*

| Algorithm | DG allocation | | Power loss (kW) | LR % |
|---|---|---|---|---|
| | Location | Size (kW) | | |
| ATGA | 13 | 833.05 | 72.80 | 65.50 |
| | 24 | 1133.3 | | |
| | 30 | 1035.8 | | |
| TGA | 13 | 797.99 | 72.86 | 65.47 |
| | 24 | 1087.6 | | |
| | 30 | 1028.4 | | |
| MVGWO [99] | 13 | 802 | 72.78 | 65.50 |
| | 24 | 1091 | | |
| | 30 | 1054 | | |
| PSO [99] | 12 | 876 | 74.22 | 64.82 |
| | 24 | 893 | | |
| | 31 | 1122 | | |
| Hybrid [60] | 13 | 790 | 72.89 | 65.45 |
| | 24 | 1070 | | |
| | 30 | 1010 | | |
| PSO [60] | 14 | 770 | 72.79 | 65.50 |
| | 24 | 1090 | | |
| | 30 | 1070 | | |
| BFOA [69] | 14 | 779 | 73.53 | 65.14 |
| | 25 | 880 | | |
| | 30 | 1083 | | |
| BSOA [68] | 13 | 632 | 89.05 | 57.76 |
| | 28 | 486 | | |
| | 31 | 550 | | |
| SKHA [70] | 13 | 802 | 72.79 | 65.50 |
| | 24 | 1091 | | |
| | 30 | 1054 | | |
| IA [61] | 6 | 900 | 81.05 | 61.62 |
| | 12 | 900 | | |
| | 31 | 720 | | |

*Table 7.18.- Comparison of LR obtained by different optimization algorithms and ATGA at Case 3 (IEEE 33-bus system)*

| Algorithm | DG allocation | | Power loss (kW) | LR % |
|---|---|---|---|---|
| | Location | Size (kVAR) | | |
| ATGA | 13 | 364.83 | 138.30 | 34.45 |
| | 24 | 523.55 | | |
| | 30 | 1032.93 | | |
| TGA | 13 | 406.88 | 138.51 | 34.35 |
| | 25 | 446.36 | | |
| | 30 | 1024.67 | | |
| MVGWO [99] | 11 | 440 | 138.39 | 34.41 |
| | 24 | 520 | | |
| | 30 | 1000 | | |
| PSO [99] | 12 | 336 | 143.58 | 31.95 |
| | 23 | 1449 | | |
| | 31 | 841 | | |
| Hybrid [60] | 13 | 360 | 138.37 | 34.42 |
| | 24 | 510 | | |
| | 30 | 1020 | | |

*Table 7.19.- Optimal sizes and locations at Case 4 (DG Type III) for IEEE 33-bus*

| Algorithm | DG allocation | | | Power loss (kW) | LR % |
|---|---|---|---|---|---|
| | Location | Size (kW) | Size (kVAR) | | |
| ATGA | 13 | 790.63 | 368.81 | 11.7 | 94.45 |
| | 24 | 1080.90 | 521.88 | | |
| | 30 | 1026.89 | 1018.05 | | |
| TGA | 15 | 635.01 | 345.32 | 17.50 | 91.70 |
| | 24 | 718.38 | 94.54 | | |
| | 30 | 1285.67 | 1086.60 | | |
| Hybrid [60] | 13 | 785.70 | 380.53 | 11.7 | 94.45 |
| | 24 | 1055.54 | 540.77 | | |
| | 30 | 1021.69 | 1013.35 | | |
| PSO [60] | 13 | 785.33 | 357.81 | 11.8 | 94.41 |
| | 24 | 1069.2 | 517.84 | | |
| | 30 | 1016.0 | 1007.7 | | |
| BFOA [69] | 12 | 85 | 400 | 15.07 | 92.56 |
| | 25 | 750 | 350 | | |
| | 30 | 860 | 850 | | |

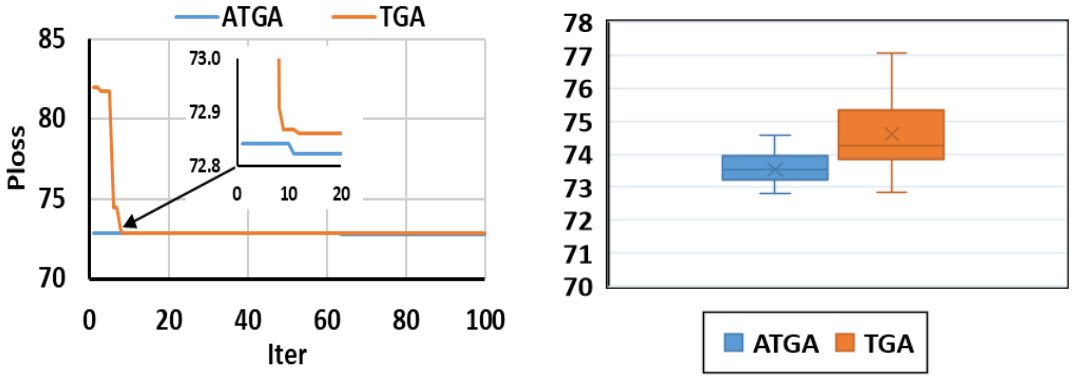


*a. Case 2*

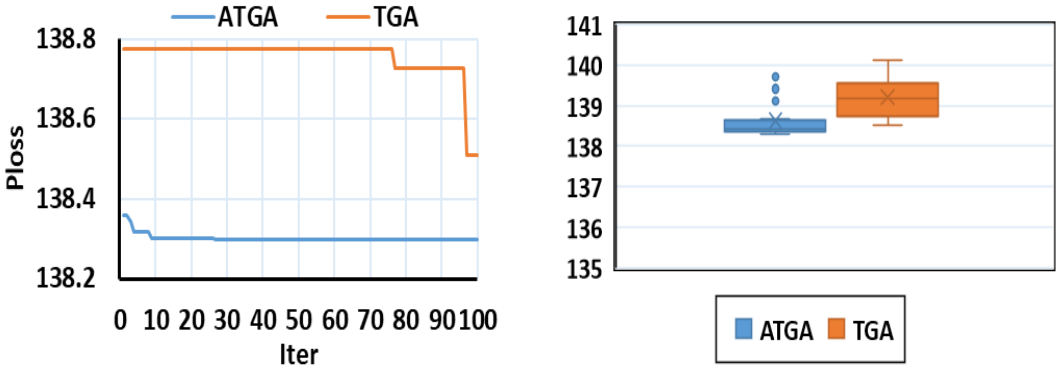


*b. Case 3*

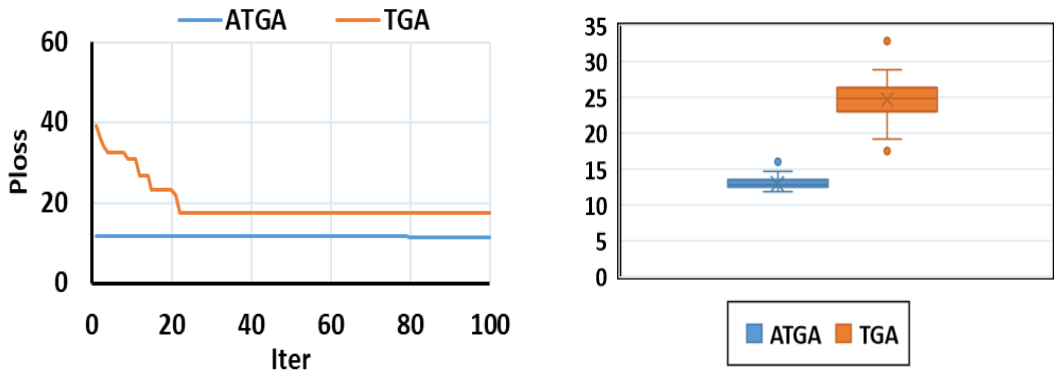


*c. Case 4*

*Fig. 7.14.- ATGA and TGA convergence rate and Boxplot in IEEE 33-bus system at different case studies*

The primary purpose of incorporating DGs into the RDS is to boost the voltage profile and increase the stability of the system voltage. Fig. 7.15 In the four studies, the voltage profiles of the IEEE 33-bus system are shown. It is apparent that Case 4's injection of active and reactive powers significantly raises the voltage profiles relative to the other three cases. However, in the voltage stability assessment for the lowest bus 18, Case 3 and Case 4 increase the system loadability $\lambda_{max}$ as shown in the P_V curve in Fig. 7.16 and written in Table 7.20. Where the $\lambda_{max}$ increased from 3.40% at Case 1 (base case) to 4.37 % in Case 3 and Case 4.

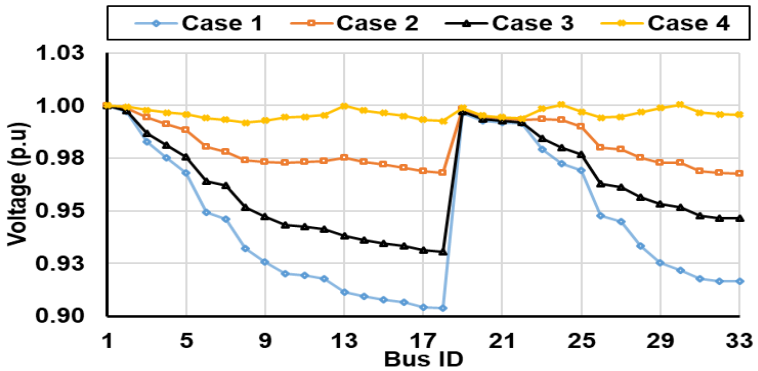


*Fig. 7.15.- Voltage profile for IEEE 33-bus at different case studies*

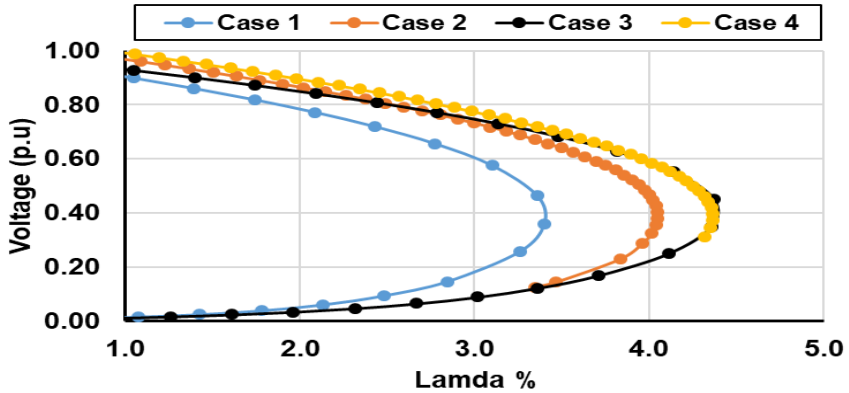


*Fig. 7.16.- P_V curve for bus 18 at different case studies*

*Table 7.20.- Maximum loadability for IEEE 33-bus at different case studies*

| Case | Case 1 | Case 2 | Case 3 | Case 4 |
|---|---|---|---|---|
| $\lambda_{max}$ % | 3.40 | 4.05 | 4.37 | 4.37 |

### 7.4.4.2 IEEE 69-bus test system

Table 7.21, Table 7.22, and Table 7.23 provide the optimal capacities and locations for various DG types into the IEEE 69-bus RDS. The highest LR is accomplished using the ATGA which goes to 69.14% when connecting three DG type I (see Table 7.21). The considerable LR is obtained in Case 4 (see Table 7.23) where the losses reduced to 4.27 kW due to the injected active and reactive power of DG type III.

*Table 7.21.- Comparison of LR obtained by different optimization algorithms and ATGA at Case 2 (IEEE 69-bus system)*

| Algorithm | DG allocation | | Power loss (kW) | LR % |
|---|---|---|---|---|
| | Location | Size (kW) | | |
| ATGA | 11 | 509.08 | 69.41 | 69.14 |
| | 17 | 382.73 | | |
| | 61 | 1723.20 | | |
| TGA | 11 | 391.12 | 69.88 | 68.94 |
| | 20 | 359.52 | | |
| | 61 | 1814.97 | | |
| MVGWO [99] | 11 | 520 | 69.43 | 69.14 |
| | 18 | 395 | | |
| | 61 | 1720 | | |
| PSO [99] | 21 | 529 | 74.29 | 66.98 |
| | 50 | 446 | | |
| | 62 | 2000 | | |
| Hybrid [60] | 11 | 510 | 69.54 | 69.09 |
| | 17 | 380 | | |
| | 61 | 1670 | | |
| PSO [60] | 11 | 460 | 69.54 | 69.09 |
| | 17 | 440 | | |
| | 61 | 1700 | | |
| SKHA [70] | 11 | 527.17 | 68.15 | 69.10 |
| | 17 | 370.88 | | |
| | 61 | 1719.07 | | |
| IA [61] | 11 | 340 | 68.38 | 68.82 |
| | 17 | 51 | | |
| | 61 | 1700 | | |

*Table 7.22.- Comparison of LR obtained by different optimization algorithms and ATGA at Case 3 (IEEE 69-bus system)*

| Algorithm | DG allocation | | Power loss (kW) | LR % |
|---|---|---|---|---|
| | Location | Size (kVAR) | | |
| ATGA | 11 | 357.36 | 145.17 | 35.47 |
| | 19 | 245.59 | | |
| | 61 | 1205.18 | | |
| TGA | 10 | 404.42 | 145.64 | 35.26 |
| | 21 | 207.81 | | |
| | 61 | 1134.83 | | |
| MVGWO [99] | 11 | 374 | 145.16 | 35.38 |
| | 18 | 240 | | |
| | 61 | 1217 | | |
| PSO [99] | 15 | 359 | 147.69 | 34.36 |
| | 40 | 1000 | | |
| | 61 | 1449 | | |
| Hybrid [60] | 11 | 330 | 145.24 | 35.45 |
| | 18 | 250 | | |
| | 61 | 1190 | | |
| PSO/GAMS [100] | 11 | 30.29 | 147.25 | 34.50 |
| | 18 | 251.63 | | |
| | 61 | 1159.57 | | |

*Table 7.23.- Comparison of LR obtained by different optimization algorithms and ATGA at Case 4 (IEEE 69-bus system)*

| Algorithm | DG allocation | | | Power loss (kW) | LR % |
|---|---|---|---|---|---|
| | Location | Size (kW) | Size (kVAR) | | |
| ATGA | 11 | 495.29 | 354.04 | 4.27 | 98.10 |
| | 17 | 378.84 | 251.65 | | |
| | 61 | 1673.56 | 1196.21 | | |
| TGA | 17 | 573.50 | 136.39 | 9.17 | 95.92 |
| | 50 | 682.27 | 741.97 | | |
| | 61 | 1846.46 | 1053.96 | | |
| Hybrid [60] | 18 | 369.60 | 306.26 | 4.3 | 98.1 |
| | 61 | 1709.80 | 1148.99 | | |
| | 66 | 434.60 | 303.35 | | |
| PSO [60] | 11 | 498.00 | 334.66 | 4.61 | 97.7 |
| | 18 | 372.60 | 269.76 | | |
| | 61 | 1668.60 | 1208.05 | | |

In relation to the original TGA, the performance of the proposed ATGA is shown in Fig. 7.17 in terms of all case studies. The figure demonstrates the ATGA 's dominance in the convergence rate. In addition, owing to the hybridization of the analytical algorithm, the boxplot for the 30 runs represents the enhancement in the proposed algorithm.

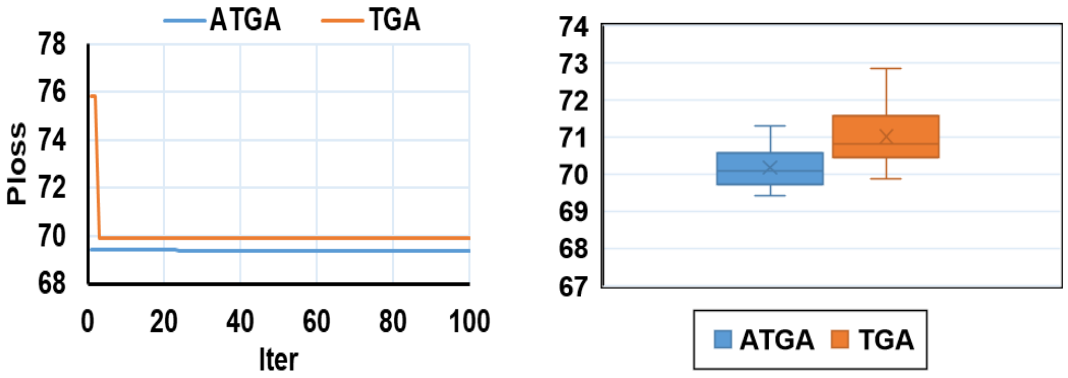


*a. Case 2*

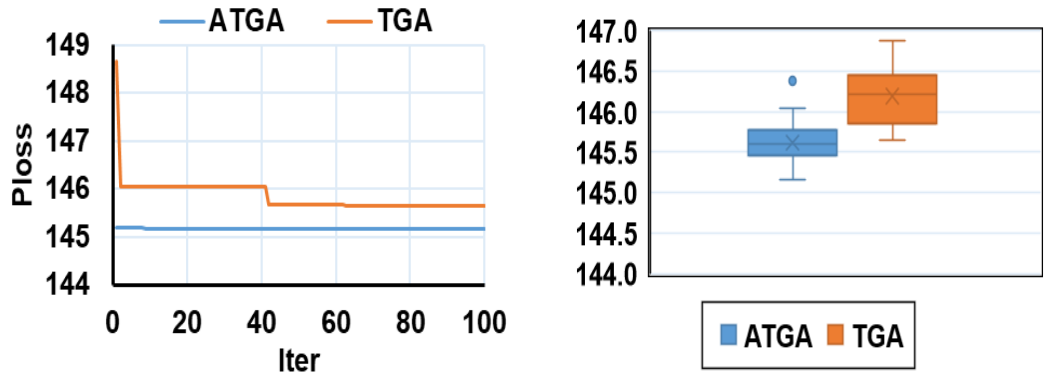


*b. Case 3*

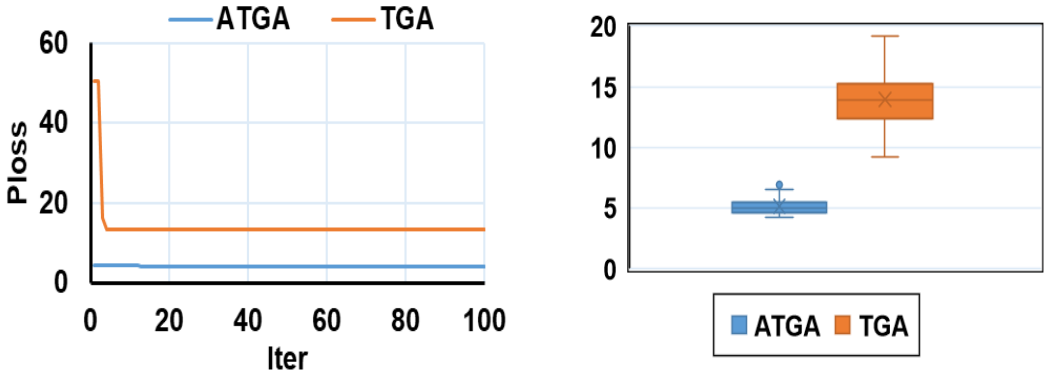


*c. Case 4*

*Fig. 7.17.- Convergence rate and Boxplot for ATGA and TGA in IEEE 69-bus at different case studies*

The voltage profile and reliability of the DG installation are also investigated to demonstrate the effect on the RDS. Fig. 7.18 explains the progress of all IEEE 69-bus buses in all case studies and it is clear that, unlike the other cases, case 4 has the greatest improvement.

Besides, the P_V curve of bus 65 is exposed in Fig. 7.19 where the maximum loadability $\lambda_{max}$ is obtained at Case 4 as given in Table 7.24 and equal 4.21 %.

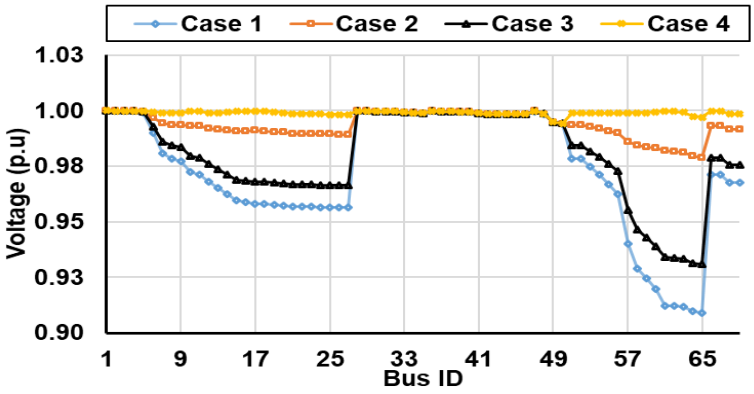


*Fig. 7.18.- Voltage profile for IEEE 69-bus at different case studies*

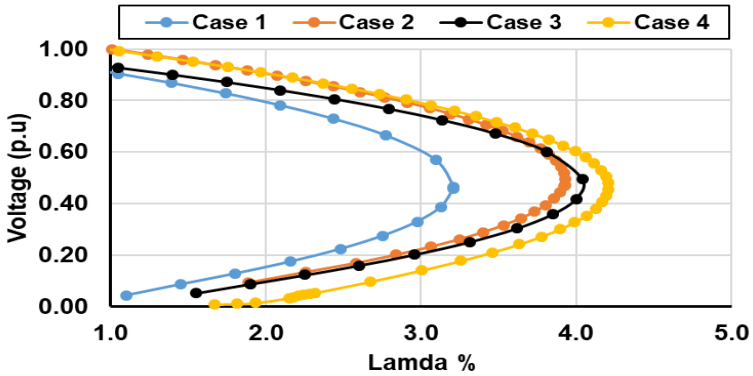


*Fig. 7.19.- P_V curve for bus 65 at different case studies*

*Table 7.24.- Maximum loadability for IEEE 69-bus at different case studies*

| Case | Case 1 | Case 2 | Case 3 | Case 4 |
|---|---|---|---|---|
| $\lambda_{max}$ % | 3.21 | 3.93 | 4.04 | 4.21 |

# 7.5.- Results of DG Allocation Using Improved Multi-Objective Optimization Algorithms

This section depicts the application of the improved multi-objective algorithms in various scenarios of DG allocation.

## 7.5.1- MOCSCA

The optimal allocation of three DGs units is achieved to minimize the total power loss, the total VD (using (2.7)) and maximize VSI as a multi-objective optimization problem. The grey relation analysis is employed with the MOCSCA to achieve the best compromise solution.

### 7.5.1.1 IEEE 33-bus test system

Compared with the MOSCA and other optimization algorithms, Table 7.25 presents the obtained results of the proposed MOCSCA based on an iterative chaos map. The suggested MOCSCA has the lowest power loss and the highest VSI (88.43 kW and

0.9572 p.u, respectively), higher than MOSCA's 89.92 kW and 0.9502 p.u. However, using TLBO, and QOTLBO, the minimum VD was obtained.

Fig. 7.20 indicates the non-dominated solution that the proposed MOCSCA and the initial MOSCA have obtained. The comparison of the initial MOSCA to the proposed MOCSCA is seen in Fig. 7.21, which illustrates the benefit of using the chaotic map to reduce the proposed algorithm's SP-metric.

*Table 7.25.- Results of MOCSCA and different optimization algorithms (IEEE 33-bus test system)*

| Algorithm | Bus | Size (MW) | $P_{loss}$ (kW) | VD (p.u) | VSI (p.u) |
|---|---|---|---|---|---|
| Base case | - | - | 202.68 | 0.1337 | 0.6691 |
| GA [73] | 11 | 1.5000 | 106.3 | 0.0407 | 0.949 |
| | 29 | 0.4228 | | | |
| | 30 | 1.0714 | | | |
| PSO [73] | 8 | 1.1768 | 105.3 | 0.0335 | 0.9255 |
| | 13 | 0.9816 | | | |
| | 32 | 0.8297 | | | |
| GA/PSO [73] | 11 | 0.9250 | 103.4 | 0.0124 | 0.9508 |
| | 16 | 0.8630 | | | |
| | 32 | 1.2000 | | | |
| TLBO [74] | 12 | 1.1826 | 124.7 | 0.0011 | 0.9503 |
| | 28 | 1.1913 | | | |
| | 30 | 1.1863 | | | |
| QOTLBO [74] | 13 | 1.0834 | 103.4 | 0.0011 | 0.9530 |
| | 26 | 1.1876 | | | |
| | 30 | 1.1992 | | | |
| TM [80] | 15 | 0.7199 | 102.30 | 0.0040 | 0.9371 |
| | 26 | 0.7199 | | | |
| | 33 | 1.4397 | | | |
| MOTA [80] | 7 | 0.9800 | 96.30 | 0.0014 | 0.9551 |
| | 14 | 0.9600 | | | |
| | 30 | 1.3400 | | | |
| MOSCA | 13 | 1.2476 | 89.92 | 0.0023 | 0.9502 |
| | 25 | 1.0617 | | | |
| | 32 | 1.2235 | | | |
| MOCSCA | 13 | 1.0980 | 88.43 | 0.0016 | 0.9572 |
| | 24 | 0.9865 | | | |
| | 30 | 1.5849 | | | |

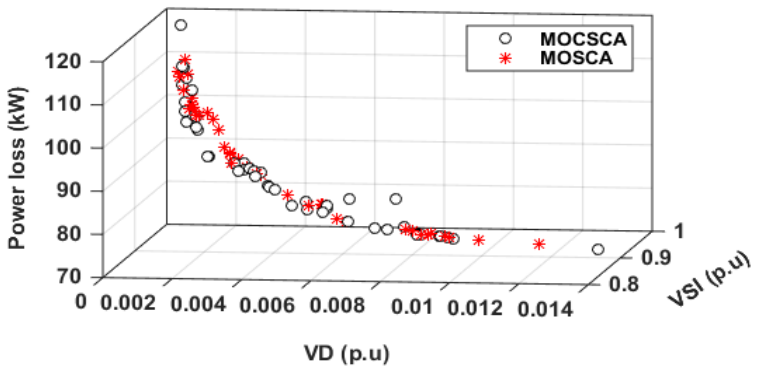


*Fig. 7.20.- MOCSCA and MOSCA Pareto optimal set in IEEE 33-bus test system*

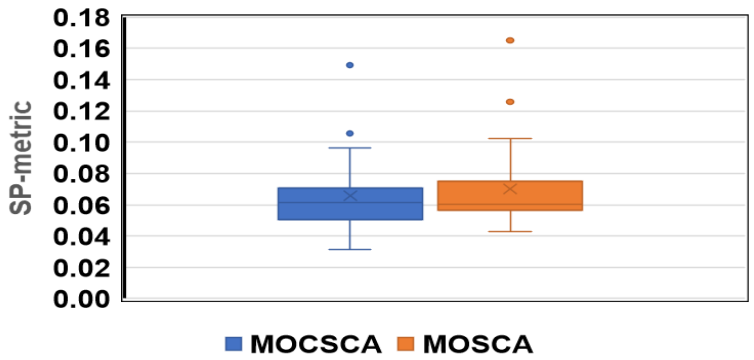


*Fig. 7.21.- MOCSCA and MOSCA's SP-metric in IEEE 33-bus test system*

### 7.5.1.2 IEEE 69-bus test system

The MOCSCA is used by the IEEE 69-bus system and Table 7.26 displays the effects of the optimum scale and location of the various DGs. The proposed MOCSCA has a minimal power loss, VD, and maximum VSI of 79.69 kW, 0.0002 p.u, and 0.9798 p.u, respectively. The better results achieved compared with the other optimization algorithms are known to be these values.

*Table 7.26.- Results of MOCSCA and different optimization algorithms (IEEE 69-bus test system)*

| Algorithm | Bus | Size (MW) | $P_{loss}$ (kW) | VD (p.u) | VSI (p.u) |
|---|---|---|---|---|---|
| Base case | - | - | 224.95 | 0.0992 | 0.6852 |
| GA [73] | 21 | 0.9297 | 89.0 | 0.0012 | 0.9705 |
| | 62 | 1.0752 | | | |
| | 64 | 0.9848 | | | |
| PSO [73] | 17 | 0.9925 | 83.2 | 0.0049 | 0.9676 |
| | 61 | 1.1998 | | | |
| | 63 | 0.7956 | | | |
| GA/PSO [73] | 21 | 0.9105 | 81.1 | 0.0031 | 0.9768 |
| | 61 | 1.1926 | | | |
| | 63 | 0.8849 | | | |
| TLBO [74] | 13 | 1.0134 | 82.2 | 0.0008 | 0.9745 |
| | 61 | 0.9901 | | | |
| | 62 | 1.1601 | | | |
| QOTLBO [74] | 15 | 0.8114 | 80.6 | 0.0007 | 0.9769 |
| | 61 | 1.1470 | | | |
| | 63 | 1.0022 | | | |
| SIMBO-Q [101] | 15 | 0.7722 | 80.0 | 0.0007 | 0.9770 |
| | 61 | 1.3526 | | | |
| | 62 | 0.8232 | | | |
| QOSIMBO-Q[101] | 15 | 0.7754 | 79.7 | 0.0007 | 0.9768 |
| | 61 | 1.4385 | | | |
| | 63 | 0.7235 | | | |
| MOSCA | 21 | 0.7858 | 83.12 | 0.0010 | 0.9782 |
| | 61 | 1.1265 | | | |
| | 61 | 1.0713 | | | |
| MOCSCA | 21 | 0.4531 | 79.69 | 0.0002 | 0.9798 |
| | 61 | 2.1917 | | | |
| | 67 | 0.6763 | | | |

The relation between the original MOSCA and the proposed MOCSCA is rendered using the Pareto ideal set and the SP-metric as seen in Fig. 7.22 , and Fig. 7.23 for example. The improved algorithm also provides better efficiency due to a chaotic iterative map.

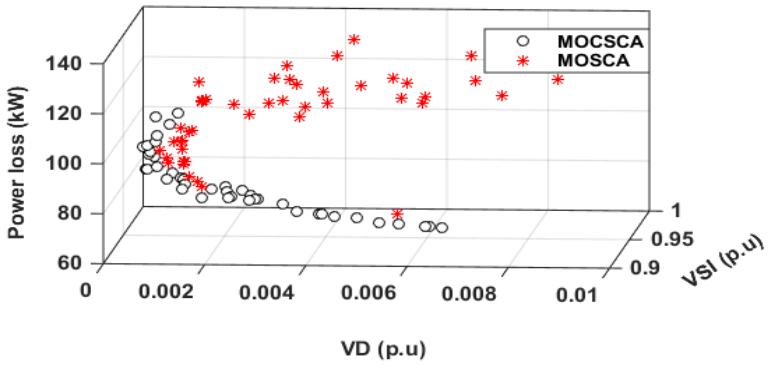


*Fig. 7.22.- MOCSCA and MOSCA's Pareto optimal set in IEEE 69-bus test system*

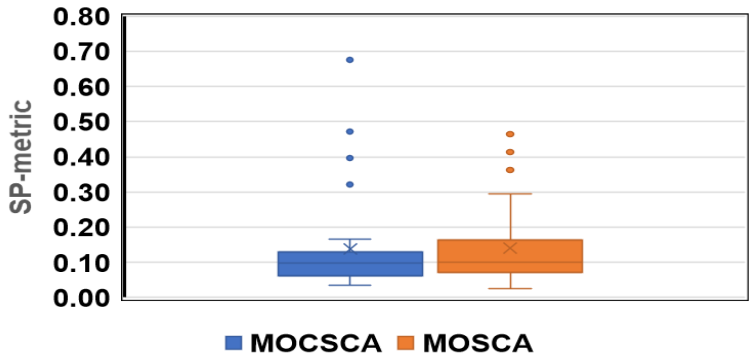


*Fig. 7.23.- MOCSCA and MOSCA's SP-metric in IEEE 69-bus test system*

## 7.5.2- MCSSA

The proposed MCSSA3 with fuzzy decision making is utilized to optimally allocate multiple PV units at rated loading condition to minimize the $P_{loss}, VD$ (using(2.8)), and maximize the $VSI$.

### 7.5.2.1 Performance analysis for MCSSA

The main objective of this analysis is to prove the effectiveness of the proposed MCSSA, its performance, and its accuracy when incorporating different chaotic maps to MSSA. Furthermore, to determine the most efficient chaotic maps among the ten maps which can be integrated into MSSA. The ten maps are used in the basic MSSA and numbered from MCSSA1 to MCSSA10 corresponding to the selected chaos map as arranged in Table 6.1. A single DG unit is employed in this analysis to be optimally allocated in the IEEE 33-bus at the rated loading condition to obtain the optimized

values for the three objective functions. The comparison among all algorithms is accomplished using the computation time and SP- metric.

*Table 7.27.- Computation time per second for different optimization algorithms*

| Algorithm | Mean | STD | Algorithm | Mean | STD |
|---|---|---|---|---|---|
| MSSA | 30.40 | 0.60 | MOPSO | 34.87 | 0.66 |
| MCSSA1 | 29.96 | 0.92 | NSGA II | 70.67 | 0.67 |
| MCSSA2 | 30.41 | 0.90 | SPEA2 | 41.93 | 0.23 |
| MCSSA3 | 28.70 | 0.14 | PESA-II | 38.08 | 0.26 |
| MCSSA4 | 30.08 | 0.64 | MOEA/D | 47.28 | 3.97 |
| MCSSA5 | 30.77 | 0.96 | MOALO | 38.54 | 1.18 |
| MCSSA6 | 30.33 | 0.78 | MOGWO | 45.22 | 0.30 |
| MCSSA7 | 30.73 | 0.98 | | | |
| MCSSA8 | 30.40 | 0.65 | | | |
| MCSSA9 | 30.44 | 0.86 | | | |
| MCSSA10 | 30.20 | 0.70 | | | |

Fig. 7.24. a exhibits the boxplot for all proposed MCSSA algorithms and the basic MSSA through 30 runs. It can be noted that the MCSSA3 which uses Gauss/mouse chaotic map gives the lowest *SP* compared with the other proposed algorithms. Nevertheless, MCSSA3 is compared with the well-known multi-objective optimization algorithms mentioned in the literature such as PAES2, NSGA-II, SPEAII, MOPSO, and new metaheuristic algorithms such as Multi-objective Ant Lion Optimizer (MOALO) and Multi-objective Grey Wolf Optimizer (MOGWO). Also, the proposed MCSSA3 proves its superiority as shown in Fig. 7.24.b. The mean and standard deviation (STD) of the computation time during 30 runs for all algorithms are summarized in Table 7.27. It can be observed that the MCSSA3 has the lowest computation time among all algorithms. Consequently, in the next section, the MCSSA3 is used to find the optimal setting and scheduling the PV and BES in RDSs.

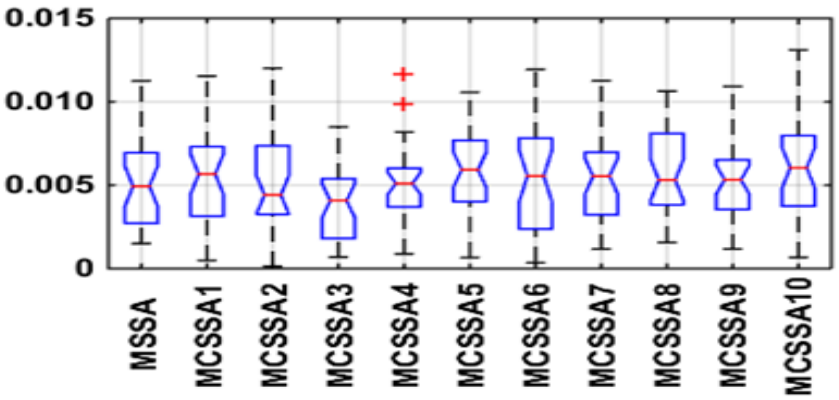


*a. MSSA with ten Chaotic maps*

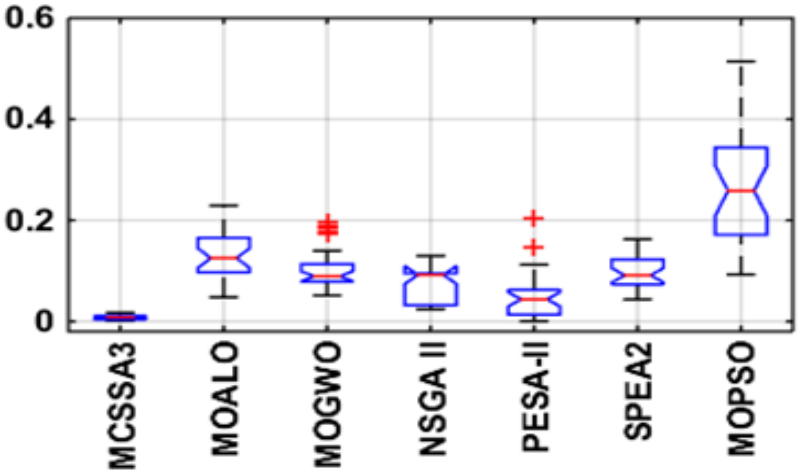


*b. Comparison between the well-known optimization algorithms*
*Fig. 7.24.- Boxplot of the SP-metric for IEEE 33-bus system*

### 7.5.2.2 IEEE 33-bus test system

At the rated demand, the power flow results indicate that the total active power losses are 202.67 kW, the minimum voltage is 0.9131 p.u at bus # 18, total VD is 11.71, and the minimum VSI is 0.6951.

The optimal sizes and locations of the PVDG units are achieved using the proposed MCSSA3 incorporated with developed fuzzy logic decision making and compared with other optimization algorithms as summarized in Table 7.28. Fig. 7.25 shows the non-dominated solutions and the best compromise solution obtained by MCSSA3 when installing one, two, and three PVDG units. For 1 PV, the best compromise solution is achieved when the three objective functions $P_{loss}$, $VD$, and $VSI$ are 106.3 kW, 2.379, and 0.8373, respectively with a maximum installed PV capacity of 2741.46 kW at bus #7.

Compared to the results in the literature as in Table 7.28, the proposed MCSSA3 gives the best results in reducing the power losses and maintaining the bus voltages within the limits where the LR reaches 47.46 %, 55.67%, and 63.26% with the minimum voltages 0.9566, 0.9742, and 0.9758 p.u for 1 PV, 2 PVs, and 3 PVs respectively. From the obtained results, it can be observed that the integration of 3 PV units into the IEEE 33-bus system significantly enhances its operational performance.

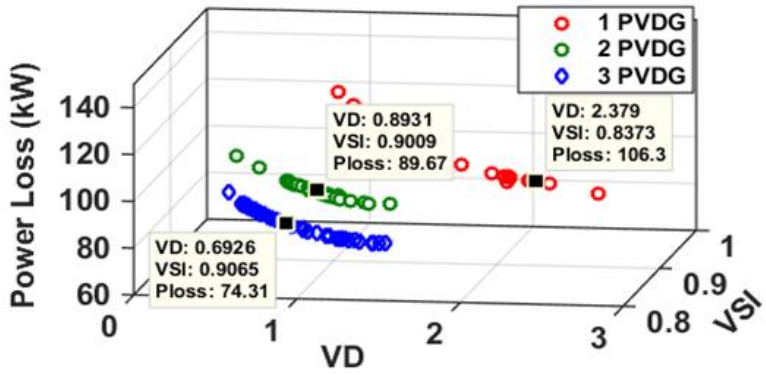


*Fig. 7.25.- Pareto Optimal Front for the IEEE 33-bus system*

*Table 7.28.- Obtained results of IEEE 33-bus with MCSSA*

| Algorithm | | DAPSO [102] | IA [61] | LSF [61] | BSOA [68] | MCSSA3 |
|---|---|---|---|---|---|---|
| 1 PVDG | (Bus) Size (kW) | (8) 1212 | (6) 2601 | (18) 743 | (8) 1857.5 | (7) 2741.46 |
| | $P_{loss}$ (kW) | 127.17 | 111.1 | 146.82 | 118.12 | 106.27 |
| | LR % | 39.7 | 47.39 | 30.48 | 44.01 | 47.46 |
| | $V_{min}$ | 0.9349 | 0.9425 | - | 0.9441 | 0.9566 |
| 2 PVDGs | (Bus)Size (kW) | (13) 1227 (32) 738 | (6) 1800 (14) 720 | (18) 720 (33) 900 | (13) 880 (31) 924 | (15) 857.62 (29) 1490.22 |
| | $P_{loss}$ (kW) | 95.93 | 91.63 | 100.69 | 89.34 | 89.67 |
| | LR % | 54.53 | 56.61 | 52.32 | 57.62 | 55.67 |
| | $V_{min}$ | 0.9651 | 0.9539 | - | 0.9665 | 0.9742 |
| 3 PVDGs | (Bus)Size (kW) | (10) 681 (18) 600 (31) 719 | (6) 900 (12) 900 (31) 720 | (18) 720 (25) 900 (33) 810 | (13) 632 (28) 487 (31) 550 | (13) 958.89 (24) 1126.39 (30) 1204.87 |
| | $P_{loss}$(kW) | 92.55 | 81.05 | 85.07 | 89.05 | 74.31 |
| | LR % | 56.13 | 61..62 | 59.72 | 57.76 | 63.26 |
| | $V_{min}$ | 0.9654 | 0.9690 | - | 0.9554 | 0.9758 |

### 7.5.2.3 94-bus Portuguese test system

The proposed MCSSA3 is applied to the real Portuguese RDS 94-bus system. The active and reactive power losses of the base case are 362.8527 kW and 504.0351 kVAR, respectively. Due to the high length of the line branch and heavy load demand, the voltage profile of this system is not subject to the limits where the minimum voltage is 0.8485 p.u on bus #92. In this system, scenario 1 and scenario 3 are used with the three PV units which give the best results.

Fig. 7.26 displays the Pareto optimal front for the three objective functions to place three PV units, the best compromise solution obtained by the developed fuzzy logic decision making is shown in the figure and Table 7.29. This table presents the optimal sizes and locations of the PV units and a comparison between the proposed MCSSA3 and MOPSO to validate the results. It is clear that by integrating three PV units at buses 21, 55, and 75 with 1276.78, 1937.40, and 1250.96 kW power generation, respectively, the obtained LR is 74.80 %, and the minimum voltage increases to 0.9561p.u compared with the MOPSO that gives 72.24 % LR and minimum voltage 0.9481p.u.

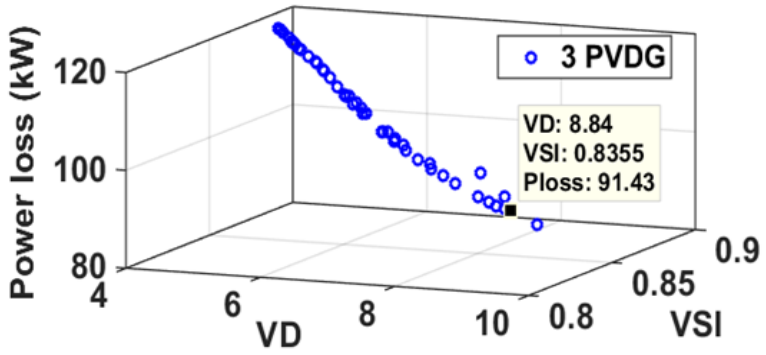


*Fig. 7.26.- Pareto Optimal Front for the 94 bus Portuguese system*

*Table 7.29.- Optimal sizes and locations of PV for 94 bus*

| | Base Case | MOPSO | MCSSA3 |
|---|---|---|---|
| (Bus)<br>Size (kW) | - | (29) 927.72<br>(56) 1075.32<br>(75) 1538.77 | (21) 1276.78<br>(55) 1937.40<br>(75) 1250.96 |
| $P_{loss}$ (kW) | 362.852 | 100.71 | 91.43 |
| LR % | - | 72.24 | 74.80 |
| VD | 104.42 | 13.01 | 8.84 |
| VSI | 0.5183 | 0.8081 | 0.8355 |
| Vmin<br>(Bus) | 0.8485 (92) | 0.9481<br>(66) | 0.9561<br>(92) |

## 7.5.3- MOIHHO

MOIHHO is applied to optimize the three objective functions (power loss, VD (using (2.7)), and VSI ) into IEEE 33-bus and 69-bus distribution systems.

### 7.5.3.1 IEEE 33-bus test system

Results of MOIHHO and different optimization algorithms at unity p.f are given in Table 7.30. The table reveals that improved MOIHHO gets the lowest power loss.

However, the VD obtained by the MOIHHO is 0.0019 p.u which is lower than 0.0020 p.u form MOHHO Besides, MOIHHO provides a high VSI which equals 0.9580 p.u

*Table 7.30.- Results of MOIHHO and different optimization algorithms at unity p.f. (IEEE 33-bus test system)*

| Algorithm | Optimal DG | | $P_{loss}$ (kW) | VD (p.u) | VSI (p.u) |
|---|---|---|---|---|---|
| | Bus | Size (kW) | | | |
| GA [73] | 11 | 1500 | 106.3 | 0.0407 | 0.949 |
| | 29 | 422.8 | | | |
| | 30 | 1071.4 | | | |
| PSO [73] | 8 | 1176.8 | 105.3 | 0.0335 | 0.9255 |
| | 13 | 981.6 | | | |
| | 32 | 829.7 | | | |
| GA/PSO [73] | 11 | 925.0 | 103.4 | 0.0124 | 0.9508 |
| | 16 | 863.0 | | | |
| | 32 | 1200.0 | | | |
| TLBO [74] | 12 | 1182.6 | 124.7 | 0.0011 | 0.9503 |
| | 28 | 1191.3 | | | |
| | 30 | 1186.3 | | | |
| QOTLBO [74] | 13 | 1083.4 | 103.4 | 0.0011 | 0.9530 |
| | 26 | 1187.6 | | | |
| | 30 | 1199.2 | | | |
| TM [80] | 15 | 719.9 | 102.30 | 0.0040 | 0.9371 |
| | 26 | 719.9 | | | |
| | 33 | 1439.7 | | | |
| MOTA [80] | 7 | 980.0 | 96.30 | 0.0014 | 0.9551 |
| | 14 | 960.0 | | | |
| | 30 | 1340.0 | | | |
| SIMBO-Q [54] | 13 | 140.0 | 104.3 | 0.0011 | 0.9615 |
| | 24 | 919.8 | | | |
| | 31 | 1400.0 | | | |
| QOSIMBO-Q [54] | 12 | 1436.8 | 101.9 | 0.0009 | 0.9669 |
| | 25 | 826.2 | | | |
| | 31 | 1443.3 | | | |
| MOHHO | 13 | 1207.0 | 92.95 | 0.0020 | 0.9654 |
| | 25 | 763.0 | | | |
| | 31 | 1400.0 | | | |
| MOIHHO | 14 | 1223.0 | 92.25 | 0.0019 | 0.9580 |
| | 24 | 1144.0 | | | |
| | 31 | 1290.0 | | | |

With 0.95 fixed p.f, the achieved results are shown in Table 7.31. In this case, power loss and VSI achieved by the improved MOIHHO are better than the ones collected by SIMBO-Q [54] and QOSIMBO-Q [54]. For optimal p.f (see Table 7.32), The results demonstrate the efficiency of the MOIHHO compared to ICA / GA [75] and the MOHHO with respect to the VD and VSI.

*Table 7.31.- Results of MOIHHO and different optimization algorithms at 0.95 p.f. (IEEE 33-bus test system)*

| Algorithm | Optimal DG | | | | $P_{loss}$ | VD | VSI |
|---|---|---|---|---|---|---|---|
| | Bus | Size | | | | | |
| | | kW | kVAR | p.f | kW | p.u | p.u |
| SIMBO-Q [54] | 30 | 1443 | 474 | 0.95 | 32.4 | 0.0003 | 0.977 |
| | 13 | 943 | 309 | 0.95 | | | |
| | 24 | 1327 | 436 | 0.95 | | | |
| QOSIMBO-Q [54] | 30 | 1419 | 467 | 0.95 | 31.7 | 0.0003 | 0.977 |
| | 24 | 1392 | 458 | 0.95 | | | |
| | 13 | 898 | 295 | 0.95 | | | |
| MOHHO | 13 | 1008 | 331 | 0.95 | 31.4 | 0.0005 | 0.976 |
| | 25 | 910 | 299 | 0.95 | | | |
| | 30 | 1334 | 439 | 0.95 | | | |
| MOIHHO | 13 | 924 | 304 | 0.95 | 30.6 | 0.0004 | 0.979 |
| | 24 | 1312 | 431 | 0.95 | | | |
| | 30 | 1356 | 446 | 0.95 | | | |

*Table 7.32.- Results of MOIHHO and different optimization algorithms at optimal p.f (IEEE 33-bus test system)*

| . Algorithm | Optimal DG | | | | $P_{loss}$ (kW) | VD (p.u) | VSI (p.u) |
|---|---|---|---|---|---|---|---|
| | Bus | Size | | | | | |
| | | kW | kVAR | p.f | | | |
| ICA/GA [75] | 13 | 795 | 376 | 0.90 | 11.9 | 0.0006 | 0.969 |
| | 24 | 1069 | 518 | 0.90 | | | |
| | 30 | 1029 | 1021 | 0.71 | | | |
| MOHHO | 12 | 951 | 516 | 0.88 | 18.8 | 0.0005 | 0.978 |
| | 25 | 786 | 436 | 0.87 | | | |
| | 30 | 1381 | 809 | 0.86 | | | |
| MOIHHO | 12 | 916 | 576 | 0.85 | 15.0 | 0.0003 | 0.978 |
| | 24 | 1088 | 386 | 0.94 | | | |
| | 30 | 1171 | 830 | 0.82 | | | |

Fig. 7.27 shows the optimal Pareto solutions achieved by MOIHHO for various operations p.f. In addition to the statistics, of all non-dominated solutions, the best compromise solution obtained by the grey interaction analysis is seen.

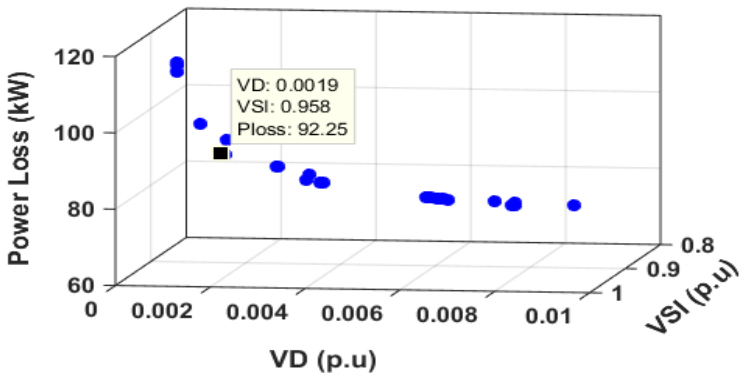

*(a) unity p.f*

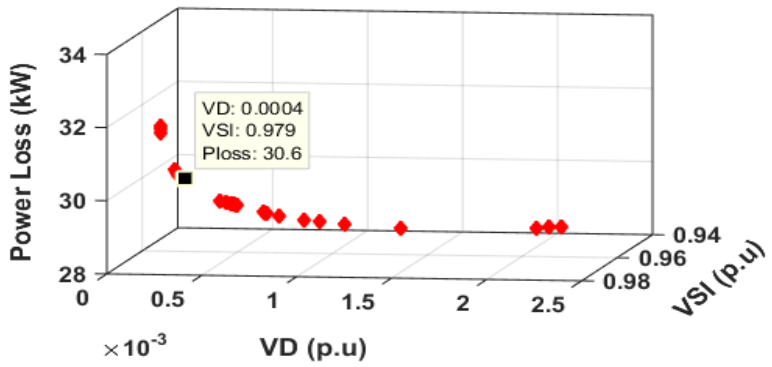


*(b) 0.95 p.f, and*

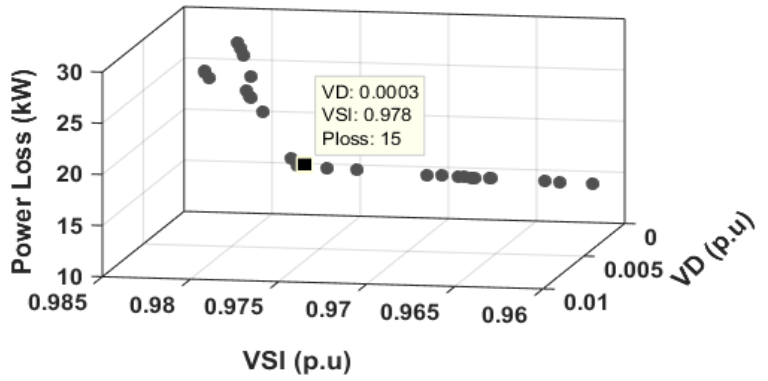


*(c) Optimal p.f*

*Fig. 7.27.- Nondominated Pareto optimal solutions obtained by MOIHHO for IEEE 33-bus considering DG operating at*

When considering VD and VSI as objective functions for the multi-objective DG allocation issue, the voltage profile of the IEEE 33-bus system has been dramatically improved. Fig. 7.28 indicates the influence of the DG on the multi-objective problem with different operating p.f, and it is clear that the voltage profile is higher than that obtained by the single-objective problem with the same operating p.f. (Fig. 7.6).

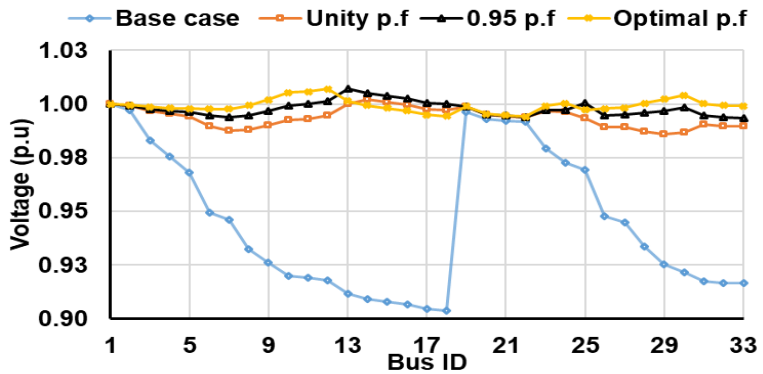


*Fig. 7.28.- Voltage profile of the IEEE 33-bus test system at different case studies for the multi-objective optimization problem.*

For the developed MOIHHO and MOHHO, the SP metric was calculated for 10 runs. Fig. 7.29 indicates that the SP parameter is compared to different operational p.f. It is evident that at the unit p.f and optimal p.f, MOIHHO has a better SP metric than MOHHO, which means that the non-dominated solutions are distributed uniformly.

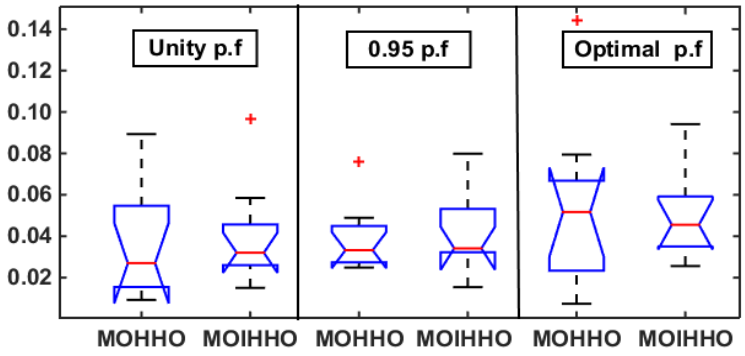


*Fig. 7.29.- Box plot for SP metric of the MOHHO and MOIHHO at different operating p.f in case of the IEEE 33-bus system.*

### 7.5.3.2 IEEE 69-bus test system

In Table 7.33, the optimum sizes and positions of the DG at unity p.f are ordered using various optimization algorithms. In this case, relative to other algorithms, MOIHHO reaches the largest VSI, which is 0.9778 p.u. The developed algorithm provides a VD of 0.0007 p.u, similar to the value obtained by QOTLBO, SIMBO-Q, and QOSIMBO-Q, and greater than the other algorithms in the table. In addition, the power loss in MOIHHO is 80.8 kW.

The result of the DG running at 0.95 p.f is given in Table 7.34, and it is mentioned that the MOIHHO provides the best results in two of the objective functions (power loss and VSI) compared to the other algorithm that proves the MOIHHO 's capability.

Finally, Table 7.35 presents the optimum p.f where the MOIHHO result is relative to MOHHO. It should be remembered that with the MOIHHO a substantial increase in the VSI is obtained and that equals 0.991 p.u, which means that the system can handle irregular conditions to become more stable. In addition to the best compromise solution achieved by the grey relationship analysis, the Pareto optimum front is exposed in Fig. 7.30 at different operating p.f.

*Table 7.33.- Results of MOIHHO and different optimization algorithms at unity p.f (IEEE 69-bus test system)*

| Algorithm | Bus | Size (kW) | $P_{loss}$ (kW) | VD (p.u) | VSI (p.u) |
|---|---|---|---|---|---|
| GA [73] | 21 | 929.7 | 89.0 | 0.0012 | 0.9705 |
| | 62 | 1075.2 | | | |
| | 64 | 984.8 | | | |
| PSO [73] | 17 | 992.5 | 83.2 | 0.0049 | 0.9676 |
| | 61 | 1199.8 | | | |
| | 63 | 795.6 | | | |
| GA/PSO [73] | 21 | 910.5 | 81.1 | 0.0031 | 0.9768 |
| | 61 | 1192.6 | | | |
| | 63 | 884.9 | | | |
| TLBO [74] | 13 | 1013.4 | 82.2 | 0.0008 | 0.9745 |
| | 61 | 990.1 | | | |
| | 62 | 1160.1 | | | |
| QOTLBO [74] | 15 | 811.4 | 80.6 | 0.0007 | 0.9769 |
| | 61 | 1147.0 | | | |
| | 63 | 1002.2 | | | |
| SIMBO-Q [54] | 61 | 1397.5 | 80.5 | 0.0007 | 0.9770 |
| | 15 | 780.3 | | | |
| | 62 | 790.7 | | | |
| QOSIMBO-Q [54] | 61 | 1498.6 | 79.8 | 0.0007 | 0.9770 |
| | 15 | 785.1 | | | |
| | 63 | 662.3 | | | |
| MOHHO | 20 | 643.6 | 81.0 | 0.0008 | 0.9720 |
| | 60 | 971.4 | | | |
| | 61 | 1328.2 | | | |
| MOIHHO | 18 | 796.2 | 80.8 | 0.0007 | 0.9778 |
| | 61 | 1447.1 | | | |
| | 64 | 707.5 | | | |

*Table 7.34.- .- Results of MOIHHO and different optimization algorithms at 0.95 p.f (IEEE 69-bus test system)*

| Algorithm | Optimal DG | | | | $P_{loss}$ kW | VD (p.u) | VSI (p.u) |
|---|---|---|---|---|---|---|---|
| | Bus | Size | | | | | |
| | | kW | kVAR | p.f | | | |
| SIMBO-Q [54] | 13 | 953 | 313 | 0.95 | 29.7 | 0.0003 | 0.977 |
| | 59 | 1002 | 329 | 0.95 | | | |
| | 62 | 1121 | 369 | 0.95 | | | |
| QOSIMBO-Q [54] | 17 | 487 | 160 | 0.95 | 31.4 | 0.0002 | 0.977 |
| | 56 | 1260 | 414 | 0.95 | | | |
| | 63 | 1500 | 493 | 0.95 | | | |
| MOHHO | 23 | 519 | 171 | 0.95 | 30.2 | 0.0010 | 0.980 |
| | 60 | 1176 | 387 | 0.95 | | | |
| | 62 | 1179 | 387 | 0.95 | | | |
| MOIHHO | 13 | 1038 | 341 | 0.95 | 28.9 | 0.0003 | 0.980 |
| | 61 | 799 | 263 | 0.95 | | | |
| | 63 | 1229 | 404 | 0.95 | | | |

*Table 7.35.- .- Results of MOIHHO and different optimization algorithms at optimal p.f (IEEE 69-bus test system)*

| Algorithm | Optimal DG | | | | $P_{loss}$ kW | VD (p.u) | VSI (p.u) |
|---|---|---|---|---|---|---|---|
| | Bus | Size | | | | | |
| | | kW | kVAR | p.f | | | |
| MOHHO | 15 | 332 | 846 | 0.37 | 21.8 | 0.0008 | 0.980 |
| | 60 | 314 | 838 | 0.35 | | | |
| | 61 | 1784 | 335 | 0.98 | | | |
| MOIHHO | 13 | 1064 | 779 | 0.81 | 13.9 | 0.0005 | 0.991 |
| | 49 | 1235 | 403 | 0.95 | | | |
| | 62 | 1610 | 1181 | 0.81 | | | |

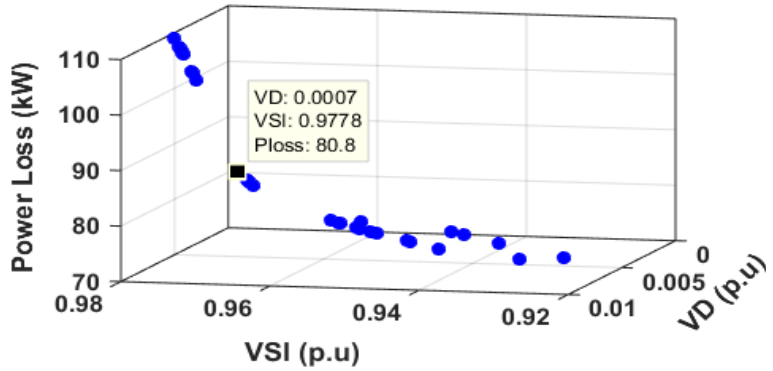


*(a) unity p.f*

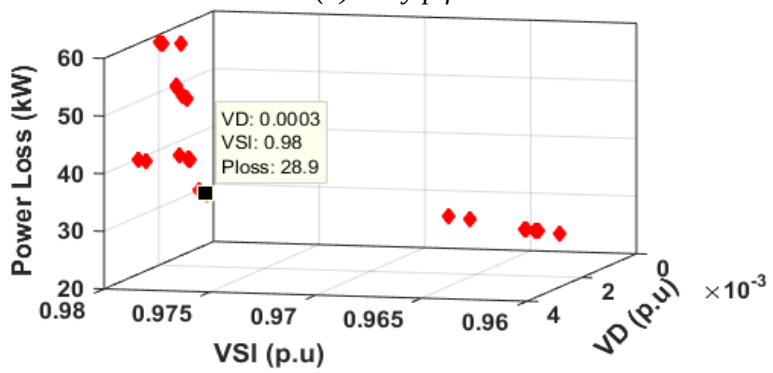


*(b) 0.95 p.f,*

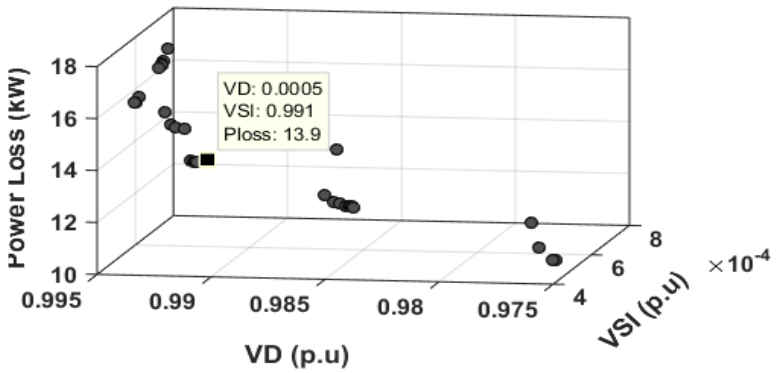


*(c) Optimal p.f*

*Fig. 7.30.- Nondominated Pareto optimal solutions obtained by MOIHHO for IEEE 69-bus considering DG operating at*

Fig. 7.31 indicates the voltage profile of the IEEE 69-bus system and substantial change is visible in the figure.

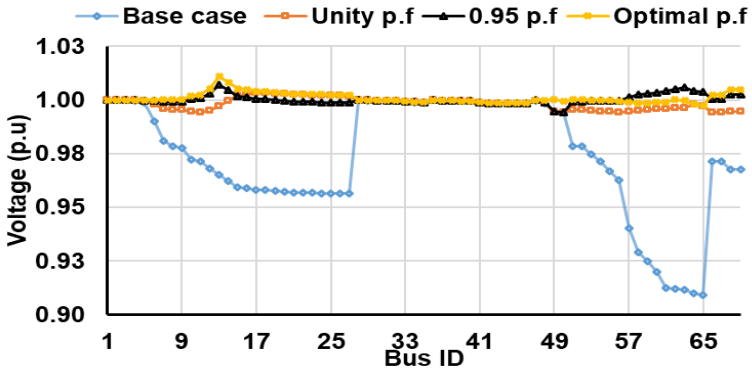


*Fig. 7.31.- Voltage profile of the IEEE 69-bus test system at different case studies for the multi-objective optimization problem.*

The box plot shown in Fig. 7.32 illustrates the SP metric of the MOHHO and MOIHHO for various operating p.f. The MOIHHO has a better distribution of the nondominated solution than the MOHHO at unity and optimal p.f.

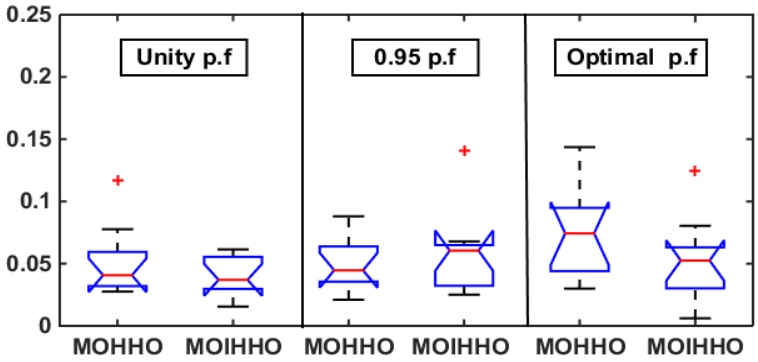


*Fig. 7.32.- Box plot for SP metric of the MOHHO and MOIHHO at different operating p.f in case of the IEEE 69-bus system.*

# 7.6.- Results of DG Allocation Based on Uncertainty and Load Variation

This section presents the application of the improved single- and multi-objective algorithms in different scenarios of DG allocation based on the uncertainty model of the PV power generation and different types of daily load curves.

## 7.6.1- CQOBMO

PV power generation based on the uncertainty model with a daily load curve is applied to present the impact of the intermittent nature of the PV on the voltage profile and the power loss for 24 hrs. The improved algorithm is employed to find the optimal PV+BES power which minimizes the total energy loss in the RDS.

#### 7.6.1.1 IEEE 33-bus test system

The improved BMO based on the quasi oppositional and sine chaotic map is used in this section to find the optimal PV+BES size after approving its feasibility in the previous sections.

In this study, a combination of residential, industrial, and commercial daily load curves (see Fig. 7.33) [103] is adopted and used to present the variation in the load demand. However, the intermittent nature of the PV is modeled using the uncertainty analysis. Hence, using the optimal sizes and location of the DG which was obtained earlier, time-series load flow is carried out using the daily load curves and PV power shown in Fig. 7.34.

The results show that at the base case (without PV), the power loss increases when the load demand is high as presented in Fig. 7.35. Besides, the voltage profile of some buses is lower than the limits (0.95 p.u) as exhibited in Fig. 7.36.

While, integrating PV at bus 13, 24, and 30 reduce the power loss and improve the voltage profile during the availability of the PV power as displayed in Fig. 7.35 and Fig. 7.37 respectively. But the power loss is still high, and the voltage profile is still lower than the limits at the time where no PV power is injected (from 19:00 to 24:00).

To avoid this problem, BES is used with the PV and the optimal size of the PV+BES power during 24 hrs is calculated using the CQOBMO_7 then the final PV power is computed using (2.29). Hence, the optimal sizes of the PV and the BES are summarized in Table 7.36. Consequently, the integration of the PV+BES minimizes the power loss as presented in Fig. 7.35 and enhances the voltage profile as shown in Fig. 7.38.

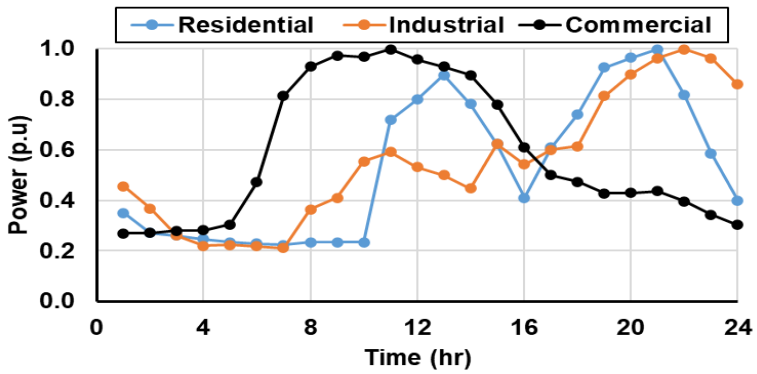


*Fig. 7.33.- Residential, industrial, and commercial daily load curves*

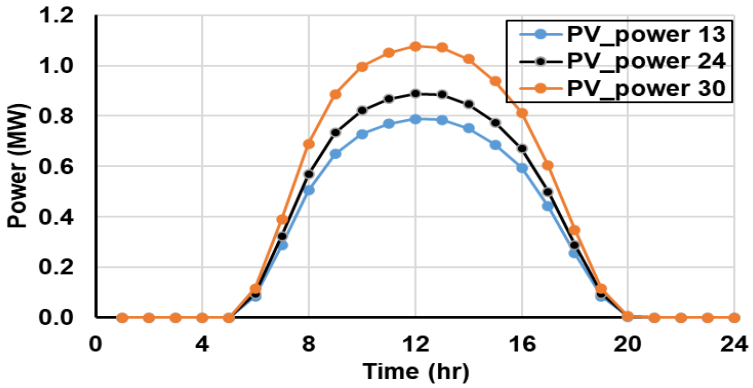


*Fig. 7.34.- PV output power at buses 13, 24, and 30.*

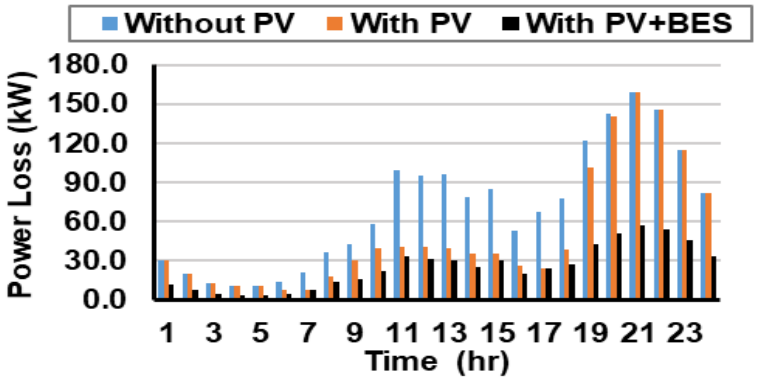


*Fig. 7.35.- Power losses in IEEE 33-bus for 24 hrs at different case studies.*

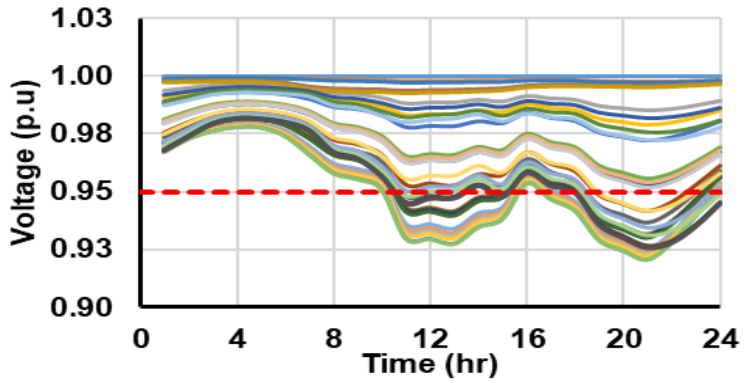


*Fig. 7.36.- Voltage profile of IEEE 33 bus for 24 hrs at base case (without PV).*

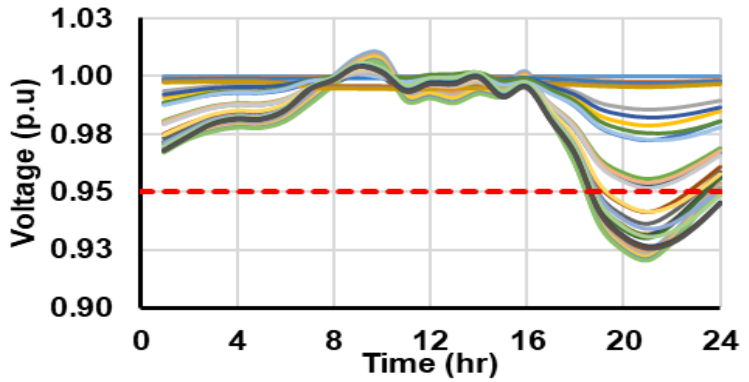


*Fig. 7.37.- Voltage profile of IEEE 33-bus for 24 hrs with PV.*

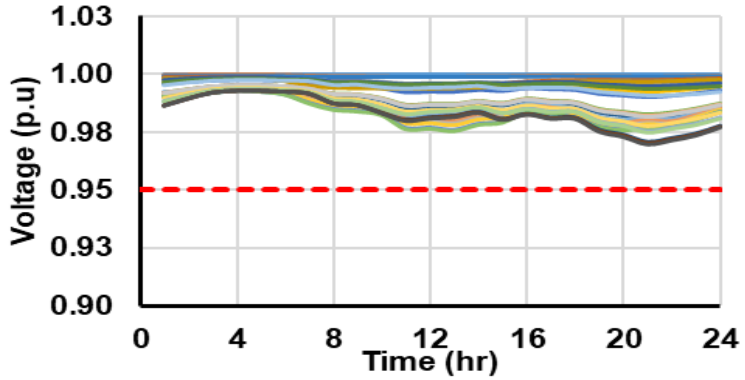


*Fig. 7.38.- Voltage profile of IEEE 33-bus for 24 hrs with PV+BES.*

Fig. 7.39 shows the BES charging and discharging power at the optimal locations and the BES capacities are calculated based on the maximum charging power of each BES and given in Table 7.36. Table 7.37 proves the benefits of the PV+BES in reducing the total energy losses where the reduction reaches 64% compared to 27.5% in the case of using the PV.

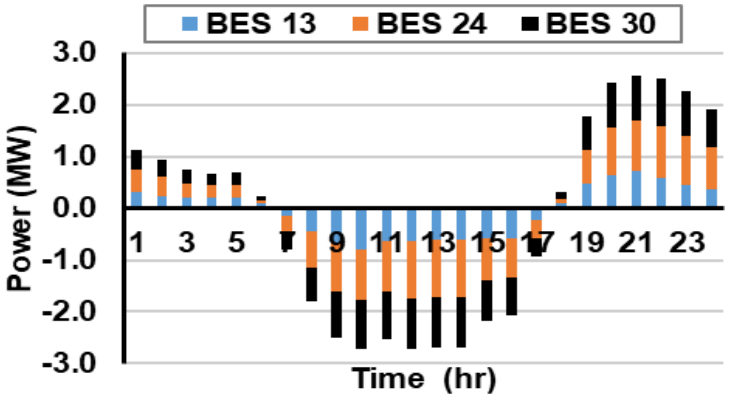


*Fig. 7.39.- Charging/ discharging powers of different BES integration in the IEEE 33 -bus.*

*Table 7.36.- Optimal size of PV+BES in IEEE 33-bus system*

| Location | PV size (MW) | BES rated power (MW) | BES capacity (MW h) |
|---|---|---|---|
| Bus 13 | 1.28 | 0.79 | 5.97 |
| Bus 24 | 1.74 | 1.11 | 9.16 |
| Bus 30 | 1.66 | 0.99 | 8.54 |

*Table 7.37.- Daily energy losses for IEEE 33-bus*

| Case | Energy losses (kW h) | Reduction % |
|---|---|---|
| Without PV | 1673.94 | - |
| With PV | 1213.35 | 27.5 |
| With PV+BES | 602.35 | 64.0 |

### 7.6.1.2 IEEE 69-bus test system

Similarly, the impact of the PV and the PV+BES is observed in the IEEE 69-bus system. Three PV units with different power generations are installed at the optimal locations as shown in Fig. 7.40. The performance of the IEEE 69-bus is improved by using the optimal power generation based on PV+BES and that is clear in Fig. 7.41. The figure shows that the power loss is significantly decreased in the case of PV+BES compared to the base case and when PV is installed.

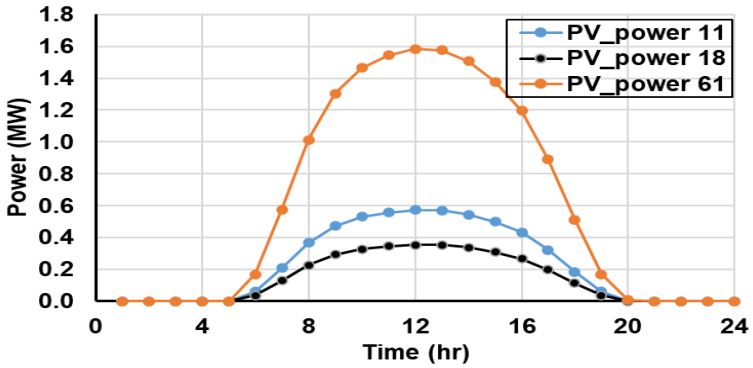


*Fig. 7.40.- PV output power at buses 11, 18, and 61.*

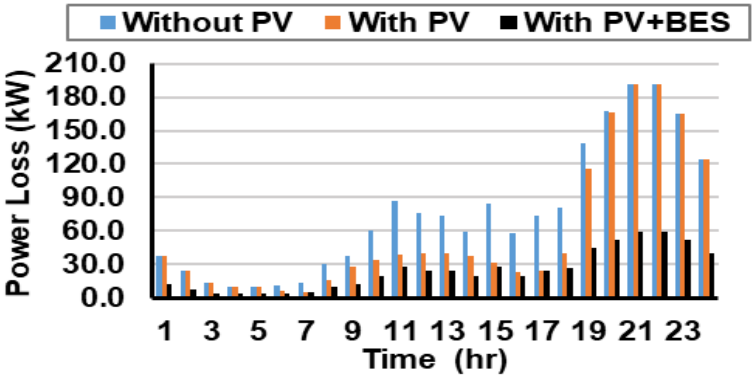


*Fig. 7.41.- Power losses in IEEE 69 bus for 24 hrs at different case studies.*

Also, the voltage profile is improved in the case of PV+BES (see Fig. 7.44) compared to the base case and PV (see Fig. 7.42 and Fig. 7.43) which show the merits of installing BES with the PV systems.

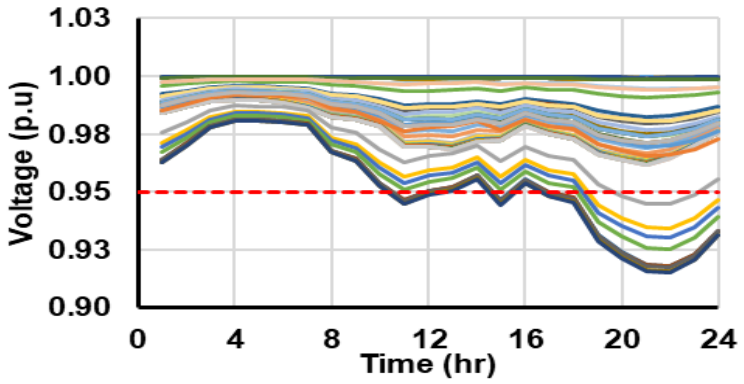


*Fig. 7.42.- Voltage profile of IEEE 69 bus for 24 hrs at base case (without PV).*

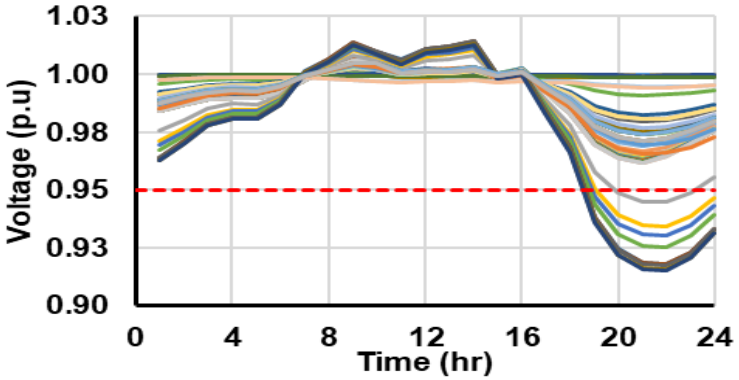


*Fig. 7.43.- Voltage profile of IEEE 69 bus for 24 hrs with PV.*

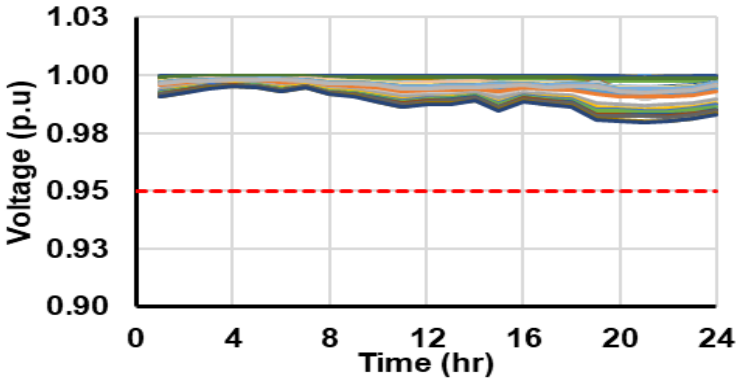


*Fig. 7.44.- Voltage profile of IEEE 69 bus for 24 hrs with PV+BES.*

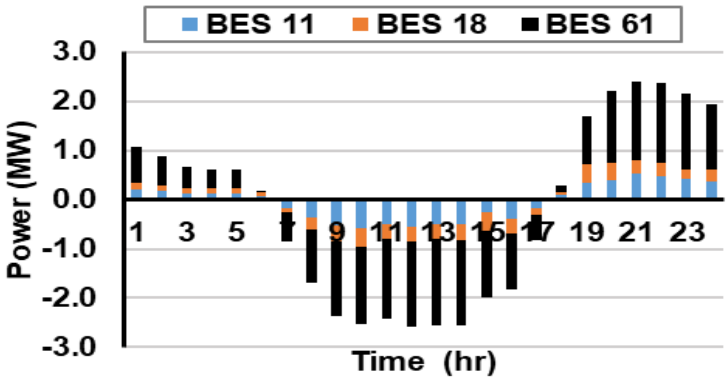


*Fig. 7.45.- Charging/ discharging powers of different BES integration in the IEEE 69 bus.*

Fig. 7.45 presents the behaviour of the BES at a different location during the 24 hrs. The BESs start discharging when the PV power is low and they charge when the PV power is high to minimize the power loss.

The optimal sizes of the PV+BES for the IEEE 69-bus system are given in Table 7.38and the reduction in the energy is summarized in Table 7.39. The table shows that a significant energy reduction is achieved in the case of PV+BES which reaches 67.80%.

*Table 7.38.- Optimal size of PV+BES in IEEE 69-bus system*

| Location | PV size (MW) | BES rated power (MW) | BES capacity (MW h) |
|---|---|---|---|
| Bus 11 | 0.88 | 0.57 | 4.55 |
| Bus 18 | 0.62 | 0.40 | 3.05 |
| Bus 61 | 2.72 | 1.77 | 14.63 |

*Table 7.39.- Daily energy losses for IEEE 69-bus*

| Case | Energy losses (kW h) | Reduction % |
|---|---|---|
| Without PV | 1822.33 | - |
| With PV | 1417.30 | 22.23 |
| With PV+BES | 586.87 | 67.80 |

## 7.6.2- MCSSA

In this section, the IEEE 33-bus and 94-bus Portuguese RDSs are used to illustrate the feasibility and efficiency of the optimal setting and scheduling of integration PV and BESs in RDSs to minimize the total power and energy losses as well as to keep the voltage within acceptable limits (0.95 – 1.05). The uncertainty PV power generation model is employed with time-varying load demand to present the impact of the intermittent nature of PV on the energy losses and voltage profile of the distribution systems. Then, **a** sequential proposed MCSSA is used to optimally schedule the PV+BES power generation for minimizing the total energy losses and enhancing the voltage profile using the three objective functions.

### 7.6.2.1 IEEE 33-bus test system

In this scenario, the PV power generation model is applied using the optimal sizes and locations obtained in scenario 1, a time-varying daily load demand that consists of three types of loads, residential, industrial, and commercial is used as displayed in Fig. 7.33 [103]. The impact of the load variation on the IEEE 33-bus voltage profile and the power losses for 24 hrs is shown in Fig. 7.47.a and Fig. 7.47.b, respectively. The voltage profile is less than the lower limit due to the increase in the load demand. To enhance the voltage profile during the 24-hr, three PV units are integrated at buses 13, 24, and 30 with the generated active power presented in Fig. 7.46.

Significant improvement occurs in the voltage profiles and LR when the PV power is available between 6:00 to 19:00 hr as exhibited in Fig. 7.47.b and Fig. 7.47.c. However, a shortage of PV integration and growth in the load demand has occurred after 19:00 hr, and this leads to a decrease in the voltage profile lower than the limit (0.95 p.u).

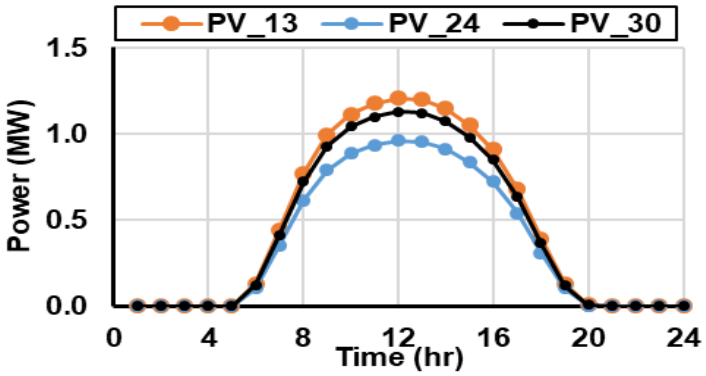


*Fig. 7.46.- PV power generation fir IEEE 33-bus system*

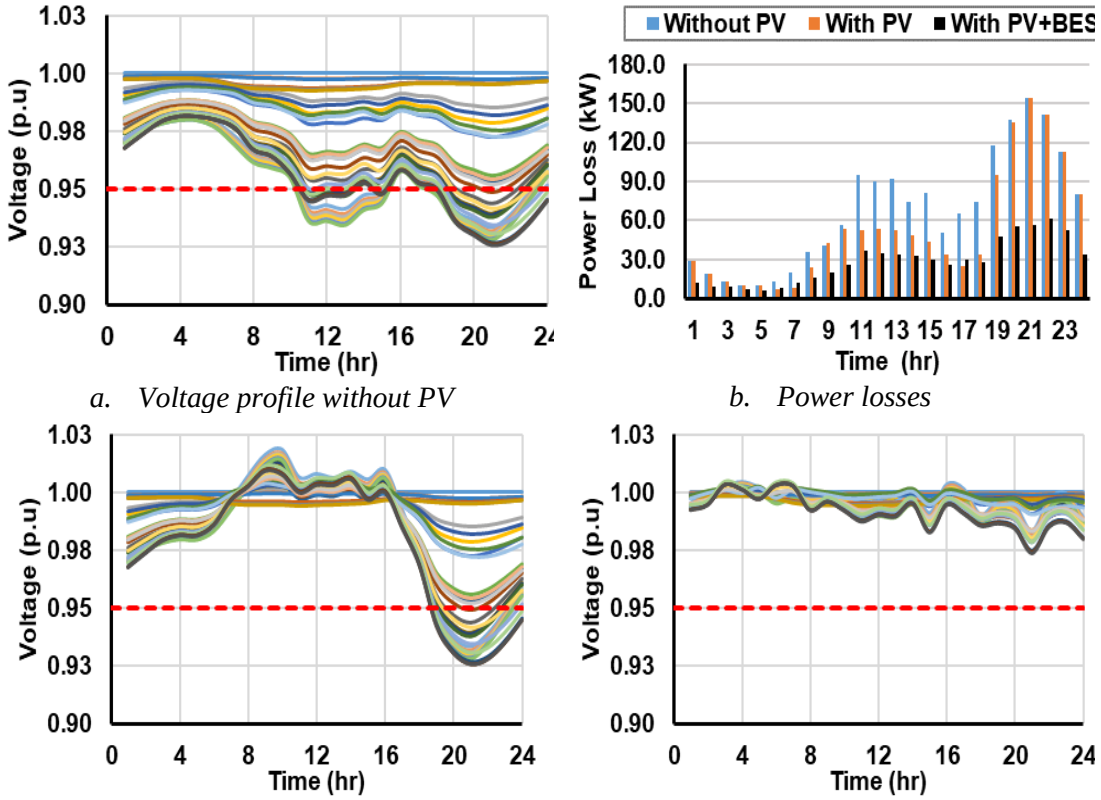


*a. Voltage profile without PV* *b. Power losses*

*c. Voltage profile with 3 PVs* *d. Voltage profile with 3PV+BES*

*Fig. 7.47.- Impact of the time-varying load and PV generation on IEEE 33 bus*

To enhance the voltage, BESs are installed at the PV locations and the proposed MCSSA is used at each hour to optimally schedule the PV+BES power to reduce the power losses, total VD, and maximize VSI. By using the PV+BES power, the optimal size for the PV and BES can be accomplished using the PV+BES modeling.

Fig. 7.48.a shows the obtained $P_{(PV+BES)_{13}}$ at bus #13 during 24-hr using the proposed MCSSA3 to minimize the total power losses and enhance the voltage profile as shown in Fig. 7.47.b and Fig. 7.47.d, respectively. Using $E_{(PV+BES)_{13}}$, the optimal $P_{PV_{13}}$ size can be obtained by applying (2.22)to (2.29).

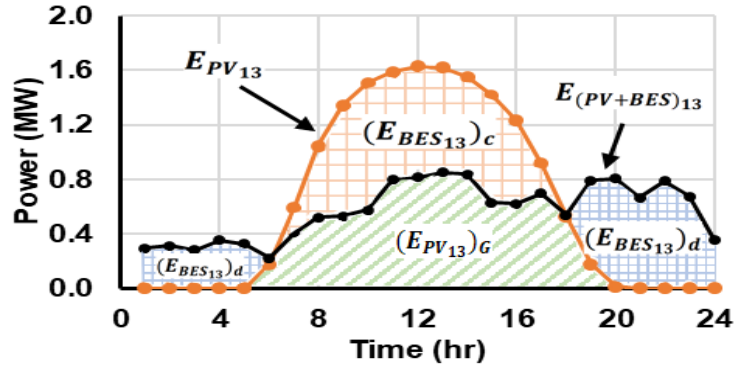


*(a) PV+BES at bus 13*

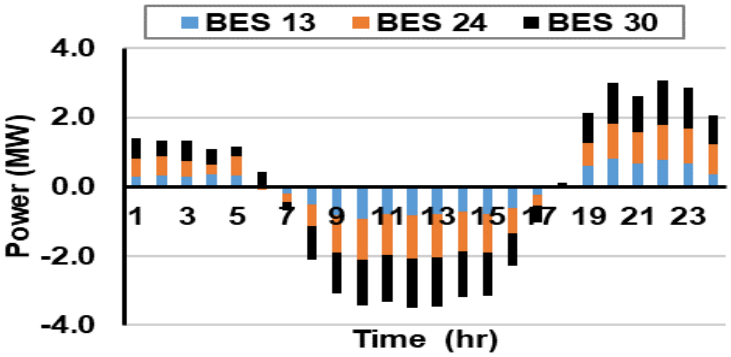


*(b) BES charging/discharging profile at buses 13, 24, and 30*

*Fig. 7.48.- PV and BES power for IEEE 33 bus*

Due to the intermittent nature of the PV power, it is considered a non-dispatchable generation unit. To convert a PV unit to dispatchable, a combination of PV and BES units is used to keep the system active power losses and VD for each load level at the minimum values. This combination can produce a daily amount of dispatchable energy, $E_{(PV+BES)}$ as shown in Fig. 7.48. a. During a 24-hr cycle, the PV unit produces an amount of energy, $E_{PV}$ based on the uncertainty model. A portion of this energy is delivered to the grid $(E_{PV})_G$. The remaining energy of the PV unit is used to charge the BES unit when the PV output is high during the day. This stored energy is then discharged to the grid when the PV output is small or zero during the night.

The maximum charging BES power $(P_{BES_{13}}^{max})_c$ can be achieved by assessing the maximum power value which should be curtailed from the $P_{PV_{13}}$ to satisfy the objective functions during 24-hr. The same analysis is performed on buses 24 and 30, the optimal sizes of PV and BES power are summarized in Table 7.40.

The BES capacity is calculated based on the maximum charging energy during the 24-hr. The charging/discharging power of the three installed BESs is shown in Fig. 7.48.b. From this figure, It is observed that the discharging occurs between 1:00 and

6:00-hr and in the second period from 19 to 24- hr to keep the power losses and the voltage profile within the satisfied operator's decision in case of no PV power is delivered. On the other hand, a charging process happens from 7 to 18-hr when high PV power is available.

*Table 7.40.- Optimal size of PV+BES in IEEE 33-bus system*

| Location | PV size (MW) | BES rated power (MW) | BES capacity (MW h) |
|---|---|---|---|
| Bus 13 | 1.63 | 0.94 | 7.18 |
| Bus 24 | 2.11 | 1.28 | 10.30 |
| Bus 30 | 2.26 | 1.42 | 11.83 |

This analysis investigates the impact of the PV and BES on the total energy losses over a day. Table 7.41 gives the percentage of the total energy reduction when installing PV and PV+BES where the energy loss is 1613.45 MW h in case of no PV integration, however after integration PV, the energy reduction reaches 20.69% and a significant reduction (57.40%) is achieved with incorporating PV+BES.

*Table 7.41 Daily energy losses for IEEE 33-bus*

| Case | Energy losses (kW h) | Reduction % |
|---|---|---|
| Without PV | 1613.45 | - |
| With PV | 1279.60 | 20.69 |
| With PV+BES | 687.40 | 57.40 |

### 7.6.2.2 94-bus Portuguese test system

Fig. 7.49. a shows the 94-bus voltage profile variation concerning the changing in the load demand and it is obvious that many buses are not subject to the voltage boundary, therefore, the MCSSA3 is applied for the 24-hr to optimally schedule the PV+BES to attain the objective functions.

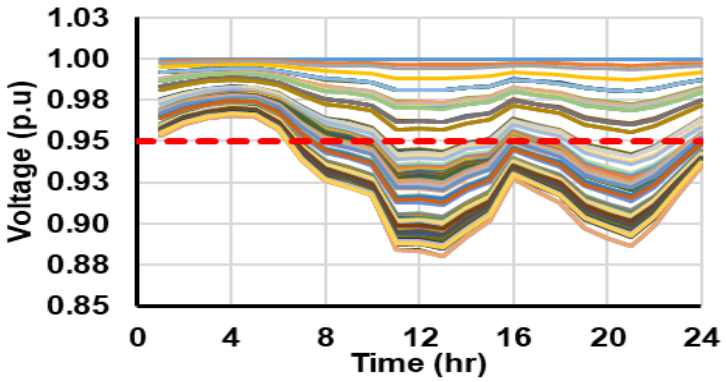


*(a) Voltage profile without PV*

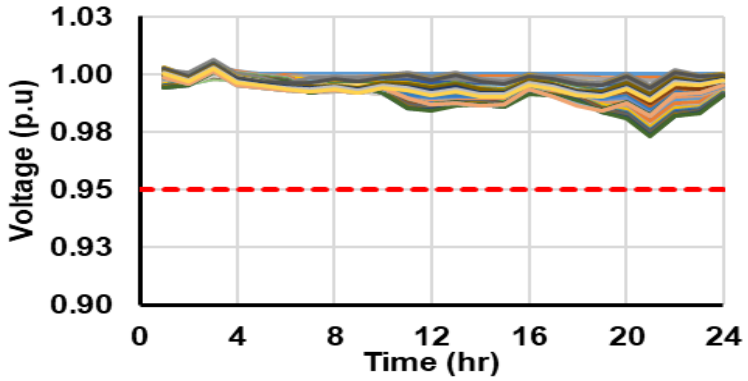


*(b) Voltage profile with PV+BES*

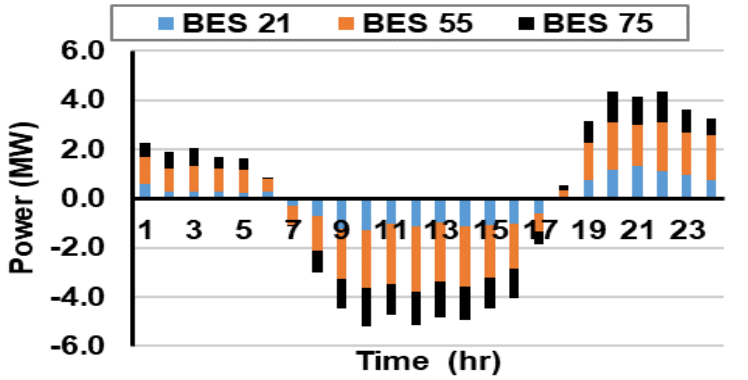


*(c) BES charging/discharging profile at buses 21, 55, and 75*

*Fig. 7.49.- Voltage profile and BES power for 94-bus Portuguese system*

As a result of utilizing the proposed optimization algorithm, the valuable improvement in the voltage profile is obtained as shown in Fig. 7.49.b. The charging/discharging power of the three connected BESs is demonstrated in Fig. 7.49.c, where the BES installed at bus #55, maintains the highest energy capacity due to the large PV size at this bus as summarized in Table 7.42.

*Table 7.42 Optimal size of PV+BES in the 94-bus Portuguese system*

| Location | PV size (MW) | BES rated power (MW) | BES capacity (MW h) |
|---|---|---|---|
| Bus 21 | 2.45 | 1.27 | 10.52 |
| Bus 55 | 4.41 | 2.66 | 21.22 |
| Bus 75 | 2.73 | 1.59 | 12.04 |

The energy loss reduction for the 94-bus system is given in Table 7.43. Similar to the previous test system, a considerable energy loss reduction is obtained when integrating PV+BES which equals 52.19%.

*Table 7.43 Daily energy losses for 94-bus Portuguese system*

| Case | Energy losses (kW h) | Reduction % |
|---|---|---|
| Without PV | 2745.23 | - |
| With PV | 1792.56 | 34.70 |
| With PV+BES | 1312.62 | 52.19 |

### 7.6.3- MOCSCA

In this analysis, using a standard PV power generation based on the uncertainty and daily demand profile during the year (Summer, Spring, Winter, and Fall), the effect of renewable energy sources on the delivery system is observed. The daily load is shown in Fig. 7.50 is used. The overall data can be found in [104]. The mean and standard deviation of the solar irradiance of the PV model are given in [105]. Fig. 7.51 shows four typical days presented in 96 hr sampling time. The power generation obtained by the Beta PDF for one PV module is shown in Fig. 7.52

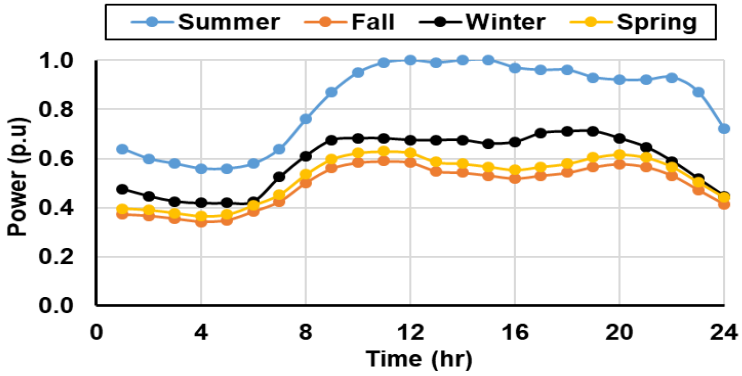


*Fig. 7.50.- Typical daily load profile*

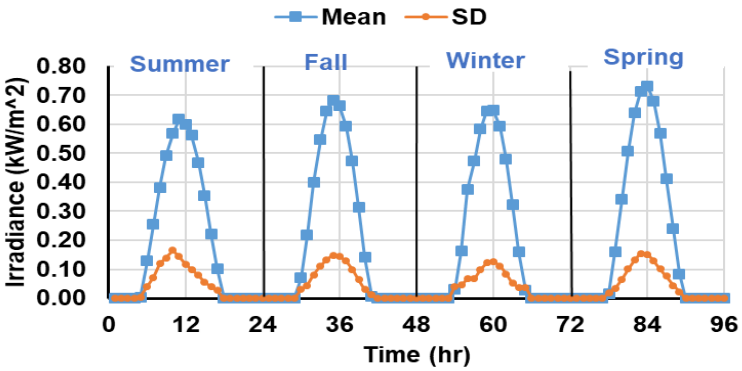


*Fig. 7.51.- Mean and Standard deviation of the solar irradiation*

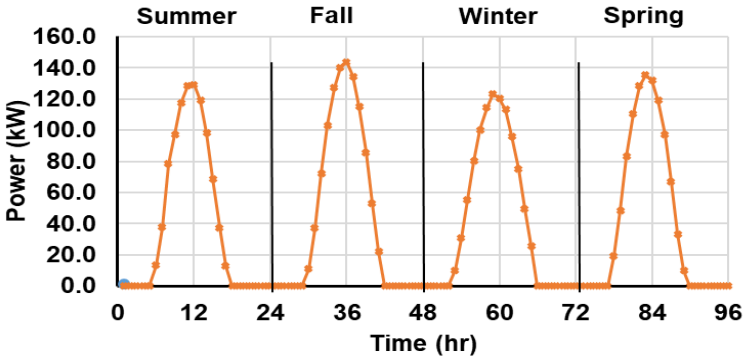


*Fig. 7.52.- PV power*

### 7.6.3.1 IEEE 33-bus test system

Fig. 7.53 indicates the IEEE 33-bus voltage profile on a normal day without PV power for each season. The figure reveals that a large voltage drop existed in the summer, but some buses met the lower limits in the winter and fall.

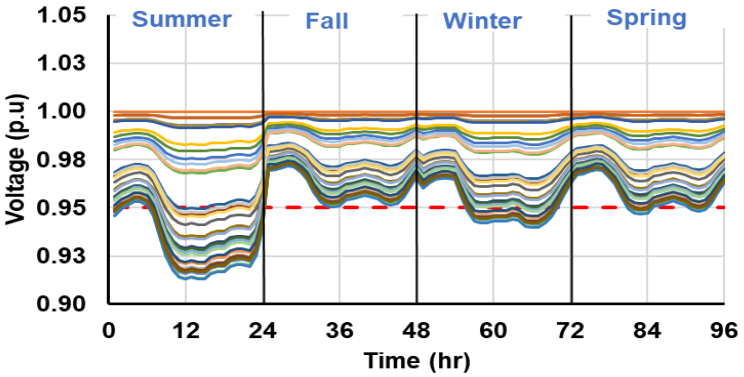


*Fig. 7.53.- Voltage profile of IEEE 33-bus for four typical days of the four seasons in the year without PV*

Using the MOCSCA, three DG units are optimally placed in the system with their maximum capacity provided in Table 7.25 to improve the voltage profile of the IEEE 33-bus and minimize power losses. Fig. 7.54 indicates the effect of the PV power on the voltage profile, if the PV power is present, the voltage is increased and lowered where the PV power is minimal.

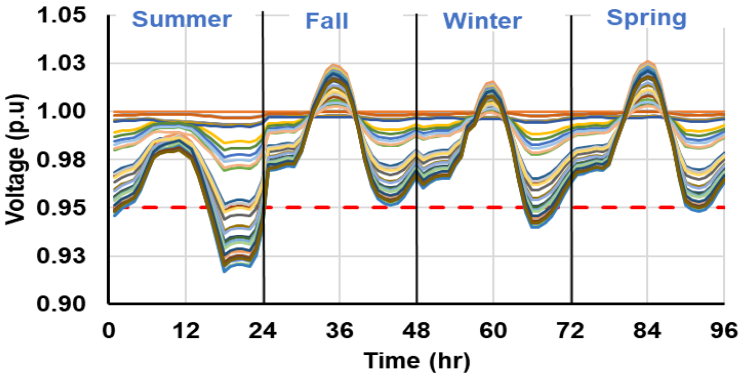


*Fig. 7.54.- Voltage profile of IEEE 33-bus for four typical days of the four seasons in the year with PV*

To decide the optimum power setting of the PV and BES, a sequential MOCSCA is used at each sampling period to preserve the voltage profile within the limits and reduce the power losses. Fig. 7.55 indicates the improvement of the voltage profile at the same PV positions by using three BESs. Using BES, substantial progress was made.

Minimizing energy loss occurs in Fig. 7.56. In the three cases examined, PV and BES are used to achieve the lowest energy loss.

Finally, the optimum BES capacity is seen in Table 7.44, and due to the high load demand and low PV power generation, the full PV and BES capacity are reached in the summer.

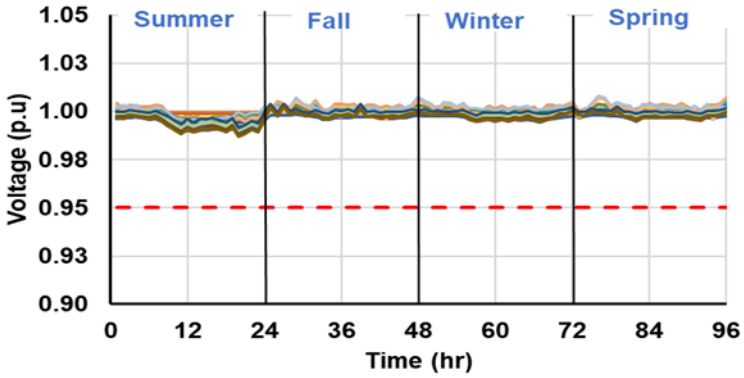


*Fig. 7.55.- Voltage profile of IEEE 33-bus for four typical days of the four seasons in the year with PV and BES*

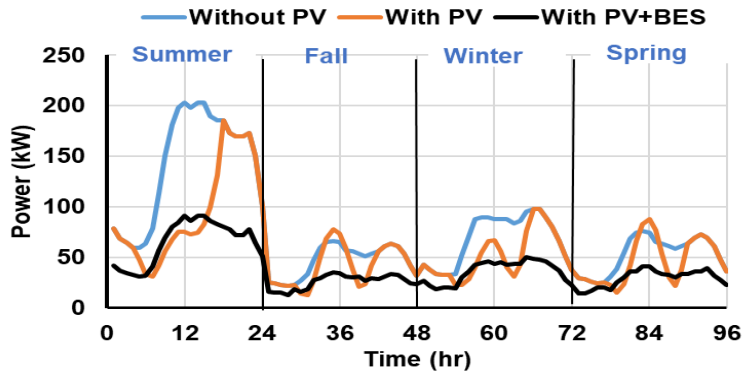


*Fig. 7.56.- Power loss minimization in IEEE 33-bus for four typical days of the four seasons in the year*

*Table 7.44.- Optimal size of PV and BES for IEEE 33-bus*

| | Summer | Fall | Winter | Spring |
|---|---|---|---|---|
| BES 13 (MW h) | 9.88 | 6.14 | 7.29 | 6.70 |
| BES 24 (MW h) | 13.01 | 9.98 | 11.32 | 10.01 |
| BES 30 (MW h) | 14.60 | 9.12 | 10.85 | 9.58 |
| PV 13 size (MW) | 3.06 | 1.92 | 2.25 | 2.06 |
| PV 24 size (MW) | 3.59 | 2.78 | 3.34 | 3.06 |
| PV 30 size (MW) | 4.60 | 2.84 | 3.36 | 2.96 |

### 7.6.3.2 IEEE 69-bus test system

Similarly, the IEEE 69-bus is studying the effect of PV and BES. The base case voltage profiles (without PV) and their improvements due to the use of PV and PV with

BES are provided in Fig. 7.57, Fig. 7.58, as well as Fig. 7.59 respectively. A large improvement in the voltage profile can be found using PV and BES during the year.

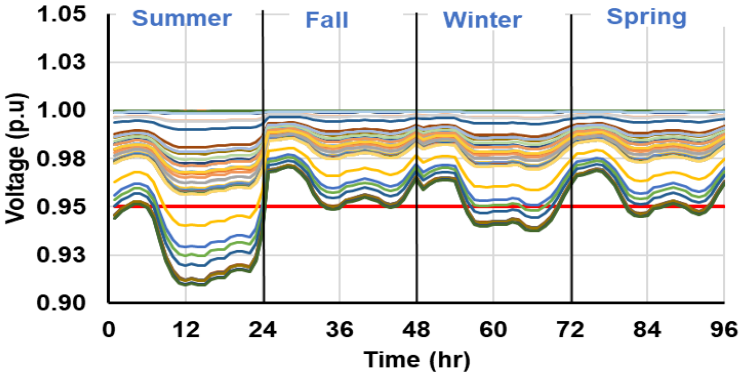


*Fig. 7.57.- Voltage profile of IEEE 69-bus for four typical days of the four seasons in the year without PV*

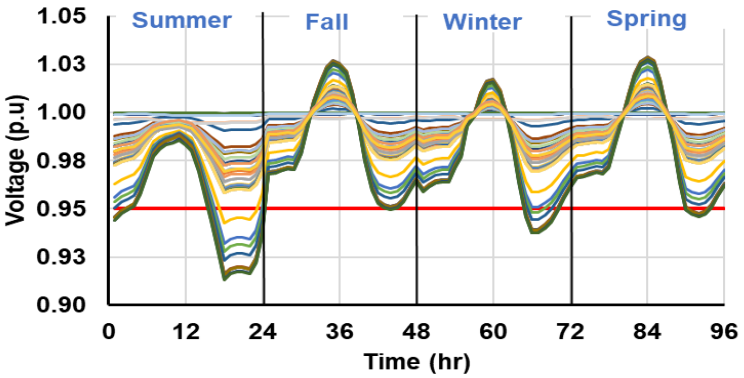


*Fig. 7.58.- Voltage profile of IEEE 69-bus for four typical days of the four seasons in the year with PV*

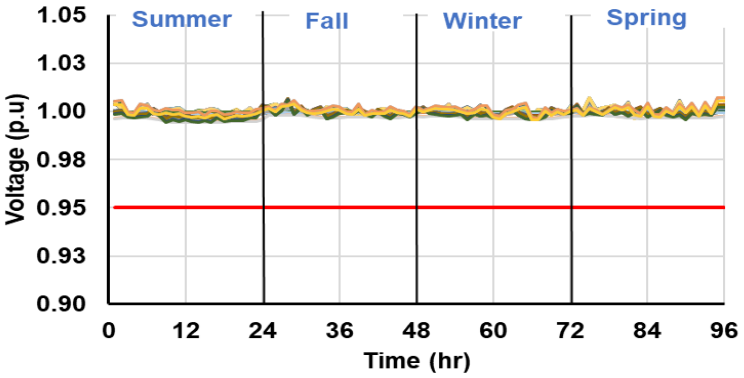


*Fig. 7.59.- Voltage profile of IEEE 69-bus for four typical days of the four seasons in the year with PV and BES*

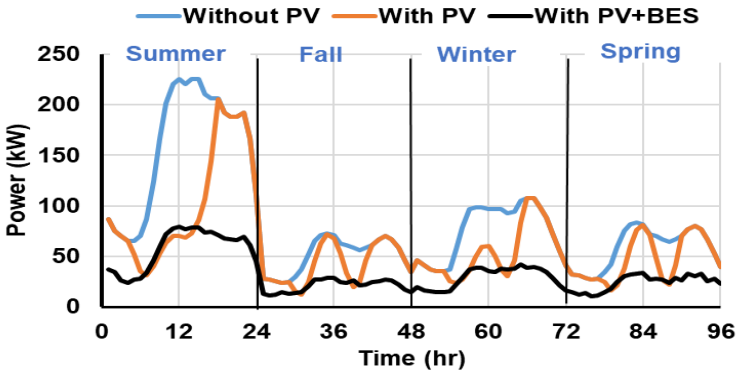


*Fig. 7.60.- Power loss minimization in IEEE 69-bus for four typical days of the four seasons in the year*

Finally, in the IEEE 69-bus system, Table 7.45 gives the optimum PV and BES sizes. It is clear that, due to the heavy load, the full sizes of the PV and BES on buses 21 and 61 are hit in summer. However, the optimum capacity is obtained in spring for BES linked to bus 67,

*Table 7.45.- Optimal size of PV and BES for IEEE 69-bus*

| | Summer | Fall | Winter | Spring |
|---|---|---|---|---|
| BES 21 (MW h) | 4.09 | 3.32 | 3.49 | 4.08 |
| BES 61 (MW h) | 19.61 | 15.59 | 16.91 | 17.90 |
| BES 67 (MW h) | 7.89 | 6.80 | 7.11 | 8.44 |
| PV 21 size (MW) | 1.30 | 0.82 | 1.00 | 0.92 |
| PV 61 size (MW) | 6.08 | 4.09 | 4.87 | 4.33 |
| PV 67 size (MW) | 2.24 | 1.74 | 1.93 | 1.92 |

# 7.7.- Conclusions

This chapter has presented various numerical results, intending to validate the studied optimization algorithms. Several standard and practical RDSs have been considered for this purpose based on three different DG allocation scenarios. Results have been presented using the same classification followed during this Thesis. Thus, the main conclusions of this section can be summarized in the following points:

- Regarding those optimization algorithms based on the single objective DG allocation problem, the improved algorithms were the most competitive algorithm. The improved algorithms gave the highest LR which proves their feasibility and robust performance. Conclusions of some of the obtained results using the improved algorithms are summarized in tables Table 7.46 IHHO and ATGA have the highest LR in the case of three DGs allocation as

presented in Table 7.46.

* *N_S= Not studied*

*Table 7.46.- Results conclusions for the improved algorithms in three DGs allocation at single-objective function*

| Algorithm | LR % | | | | | |
|---|---|---|---|---|---|---|
| | IEEE 33- bus | | | IEEE 69- bus | | |
| | DG type I | DG type II | DG type III | DG type I | DG type II | DG type III |
| CSCA | 64.5 | N_S | N_S | 68.86 | N_S | N_S |
| IHHO | 65.50 | N_S | 94.39 | 69.15 | N_S | 98.0 |
| CQOBMO | 65.26 | N_S | N_S | 68.86 | N_S | N_S |
| ATGA | 65.50 | 34.45 | 94.45 | 69.14 | 35.47 | 98.10 |

* *N_S= Not studied*

- The problem of DG allocation has been studied using improved multi-objective optimization algorithms. Three objectives have been considered in this case namely power loss, voltage deviation, and VSI. As well the improved algorithms with the developed decision-making proved their efficiency compared to the other competitive algorithms. Table 7.47 presents the conclusion of the obtained results using the improved multi-objective algorithms for DG allocation type I, the results show the feasibility of the MOCSCA compared to the other algorithms.

*Table 7.47.- Results conclusions for the improved algorithms in three DGs allocation at Multi-objective functions (DG type I)*

| Algorithm | IEEE 33- bus | | | IEEE 69- bus | | |
|---|---|---|---|---|---|---|
| | $P_{loss}$ (kW) | VD (p.u) | VSI (p.u) | $P_{loss}$ (kW) | VD (p.u) | VSI (p.u) |
| MOCSCA | 88.43 | 0.0016 | 0.9572 | 79.69 | 0.0002 | 0.9798 |
| MCSSA | 74.31 | 0.6926** | 0.9065 | N_S | N_S | N_S |
| MOIHHO | 92.25 | 0.0019 | 0.9580 | 80.8 | 0.0007 | 0.9778 |

* *N_S= Not studied*

* * *VD is calculated using(2.8)*

- Finally, the DG allocation problem has been solved considering the uncertainty of the power generation and the load variation. A suitable PV+BES power has been optimally calculated using the improved single- and multi-objective optimization algorithms. Considerable enhancements have been achieved in the energy loss reduction and voltage profile using the PV+BES integration. Table 7.48 summarizes the reduction in energy loss using the CQOBMO and MCSSA. It is clear that the percentage obtained by

CQOBMO is higher than the MCSSA and that is because the CQOBMO is applied for a single optimization problem that uses the power loss as the main objective function.

*Table 7.48.- Results conclusions for the reduction in the energy with optimal PV+BES sizing*

| Algorithm | Energy losses Reduction % | |
|---|---|---|
| | IEEE 33- bus | IEEE 69- bus |
| CQOBMO | 64.0 | 67.80 |
| MCSSA | 57.40 | N_S |

* *N_S= Not studied*

# 7.8.- Developed GUI Program

A developed GUI is implemented for the DG allocation in RDSs using MATLAB m-file code as shown in Fig A.5. the figure presents the simplicity of entering the input data for the DG allocation problem. The user can choose the test study from various test systems. Besides, several optimization algorithms can be chosen to perform the optimization problem. The main parameters of the optimization algorithm such as the population and iteration numbers. The program performs a statistical analysis (mean, best, and worst values) for the optimization algorithm by running the algorithm many times by writing the number of runs to.

Various improvement methods are included in the program as presented in this thesis such as fuzzy, analytical, and chaotic theory. Besides, different types of DG allocation can be carried out with different numbers. The program provides two file formats for the output results (excel and text), Finally, the convergence chrematistic is plotted on the screen to check the performance of the optimization algorithm.

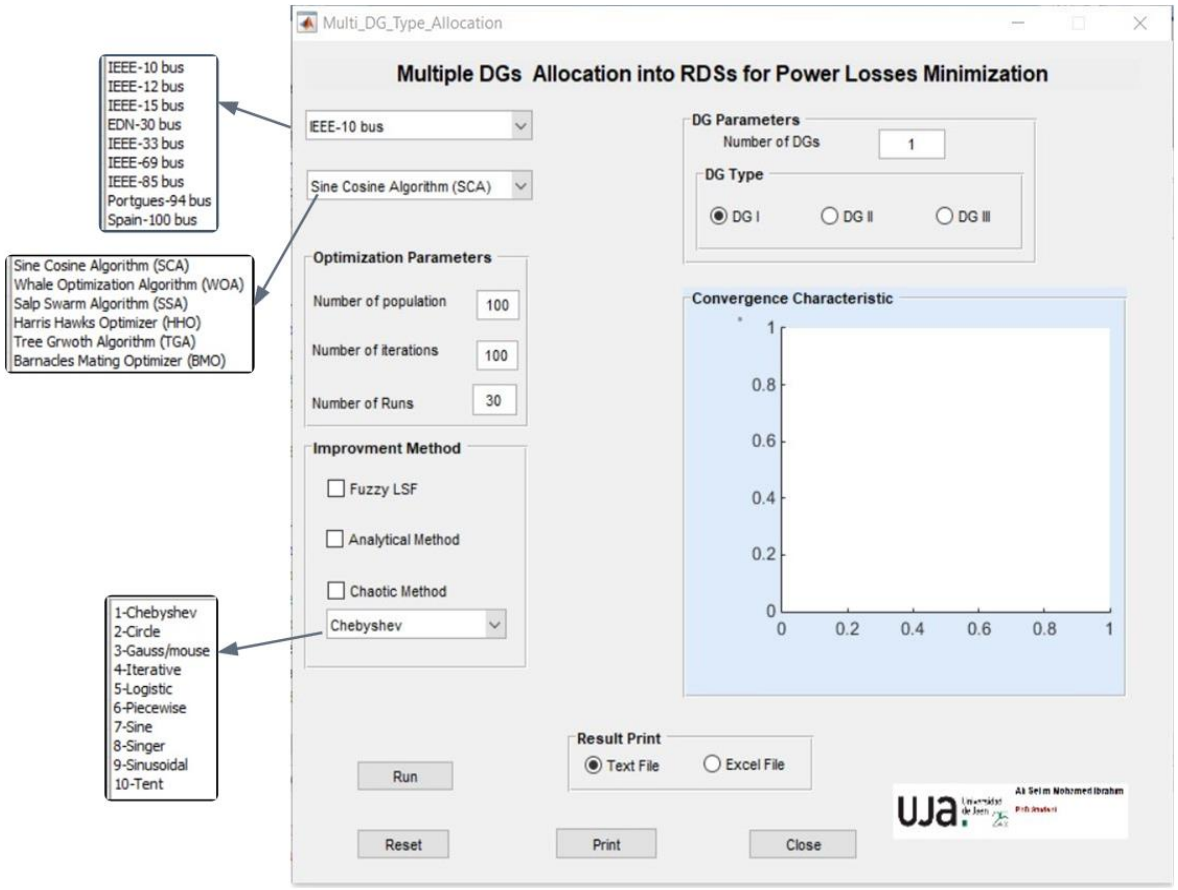


*Fig. 7.61.- A developed GUI for the DG allocation using improved single-objective optimization algorithms*

# Chapter 8

# Conclusions and Future Works

This chapter presents the conclusions of the presented research in this thesis and highlights its impact. Furthermore, it provides the main research opportunities for extending the presented work in the future.

## 8.1.- Conclusions

Optimal DG allocation has been studied in this thesis to enhance the performance of the RDSs. The DG allocation problem has been introduced as a single- and multi-objective problem. In the single-objective problem, minimizing the total power loss has been taken as the main objective function, on the other hand, three objective functions namely power loss, voltage deviation, and VSI have been optimized. The uncertainty model for DG based PV power generation has been formulated to represent the intermittent nature of DG based renewable energy. Besides, BES charging/discharging model has been implemented to compensate for the active power generation of the PV. Several optimization algorithms have been used to allocate the DG in RDSs and many results have been achieved in this regard. Hence, to check the performance of these algorithms, the conclusions for the main contributions that have been accomplished in this thesis can be summarized as follows:

- The forward/backward load flow solver has been adopted to calculate the main objective functions. The forward/backward has been applied due to its computational efficiencies and solution accuracies in solving RDSs.
- Different types of optimization algorithms have been applied for the DG allocation such as analytical, metaheuristic, hybrid optimization algorithms. In the analytical algorithms, a mathematical formulation has been constructed based on the derivative of the objective function. However, the metaheuristic algorithms used the nature-inspired technique without going so far in the optimization problem.
- Improved single- and multi-objective optimization algorithms have been applied to the DG allocation. To check the performance of these algorithms, various standard (IEEE systems) and practical (Portuguese) RDSs have been used in the numerical results section and compared to the other competitive algorithms.
- The impact of the intermittent nature of the PV power and the load variation for 24 hrs and one year on the RDSs has been studied in this thesis. To overcome the intermittent issue, BES has been optimally integrated into RDSs using the improved optimization algorithms. Significant enhancements in the energy reduction and voltage profile have been achieved with the scheduling of the PV+BES power generation.

## 8.2.- Future works

Based on the obtained results in this work, several ideas and research works could be carried out in the future.

Some of these ideas can be summarized in the following lines:

- Further DG based renewable energy resources such as wind could be modeled using uncertainty and optimally allocated in the RDSs.
- Long-term analysis considering both capital and operational expenditure of the PV and BES system will be optimized.
- Scheduling the active and reactive power of the PV based on the PV inverter technology could be studied using different optimization algorithms and

different power generation and load scenarios.

- Optimal coordination of the Plug-in hybrid electric vehicles in the RDSs can be formulated.
- Using Plug-in hybrid electric vehicles charging/discharging control strategies to support the voltage profile in the distribution systems.

# Appendix A

# Curriculum Vitae

**Name:** Ali Selim Mohamed

**Birthday:** July 2, 1988

**Nationality:** Egyptian

**Education and qualifications:**

- ***Graduate Degree:*** *Electrical Engineering by Aswan University, Egypt. 2010 Very good with the first honor degree (82.9 %).*

- ***Master's Degree:*** *Master of Science in Electrical Engineering by Aswan University, Egypt in 2016 Excellent with the first university rank (92.8 %).*

**Experience**

- *September - December 2019: Academic visitor Laboratory of Electric Power Supply, Faculty of Electrical Engineering, University of Ljubljana, Slovenia.*

- *February - May 2018: Academic visitor, Institute for Systems and Computer Engineering, Technology and Science (INESC TEC), Porto, Portugal.*
- *Nov. 2017 - Until now: Ph.D. student, Electrical Engineering Department, University of Jaén, Spain.*
- *December 2016 - Until now: Assistant lecture, Department of Electrical Engineering. Aswan University, Aswan, Egypt.*
- *December 2015 - June 2016: Academic visitor, Department of Electrical and Electronics Engineering. University of the Ryukyus, Okinawa, Japan.*
- *June 2012 - December 2016: Demonstrator, Department of Electrical Engineering. Aswan University, Aswan, Egypt.*

**Honors and Awards**

- 2016 Aswan University: *Academic Award.*
- 2010 Aswan University: *Academic Award.*

# Appendix B

# List of Publications

As a result of the contributions of this Thesis, the following papers have been published or accepted for publication in international journals and conferences.

## B.1 Journal papers

- A. Selim, S. Kamel, and F. Jurado, "Voltage stability analysis based on optimal placement of multiple DG types using hybrid optimization technique," International Transactions on Electrical Energy Systems, p. e12551, 2020. DOI: 10.1002/2050-7038.12551
- A. Selim, S. Kamel, L. S. Nasrat, and F. Jurado, "Voltage Stability Assessment of Radial Distribution Systems Including Optimal Allocation of Distributed Generators," International Journal of Interactive Multimedia Artificial Intelligence, vol. 6, no. 1, 2020. DOI: 10.9781/ijimai.2020.02.004
- W. Ahmed, A. Selim, S. Kamel, J. Yu, and F. J. Melguizo, "Probabilistic Load Flow Solution Considering Optimal Allocation of SVC in Radial Distribution System," International Journal of Interactive Multimedia Artificial Intelligence, vol. 5, no. 3, pp. 152-161, 2018. DOI: 10.9781/ijimai.2018.11.001
- A. Selim, S. Kamel, A. S. Alghamdi, and F. Jurado, "Optimal Placement of DGs in Distribution System Using an Improved Harris Hawks Optimizer Based on Single-and Multi-Objective Approaches," IEEE Access, vol. 8, pp. 52815-

52829, 2020. DOI: 10.1109/ACCESS.2020.2980245

- S. Kamel, A. Selim, W. Ahmed, and F. Jurado, "Single-and multi-objective optimization for photovoltaic distributed generators implementation in probabilistic power flow algorithm," Electrical Engineering, pp. 1-17, 2019. DOI: 10.1007/s00202-019-00878-7
- A. Selim, S. Kamel, and F. Jurado, "Optimal allocation of distribution static compensators using a developed multi-objective sine cosine approach," Computers Electrical Engineering, vol. 85, p. 106671, 2020. DOI: 10.1016/j.compeleceng.2020.106671
- A. Selim, S. Kamel, and F. Jurado, "Capacitors Allocation in Distribution Systems Using a Hybrid Formulation Based on Analytical and Two Metaheuristic Optimization Techniques," Computers Electrical Engineering, vol. 85, p. 106675, 2020. DOI: 10.1016/j.compeleceng.2020.106675
- A. Selim, S. Kamel, and F. Jurado, "Efficient optimization technique for multiple DG allocation in distribution networks," Applied Soft Computing, vol. 86, p. 105938, 2020. DOI: 10.1016/j.asoc.2019.105938
- A. Selim, S. Kamel, and F. Jurado, João Peças Lopes, Manuel A. Matos "Optimal Setting of PV and Battery Energy Storage in Radial Distribution Systems using Multi-Objective Criteria with Fuzzy Logic Decision Making" Accepted in IET Generation Transmission & Distribution vol. 15, p. 135-148, 2020. DOI: doi.org/10.1049/gtd2.12019

## B.2 Conference papers

- S. Kamel, A. Selim, F. Jurado, J. Yu, K. Xie, and C. Yu, "Multi-Objective Whale Optimization Algorithm for Optimal Integration of Multiple DGs into Distribution Systems," in 2019 IEEE Innovative Smart Grid Technologies-Asia (ISGT Asia), 2019, pp. 1312-1317: IEEE.
- S. Kamel, A. Selim, F. Jurado, J. Yu, K. Xie, and T. Wu, "Capacitor Allocation in Distribution Systems Using Fuzzy Loss Sensitivity Factor with Sine Cosine Algorithm," in 2019 IEEE Innovative Smart Grid Technologies-Asia (ISGT Asia), 2019, pp. 1276-1281: IEEE.
- A. Selim, S. Kamel, F. Jurado, and S. Marrouchi, "Developed Algorithm Based

on Lightning Search optimizer and Analytical Technique for Allocation of Distribution Generators," in 2019 21st International Middle East Power Systems Conference (MEPCON), 2019, pp. 970-975: IEEE.

- A. Selim, S. Kamel, and F. Jurado, "Power losses and Energy Cost Minimization Using Shunt Capacitors Installation in Distribution Systems," in 2019 10th International Renewable Energy Congress (IREC), 2019: IEEE.
- A. Selim, S. Kamel, and F. Jurado, "Voltage Profile Enhancement Using Multi-Objective Sine Cosine Algorithm for Optimal Installation of DSTACOMs into Distribution Systems," in 2019 10th International Renewable Energy Congress (IREC), 2019: IEEE.
- S. Kamel, M. Mohamed, A. Selim, L. S. Nasrat, and F. Jurado, "Power System Voltage Stability Based on Optimal Size and Location of Shunt Capacitor Using Analytical," in 2019 10th International Renewable Energy Congress (IREC), 2019: IEEE.
- S. Kamel, W. Hamdy, S. Abd-elgwad, A. Selim, and F. Jurado, "Development of Probabilistic Power Flow Algorithm for Radial Distribution Systems with Capacitors Using Analytical Approach," in 2019 10th International Renewable Energy Congress (IREC), 2019: IEEE.
- A. Selim, S. Kamel, and F. Jurado, "Voltage Profile Improvement in Active Distribution Networks Using Hybrid WOA-SCA Optimization Algorithm," in 2018 Twentieth International Middle East Power Systems Conference (MEPCON), 2018, pp. 1064-1068: IEEE.
- A. Selim, S. Kamel, and F. Jurado, "Hybrid Optimization Technique for Optimal Placement of DG and D-STATCOM in Distribution Networks," in 2018 Twentieth International Middle East Power Systems Conference (MEPCON), 2018, pp. 689-693: IEEE.

# Bibliography

[1] A. Y. Saber and G. K. Venayagamoorthy, "Plug-in vehicles and renewable energy sources for cost and emission reductions," *IEEE Transactions on Industrial electronics,* vol. 58, no. 4, pp. 1229-1238, 2011.

[2] L. L. Lai and T. F. Chan, *Distributed generation: Induction and permanent magnet generators*. John Wiley & Sons, 2008.

[3] S. Kamel, A. Selim, W. Ahmed, and F. J. E. E. Jurado, "Single-and multi-objective optimization for photovoltaic distributed generators implementation in probabilistic power flow algorithm," pp. 1-17, 2019.

[4] A. Selim, M. Abdel-Akher, M. M. Aly, and S. Kamel, "Efficient time series simulation of distribution systems with voltage regulation and PV penetration," in *Power Systems Conference (MEPCON), 2016 Eighteenth International Middle East*, 2016, pp. 717-722: IEEE.

[5] T. T. Hashim, A. Mohamed, and H. Shareef, "A review on voltage control methods for active distribution networks," *Electrical review,* vol. 88, no. 6, pp. 304-312, 2012.

[6] A. Selim, M. Abdel-Akher, M. M. Aly, S. Kamel, and T. Senjyu, "Fast quasi-static time-series analysis and reactive power control of unbalanced distribution systems," *International Transactions on Electrical Energy Systems,* p. e2673, 2018.

[7] S. M. Said, A. Selim, and B. Hartmann, "Enhancement of voltage profile for unbalanced distribution system with wind energy and superconducting magnetic energy storage," in *Innovative Trends in Computer Engineering (ITCE), 2018 International Conference on*, 2018, pp. 289-295: IEEE.

[8] J. P. Lopes, Â. Mendonça, N. Fonseca, and L. Seca, "Voltage and reactive power control provided by DG units," in *CIGRE Symposium: Power Systems with Dispersed Generation, Athens, Greece*, 2005.

[9] M. H. Sulaiman, Z. Mustaffa, M. M. Saari, and H. Daniyal, "Barnacles Mating Optimizer: A new bio-inspired algorithm for solving engineering optimization problems," *Engineering Applications of Artificial Intelligence*, vol. 87, p. 103330, 2020.

[10] W. Zhao, L. Wang, and Z. Zhang, "Artificial ecosystem-based optimization: a novel nature-inspired meta-heuristic algorithm," *Neural Computing Applications*, pp. 1-43, 2019.

[11] T. Dutta, S. Bhattacharyya, S. Dey, and J. Platos, "Border Collie Optimization," *IEEE Access*, 2020.

[12] X.-S. Yang, *Nature-inspired metaheuristic algorithms*. Luniver press, 2010.

[13] S. Mirjalili and A. Lewis, "The whale optimization algorithm," *Advances in engineering software*, vol. 95, pp. 51-67, 2016.

[14] M. Mitchell, *An introduction to genetic algorithms*. MIT press, 1998.

[15] R. Storn and K. Price, "Differential evolution–a simple and efficient heuristic for global optimization over continuous spaces," *%J Journal of global optimization*, vol. 11, no. 4, pp. 341-359, 1997.

[16] O. Montiel, O. Castillo, P. Melin, A. R. Díaz, and R. Sepúlveda, "Human evolutionary model: A new approach to optimization," *Information Sciences*, vol. 177, no. 10, pp. 2075-2098, 2007.

[17] X. Chen, Y. Liu, X. Li, Z. Wang, S. Wang, and C. Gao, "A new evolutionary multiobjective model for traveling salesman problem," *IEEE Access*, vol. 7, pp. 66964-66979, 2019.

[18] D. Simon, "Biogeography-based optimization," *IEEE transactions on evolutionary computation*, vol. 12, no. 6, pp. 702-713, 2008.

[19] J. Kennedy and R. Eberhart, "Particle swarm optimization," in *Proceedings of ICNN'95-International Conference on Neural Networks*, 1995, vol. 4, pp. 1942-1948: IEEE.

[20] E. Cuevas and M. Cienfuegos, "A new algorithm inspired in the behavior of the social-spider for constrained optimization," *Expert Systems with Applications*, vol. 41, no. 2, pp. 412-425, 2014.

[21] D. Karaboga and B. Basturk, "A powerful and efficient algorithm for numerical function optimization: artificial bee colony (ABC) algorithm," *Journal of global optimization*, vol. 39, no. 3, pp. 459-471, 2007.

[22] S. Mirjalili, "Moth-flame optimization algorithm: A novel nature-inspired heuristic paradigm," *Knowledge-based systems*, vol. 89, pp. 228-249, 2015.

[23] S. Mirjalili, S. M. Mirjalili, and A. Lewis, "Grey wolf optimizer," *Advances in engineering software*, vol. 69, pp. 46-61, 2014.

[24] S. Saremi, S. Mirjalili, and A. Lewis, "Grasshopper optimisation algorithm: theory and application," *Advances in Engineering Software*, vol. 105, pp. 30-47, 2017.

[25] S. Mirjalili, A. H. Gandomi, S. Z. Mirjalili, S. Saremi, H. Faris, and S. M. Mirjalili, "Salp Swarm Algorithm: A bio-inspired optimizer for engineering design problems," *Advances in Engineering Software*, vol. 114, pp. 163-191, 2017.

[26] A. A. Heidari, S. Mirjalili, H. Faris, I. Aljarah, M. Mafarja, and H. Chen, "Harris hawks optimization: Algorithm and applications," *Future Generation Computer Systems*, vol. 97, pp. 849-872, 2019.

[27] A. K. Das and D. K. Pratihar, "A new bonobo optimizer (BO) for real-parameter optimization," in *2019 IEEE Region 10 Symposium (TENSYMP)*, 2019, pp. 108-113: IEEE.

[28] S. Kirkpatrick, C. D. Gelatt, and M. P. Vecchi, "Optimization by simulated annealing," *science,* vol. 220, no. 4598, pp. 671-680, 1983.

[29] B. Webster and P. J. Bernhard, "A local search optimization algorithm based on natural principles of gravitation," 2003.

[30] H. Eskandar, A. Sadollah, A. Bahreininejad, and M. Hamdi, "Water cycle algorithm–A novel metaheuristic optimization method for solving constrained engineering optimization problems," *Computers & Structures,* vol. 110, pp. 151-166, 2012.

[31] A. Kaveh and T. Bakhshpoori, "Water evaporation optimization: a novel physically inspired optimization algorithm," *Computers & Structures,* vol. 167, pp. 69-85, 2016.

[32] W. Zhao, L. Wang, and Z. Zhang, "Atom search optimization and its application to solve a hydrogeologic parameter estimation problem," *Knowledge-Based Systems,* vol. 163, pp. 283-304, 2019.

[33] A. Faramarzi, M. Heidarinejad, B. Stephens, and S. Mirjalili, "Equilibrium optimizer: A novel optimization algorithm," *Knowledge-Based Systems,* vol. 191, p. 105190, 2020.

[34] H. Shareef, A. A. Ibrahim, and A. H. Mutlag, "Lightning search algorithm," *Applied Soft Computing,* vol. 36, pp. 315-333, 2015.

[35] L. M. Zhang, C. Dahlmann, and Y. Zhang, "Human-inspired algorithms for continuous function optimization," in *2009 IEEE international conference on intelligent computing and intelligent systems,* 2009, vol. 1, pp. 318-321: IEEE.

[36] S. Satapathy and A. Naik, "Social group optimization (SGO): a new population evolutionary optimization technique," *Complex & Intelligent Systems,* vol. 2, no. 3, pp. 173-203, 2016.

[37] R. V. Rao, V. J. Savsani, and D. Vakharia, "Teaching–learning-based optimization: an optimization method for continuous non-linear large scale problems," *Information sciences,* vol. 183, no. 1, pp. 1-15, 2012.

[38] H. Bouchekara, "Most Valuable Player Algorithm: a novel optimization algorithm inspired from sport," *Operational Research,* pp. 1-57, 2017.

[39] A. H. Kashan, "League Championship Algorithm (LCA): An algorithm for global optimization inspired by sport championships," *Applied Soft Computing,* vol. 16, pp. 171-200, 2014.

[40] D. H. Wolpert and W. G. Macready, "No free lunch theorems for optimization," *IEEE transactions on evolutionary computation,* vol. 1, no. 1, pp. 67-82, 1997.

[41] L. M. Pecora and T. L. Carroll, "Synchronization in chaotic systems," *Physical review letters,* vol. 64, no. 8, p. 821, 1990.

[42] E. Emary and H. M. Zawbaa, "Impact of chaos functions on modern swarm optimizers," *PloS one,* vol. 11, no. 7, p. e0158738, 2016.

[43] Y. Li-Jiang and C. Tian-Lun, "Application of chaos in genetic algorithms," *Communications in Theoretical Physics,* vol. 38, no. 2, p. 168, 2002.

[44] B. Liu, L. Wang, Y.-H. Jin, F. Tang, and D.-X. Huang, "Improved particle swarm optimization combined with chaos," *Chaos, Solitons & Fractals,* vol. 25, no. 5, pp. 1261-1271, 2005.

[45] H. M. Zawbaa, E. Emary, and C. Grosan, "Feature selection via chaotic antlion optimization," *PloS one,* vol. 11, no. 3, p. e0150652, 2016.

[46] G. Kaur and S. Arora, "Chaotic whale optimization algorithm," *Journal of Computational Design and Engineering,* vol. 5, no. 3, pp. 275-284, 2018.

[47] M. Kohli and S. Arora, "Chaotic grey wolf optimization algorithm for constrained optimization problems," *Journal of computational design and engineering,* vol. 5, no. 4, pp. 458-472, 2018.

[48] S. Saremi, S. Mirjalili, and A. Lewis, "Biogeography-based optimisation with chaos," *Neural Computing and Applications,* vol. 25, no. 5, pp. 1077-1097, 2014.

[49] A. Selim, S. Kamel, and F. Jurado, "Efficient optimization technique for multiple DG allocation in distribution networks," *Applied Soft Computing,* vol. 86, p. 105938, 2020.

[50] A. S. Menesy, H. M. Sultan, A. Selim, M. G. Ashmawy, and S. Kamel, "Developing and applying chaotic harris hawks optimization technique for extracting parameters of several proton exchange membrane fuel cell stacks," *IEEE Access,* vol. 8, pp. 1146-1159, 2019.

[51] H. R. Tizhoosh, "Opposition-based learning: a new scheme for machine intelligence," in *International Conference on Computational Intelligence for Modelling, Control and Automation and International Conference on Intelligent Agents, Web Technologies and Internet Commerce (CIMCA-IAWTIC'06)*, 2005, vol. 1, pp. 695-701: IEEE.

[52] P. K. Roy and S. Bhui, "Multi-objective quasi-oppositional teaching learning based optimization for economic emission load dispatch problem," *International Journal of Electrical Power Energy Systems,* vol. 53, pp. 937-948, 2013.

[53] S. Sultana and P. K. Roy, "Multi-objective quasi-oppositional teaching learning based optimization for optimal location of distributed generator in radial distribution systems," *International Journal of Electrical Power Energy Systems,* vol. 63, pp. 534-545, 2014.

[54] S. Sharma, S. Bhattacharjee, and A. Bhattacharya, "Quasi-Oppositional Swine Influenza Model Based Optimization with Quarantine for optimal allocation of DG in radial distribution network," *International Journal of Electrical Power Energy Systems,* vol. 74, pp. 348-373, 2016.

[55] J. Yu, C.-H. Kim, and S.-B. Rhee, "Oppositional Jaya Algorithm With Distance-Adaptive Coefficient in Solving Directional Over Current Relays Coordination Problem," *IEEE Access,* vol. 7, pp. 150729-150742, 2019.

[56] J. Lian, Y. Zhang, C. Ma, Y. Yang, and E. Chaima, "A review on recent sizing methodologies of hybrid renewable energy systems," *Energy Conversion and Management,* vol. 199, p. 112027, 2019.

[57] L. Mingxue, Y. Guolai, L. Xiaoqing, and B. Guixiang, "Variable universe fuzzy control of adjustable hydraulic torque converter based on multi-population genetic algorithm," *IEEE Access,* vol. 7, pp. 29236-29244, 2019.

[58] P. Prakash and D. K. Khatod, "Optimal sizing and siting techniques for distributed generation in distribution systems: A review," *Renewable and Sustainable Energy Reviews,* vol. 57, pp. 111-130, 2016.

[59] M. P. HA, P. D. Huy, and V. K. Ramachandaramurthy, "A review of the optimal allocation of distributed generation: Objectives, constraints, methods, and algorithms," *Renewable and Sustainable Energy Reviews,* vol. 75, pp. 293-312, 2017.

[60] S. Kansal, V. Kumar, and B. Tyagi, "Hybrid approach for optimal placement of multiple DGs of multiple types in distribution networks," *International Journal of Electrical Power & Energy Systems,* vol. 75, pp. 226-235, 2016.

[61] D. Q. Hung and N. Mithulananthan, "Multiple distributed generator placement in primary distribution networks for loss reduction," *IEEE Transactions on industrial electronics,* vol. 60, no. 4, pp. 1700-1708, 2013.

[62] S. N. G. Naik, D. K. Khatod, and M. P. Sharma, "Analytical approach for optimal siting and sizing of distributed generation in radial distribution networks," *IET Generation, Transmission & Distribution*, vol. 9, no. 3, pp. 209-220, 2014.

[63] A. Ehsan and Q. Yang, "Optimal integration and planning of renewable distributed generation in the power distribution networks: A review of analytical techniques," *Applied Energy*, vol. 210, pp. 44-59, 2018.

[64] M. H. Moradi, M. Abedinie, and H. B. Tolabi, "Optimal multi-distributed generation location and capacity by genetic algorithms," in *2010 Conference Proceedings IPEC*, 2010, pp. 614-618: IEEE.

[65] A. El-Zonkoly, "Optimal placement of multi-distributed generation units including different load models using particle swarm optimization," *Swarm Evolutionary Computation*, vol. 1, no. 1, pp. 50-59, 2011.

[66] G. Celli, E. Ghiani, S. Mocci, and F. Pilo, "A multiobjective evolutionary algorithm for the sizing and siting of distributed generation," *IEEE Transactions on power systems*, vol. 20, no. 2, pp. 750-757, 2005.

[67] M. P. Lalitha, V. V. Reddy, N. S. Reddy, and V. U. Reddy, "DG source allocation by fuzzy and clonal selection algorithm for minimum loss in distribution system," *Distributed Generation & Alternative Energy Journal*, vol. 26, no. 4, pp. 17-35, 2011.

[68] A. El-Fergany, "Optimal allocation of multi-type distributed generators using backtracking search optimization algorithm," *International Journal of Electrical Power & Energy Systems*, vol. 64, pp. 1197-1205, 2015.

[69] K. Devabalaji and K. Ravi, "Optimal size and siting of multiple DG and DSTATCOM in radial distribution system using Bacterial Foraging Optimization Algorithm," *Ain Shams Engineering Journal*, vol. 7, no. 3, pp. 959-971, 2016.

[70] S. ChithraDevi, L. Lakshminarasimman, and R. Balamurugan, "Stud Krill herd Algorithm for multiple DG placement and sizing in a radial distribution system," *Engineering Science and Technology, an International Journal*, vol. 20, no. 2, pp. 748-759, 2017.

[71] P. D. P. Reddy, V. V. Reddy, and T. G. Manohar, "Whale optimization algorithm for optimal sizing of renewable resources for loss reduction in distribution systems," *Renewables: Wind, Water, and Solar*, vol. 4, no. 1, p. 3, 2017.

[72] A. Selim, S. Kamel, and F. Jurado, "Efficient optimization technique for multiple DG allocation in distribution networks," *Applied Soft Computing*, vol. 86, p. 105938, 2020.

[73] M. H. Moradi and M. Abedini, "A combination of genetic algorithm and particle swarm optimization for optimal DG location and sizing in distribution systems," *International Journal of Electrical Power & Energy Systems*, vol. 34, no. 1, pp. 66-74, 2012.

[74] S. Sultana and P. K. Roy, "Multi-objective quasi-oppositional teaching learning based optimization for optimal location of distributed generator in radial distribution systems," *International Journal of Electrical Power & Energy Systems*, vol. 63, pp. 534-545, 2014.

[75] M. H. Moradi, A. Zeinalzadeh, Y. Mohammadi, and M. Abedini, "An efficient hybrid method for solving the optimal sitting and sizing problem of DG and shunt capacitor banks simultaneously based on imperialist competitive algorithm and genetic algorithm," *International Journal of Electrical Power Energy Systems*, vol. 54, pp. 101-111, 2014.

[76] C. A. C. Coello, G. T. Pulido, and M. S. Lechuga, "Handling multiple objectives with particle swarm optimization," *IEEE Transactions on evolutionary computation*, vol. 8, no. 3, pp. 256-279, 2004.

[77] S. Kamel, A. Selim, W. Ahmed, and F. Jurado, "Single-and multi-objective optimization for photovoltaic distributed generators implementation in probabilistic power flow algorithm," *Electrical Engineering*, pp. 1-17, 2019.

[78] S. Kamel, A. Selim, F. Jurado, J. Yu, K. Xie, and C. Yu, "Multi-Objective Whale Optimization Algorithm for Optimal Integration of Multiple DGs into Distribution Systems," in *2019 IEEE Innovative Smart Grid Technologies-Asia (ISGT Asia)*, 2019, pp. 1312-1317: IEEE.

[79] C. Yammani, S. Maheswarapu, and S. K. Matam, "A Multi-objective Shuffled Bat algorithm for optimal placement and sizing of multi distributed generations with different load models," *International Journal of Electrical Power & Energy Systems*, vol. 79, pp. 120-131, 2016.

[80] N. K. Meena, A. Swarnkar, N. Gupta, and K. R. Niazi, "Multi-objective Taguchi approach for optimal DG integration in distribution systems," *IET Generation, Transmission & Distribution*, vol. 11, no. 9, pp. 2418-2428, 2017.

[81] Y. Atwa, E. El-Saadany, M. Salama, and R. Seethapathy, "Optimal renewable resources mix for distribution system energy loss minimization," *IEEE Transactions on Power Systems*, vol. 25, no. 1, pp. 360-370, 2010.

[82] D. Q. Hung, N. Mithulananthan, and R. Bansal, "Analytical strategies for renewable distributed generation integration considering energy loss minimization," *Applied Energy*, vol. 105, pp. 75-85, 2013.

[83] D. Q. Hung, N. Mithulananthan, and K. Y. Lee, "Determining PV penetration for distribution systems with time-varying load models," *IEEE Transactions on Power Systems*, vol. 29, no. 6, pp. 3048-3057, 2014.

[84] D. Q. Hung, N. Mithulananthan, and R. Bansal, "Integration of PV and BES units in commercial distribution systems considering energy loss and voltage stability," *Applied Energy*, vol. 113, pp. 1162-1170, 2014.

[85] S. Chen, H. B. Gooi, and M. Wang, "Sizing of energy storage for microgrids," *IEEE Transactions on Smart Grid*, vol. 3, no. 1, pp. 142-151, 2012.

[86] S. Mirjalili, "SCA: a sine cosine algorithm for solving optimization problems," *Knowledge-Based Systems*, vol. 96, pp. 120-133, 2016.

[87] A. Cheraghalipour, M. Hajiaghaei-Keshteli, and M. M. J. E. A. o. A. I. Paydar, "Tree Growth Algorithm (TGA): A novel approach for solving optimization problems," vol. 72, pp. 393-414, 2018.

[88] M. Balasubbareddy and D. Dwivedi, "Optimal Power Flow Solution for multi-fuel system using Tree Growth Algorithm," *Pramana Research Journal*, vol. 9, no. 4, 2019.

[89] S. Mirjalili, S. Saremi, S. M. Mirjalili, and L. d. S. Coelho, "Multi-objective grey wolf optimizer: a novel algorithm for multi-criterion optimization," *Expert Systems with Applications*, vol. 47, pp. 106-119, 2016.

[90] A. Selim, S. Kamel, and F. Jurado, "Voltage Profile Enhancement Using Multi-Objective Sine Cosine Algorithm for Optimal Installation of DSTACOMs into Distribution Systems," in *2019 10th International Renewable Energy Congress (IREC)*, 2019, pp. 1-6.

[91] W. Ahmed, A. Selim, S. Kamel, J. Yu, and F. Jurado, "Probabilistic Load Flow Solution Considering Optimal Allocation of SVC in Radial Distribution System," *International Journal of Interactive Multimedia & Artificial Intelligence*, vol. 5, no. 3, 2018.

[92] Y. Kuo, T. Yang, and G.-W. Huang, "The use of grey relational analysis in solving multiple attribute decision-making problems," *Computers & industrial engineering*, vol. 55, no. 1, pp. 80-93, 2008.

[93] J. R. Schott, "Fault Tolerant Design Using Single and Multicriteria Genetic Algorithm Optimization," AIR FORCE INST OF TECH WRIGHT-PATTERSON AFB OH1995.

[94] G. Kaur and S. Arora, "Chaotic Whale Optimization Algorithm," *Journal of Computational Design and Engineering*, 2018.

[95] M. E. Baran and F. F. Wu, "Network reconfiguration in distribution systems for loss reduction and load balancing," *IEEE Transactions on Power delivery*, vol. 4, no. 2, pp. 1401-1407, 1989.

[96] J. Liu, M. Salama, and R. Mansour, "An efficient power flow algorithm for distribution systems with polynomial load," *International Journal of Electrical Engineering Education*, vol. 39, no. 4, pp. 371-386, 2002.

[97] D. F. Pires, C. H. Antunes, and A. G. Martins, "NSGA-II with local search for a multi-objective reactive power compensation problem," *International Journal of Electrical Power & Energy Systems*, vol. 43, no. 1, pp. 313-324, 2012.

[98] K. Nadhir, D. Chabane, and B. Tarek, "Distributed generation location and size determination to reduce power losses of a distribution feeder by Firefly Algorithm," *International journal of advanced science and technology*, vol. 56, pp. 61-72, 2013.

[99] S. Nagaballi and V. S. Kale, "Optimal Deployment of DG and DSTATCOM in Distribution System Using Swarm Intelligent Techniques," in *Proceedings of the 2018 International Conference on Robotics, Control and Automation Engineering*, 2018, pp. 65-70: ACM.

[100] V. V. S. N. Murty and A. Kumar, "Impact of D-STATCOM in distribution systems with load growth on stability margin enhancement and energy savings using PSO and GAMS," *International Transactions on Electrical Energy Systems*, vol. 28, no. 11, p. e2624, 2018.

[101] S. Sharma, S. Bhattacharjee, and A. Bhattacharya, "Quasi-Oppositional Swine Influenza Model Based Optimization with Quarantine for optimal allocation of DG in radial distribution network," *International Journal of Electrical Power & Energy Systems*, vol. 74, pp. 348-373, 2016.

[102] H. Manafi, N. Ghadimi, M. Ojaroudi, and P. Farhadi, "Optimal placement of distributed generations in radial distribution systems using various PSO and DE algorithms," *Elektronika ir Elektrotechnika*, vol. 19, no. 10, pp. 53-57, 2013.

[103] E. Lopez, H. Opazo, L. Garcia, and P. Bastard, "Online reconfiguration considering variability demand: Applications to real networks," *IEEE Transactions on Power systems*, vol. 19, no. 1, pp. 549-553, 2004.

[104] Y. Atwa, E. El-Saadany, M. Salama, and R. J. I. T. o. P. S. Seethapathy, "Optimal renewable resources mix for distribution system energy loss minimization," vol. 25, no. 1, pp. 360-370, 2009.

[105] P. Kayal and C. J. R. e. Chanda, "Optimal mix of solar and wind distributed generations considering performance improvement of electrical distribution network," vol. 75, pp. 173-186, 2015.